PLTMG:
A Software Package for Solving Elliptic Partial Differential Equations
Users' Guide 12.0

Randolph E. Bank

Department of Mathematics
University of California at San Diego
La Jolla, California 92093-0112

June, 2016

This work was supported by the National Science Foundation
under grants DMS-1318480, DMS-1345103, and MRI-0821816.

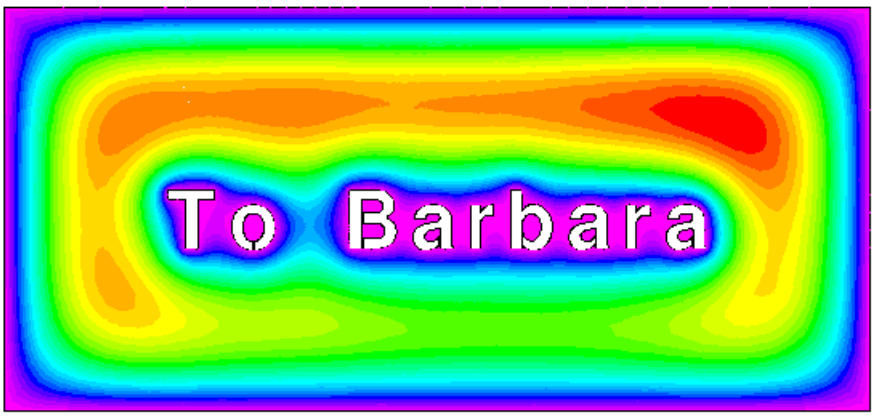
To Barbara

Contents

Preface

Many people have made contributions to the development of this version of *PLTMG*; I am indebted to them all for their help. The original grid refinement algorithms used in *PLTMG* were derived in 1976 as joint work with Todd Dupont of the University of Chicago. The approximate Newton strategies incorporated in the present version of *PLTMG* represent joint work with Donald J. Rose. The gradient recovery and a posteriori error estimation procedures are joint work with Jinchao Xu of Pennsylvania State University and Bin Zheng of Pacific Northwest National Laboratory. The algorithms used in the pseudo-arclength continuation procedures are joint work with Tony Chan of the Hong Kong University of Science and Technology and Hans Mittelmann of Arizona State University. The interior point algorithms used in the optimization problems treated in this version are joint work with Philip Gill of University of California at San Diego. The adaptive mesh smoothing algorithms are joint work with R. Kent Smith. The *hp* refinement algorithms and associated data structures are joint work with Hieu Nguyen of the Universitat Politècnica De Catalunya and Chris Deotte of the University of California at San Diego. The load balance algorithms for parallel computations are also joint work with Chris Deotte. The X-Windows interface and many of the graphics enhancements were jointly developed with Michael Holst of the University of California at San Diego. The parallel adaptive paradigm is joint work with Michael Holst. The parallel domain decomposition solver is joint work with Shaoying Lu of the University of California at San Diego and Panayot Vassilevski of Lawrence Livermore National Laboratory. The dual function used for parallel adaptive meshing is joint work with Jeffrey Ovall of Portland State University. Many people made contributions to the test problems, reported bugs and suggested improvements that have been incorporated in the current version.

This version of *PLTMG* was supported by the National Science Foundation through grants DMS-1318480 and DMS-1345013 (University of California at San Diego). The UCSD Scicomp Beowulf cluster was built using funds provided by the National Science Foundation through MRI-0821816.

University of California at San Diego Randolph E. Bank
June, 2016

Chapter 1
Introduction

1.1 Problem Specification.

Consider the elliptic boundary value problem

$$-\nabla \cdot a(x, y, u, \nabla u, \lambda) + f(x, y, u, \nabla u, \lambda) = 0 \qquad \text{in } \Omega, \tag{1.1}$$

with boundary conditions

$$\begin{aligned} u &= g_2(x, y, \lambda) && \text{on } \partial\Omega_2, \\ a{\cdot}n &= g_1(x, y, u, \lambda) && \text{on } \partial\Omega_1, \\ u, a{\cdot}n &\quad \text{continuous} && \text{on } \partial\Omega_0. \end{aligned} \tag{1.2}$$

Here Ω is a bounded region in $\mathcal{R}^2$, n is the unit normal, a is the vector $(a_1, a_2)^t$, a_1, a_2, f, g_1, and g_2 are scalar functions. $\partial\Omega_0$ is a portion of $\partial\Omega$ where periodic boundary conditions are applied. In some problems solved by *PLTMG*, the parameter λ is not used, while in others $\lambda \in \mathcal{R}^k$, $k \geq 1$, is a vector of scalar parameters or $\lambda \in \mathcal{H}^1(\Omega)$, where $\mathcal{H}^1(\Omega)$ denotes the usual Sobolev space. Let

$$\begin{aligned} \mathcal{H}^1_p &= \{\phi \in \mathcal{H}^1(\Omega) \,|\, \phi \text{ is continuous on } \partial\Omega_0\}, \\ \mathcal{H}^1_g &= \{\phi \in \mathcal{H}^1_p \,|\, \phi = g_2 \text{ on } \partial\Omega_2\}, \\ \mathcal{H}^1_e &= \{\phi \in \mathcal{H}^1_p \,|\, \phi = 0 \text{ on } \partial\Omega_2\}. \end{aligned}$$

Then the weak form of (1.1)-(1.2) is: find $u \in \mathcal{H}^1_g$ such that

$$a(u, v) = 0 \qquad \text{for all } v \in \mathcal{H}^1_e, \tag{1.3}$$

where

$$a(u, v) = \int_\Omega a(u, \nabla u, \lambda) \cdot \nabla v + f(u, \nabla u, \lambda) v \, dx \, dy - \int_{\partial\Omega_1} g_1(u, \lambda) v \, ds. \tag{1.4}$$

In some problems solved by *PLTMG*, a functional $\rho(u, \lambda)$ plays an important role. Functionals we consider are of the form

$$\rho(u,\lambda) = \int_\Omega p_1(x, y, u, \nabla u, \lambda)\, dx\, dy + \int_\Gamma p_2(x, y, u, \nabla u, \lambda)\, ds, \tag{1.5}$$

where p_1 and p_2 are scalar functions. Here $\Gamma = \partial\Omega \cup \Gamma_0$, where Γ_0 consists of certain internal curves specified by the user.

This version of the *PLTMG* package addresses five major problem classes. These are briefly described below.

1.1.1 Approximation Spaces.

PLTMG is based on a family of conforming C^0 finite element spaces. Let $\mathcal{T}$ denote a triangulation of Ω and let $\mathcal{M}$ be the space of C^0 piecewise polynomials associated with $\mathcal{T}$. In this version of *PLTMG*, the degree of the polynomial can vary element by element. The maximum degree allowed at present is $p = 9$, a condition imposed by the availability of suitable quadrature formulas.[1] *PLTMG* represents such a piecewise polynomial using the standard Lagrange nodal basis; a function can then be specified by giving its values at the principle lattice points of the element, as illustrated in Figure 1.1 for the cases $1 \le p \le 3$.

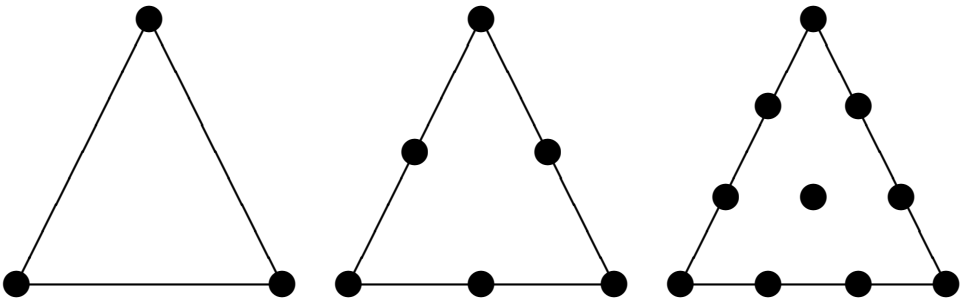

Figure 1.1. *Nodal degrees of freedom for the continuous piecewise linear element, $p = 1$ (left), the continuous piecewise quadratic element, $p = 2$ (middle), and the continuous piecewise cubic element, $p = 3$ (right).*

When two elements of different degrees share a common edge, the element of lower degree becomes a *transition element*. If such a element is of degree p, sharing an edge with an element of degree $q > p$, the element contains all polynomials of degree p plus some additional polynomials of degree q, which allow the overall finite element space to remain conforming. In particular, along the shared edge, the degrees of freedom correspond to those of the higher degree element. Some examples are given in Figure 1.2. Finally, *PLTMG* allows the use of isoparametric versions

[1] *PLTMG* uses quadrature formulas given in Zhang, Cui, and Liu [64].

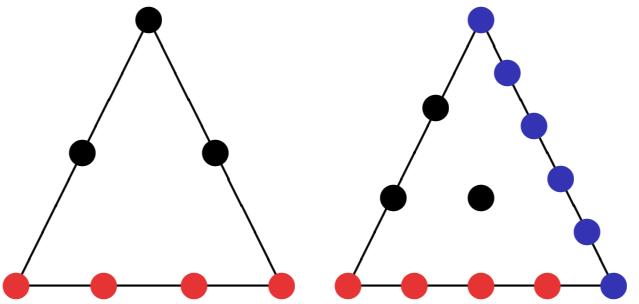

Figure 1.2. *Nodal degrees of freedom for the a quadratic transition element with a cubic edge (left), and a cubic transition element with one edge of degree four and one edge of degree five (right).*

of this family of Lagrange elements to address problems with curved boundaries or interfaces.

1.1.2 Elliptic Boundary Value Problem.

For this problem, *PLTMG* solves a discrete analog of (1.3). The parameter λ does not play a role in this problem. Let $\mathcal{I} : \mathcal{H}^1(\Omega) \to \mathcal{M}$ denote continuous piecewise polynomial interpolation operator that interpolates at the degrees of freedom of $\mathcal{T}$. Then

$$\begin{aligned}\mathcal{M}_p &= \{\phi \in \mathcal{M} \,|\, \phi \text{ is continuous on } \partial\Omega_0\},\\ \mathcal{M}_g &= \{\phi \in \mathcal{M}_p \,|\, \phi = \mathcal{I}(g_2) \text{ on } \partial\Omega_2\},\\ \mathcal{M}_e &= \{\phi \in \mathcal{M}_p \,|\, \phi = 0 \text{ on } \partial\Omega_2\}.\end{aligned}$$

The discrete equations solved by *PLTMG* are formulated as follows: find $u_h \in \mathcal{M}_d$ such that

$$a(u_h, v) = 0 \qquad \text{for all } v \in \mathcal{M}_e. \tag{1.6}$$

1.1.3 Obstacle Problem.

The second class of problems addressed by *PLTMG* are the subset of variational inequalities known as obstacle problems. Let

$$\mathcal{K} = \{\phi \in \mathcal{H}^1_g \,|\, \underline{u} \le \phi \le \overline{u}\}.$$

The obstacle problem is formulated as

$$\min_{u \in \mathcal{K}} \rho(u) \tag{1.7}$$

where ρ is a functional of the form (1.5). The parameter λ is not used in this problem. Implicit in our formulation of this problem is an assumption that the

Frechet derivative of ρ corresponds to an elliptic boundary problem of the form (1.3). We also assume that the bound constraints are consistent with the boundary conditions.

The discrete form of this problem is as follows. Let

$$\mathcal{K}_h = \{\phi \in \mathcal{M}_g \,|\, \mathcal{I}(\underline{u}) \le \phi \le \mathcal{I}(\overline{u})\}.$$

We then seek $u_h \in \mathcal{K}_h$ that satisfies

$$\min_{u_h \in \mathcal{K}_h} \rho(u_h) \tag{1.8}$$

1.1.4 Continuation Problem.

Continuation problems addressed by *PLTMG* are all of the form (1.3), where the parameter $\lambda \in \mathcal{R}$. Continuation problems also require a functional ρ as in (1.5). Solutions of (1.3)–(1.5) in general define a family of curves on the (λ, ρ) plane. Typical curves are shown in Figure 1.3.

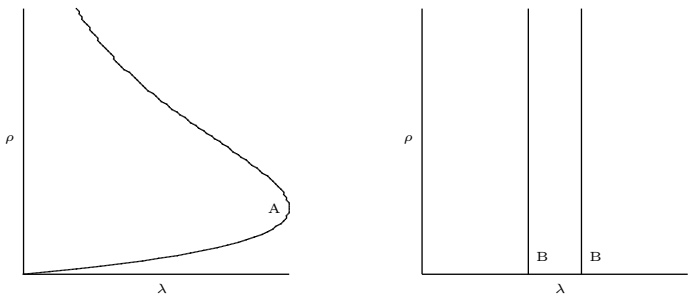

Figure 1.3. *Continuation curves* $\rho = \rho(\lambda)$.

The singular point labeled "A" in the figure on the left is a limit (turning) point, and those labeled "B" in the figure on the right are bifurcation points (this figure corresponds to the special case of a linear eigenvalue problem). The purpose of the continuation process is to compute solutions (u, λ) corresponding to points on these curves.

PLTMG provides a suite of options for solving continuation problems. Among them are options for following a solution curve to a target value in λ or ρ, locating limit and bifurcation points, and switching branches at bifurcation points. Because some problems might have more than one parameter of interest, *PLTMG* also has options for switching parameters and functionals (changing the definitions of λ and ρ) during the calculation, as a means of exploring higher dimensional spaces.

1.1.5 Parameter Identification Problem.

In this problem, a partial differential equation of the form (1.3) appears as a constraint in an optimization problem. Here we seek $\lambda \in \mathcal{R}^k$, $1 \le k \le 10$, and $u \in \mathcal{H}_g$

that satisfy

$$\min \rho(u, \lambda) \tag{1.9}$$

subject to the constraint (1.3) and the simple bounds

$$\underline{\lambda}_j \leq \lambda_j \leq \overline{\lambda}_j, \tag{1.10}$$

for $1 \leq j \leq k$. In addition to appearing within the coefficients of the partial differential equation and the boundary conditions, parameters λ_j can be used to describe the shape of the boundary of Ω or some internal interface. This allows the solution of problems where certain geometric properties of Ω are to be optimized.

We define the Lagrangian

$$L(u, v, \lambda) = \rho(u, \lambda) + a(u, v), \tag{1.11}$$

where $v \in \mathcal{H}_e$ is a Lagrange multiplier. We can solve the optimization problem by seeking stationary points of $L(u, v, \lambda)$ constrained by the simple bounds (1.10).

In the discretized problem, we seek $u_h \in \mathcal{M}_g$, a discrete Lagrange multiplier $v_h \in \mathcal{M}_e$, and $\lambda_h \in \mathcal{R}^k$ that correspond to a stationary point of $L(u_h, v_h, \lambda_h)$, constrained by the simple bounds

$$\underline{\lambda}_j \leq \lambda_{h,j} \leq \overline{\lambda}_j, \tag{1.12}$$

for $1 \leq j \leq k$.

1.1.6 Optimal Control Problem.

This problem is very similar to the parameter identification problem, except now $\lambda \in \mathcal{H}^1(\Omega)$ (or perhaps some weaker space where pointwise values of (1.14) below are defined). Thus we seek $u \in \mathcal{H}_g$ and $\lambda \in \mathcal{H}^1(\Omega)$ that satisfy

$$\min \rho(u, \lambda) \tag{1.13}$$

subject to the constraint (1.3) and the simple bounds

$$\underline{\lambda}(x, y) \leq \lambda \leq \overline{\lambda}(x, y) \tag{1.14}$$

for $(x, y) \in \Omega$. As before, we define the Lagrangian

$$L(u, v, \lambda) = \rho(u, \lambda) + a(u, v), \tag{1.15}$$

where $v \in \mathcal{H}_e$ is a Lagrange multiplier. We seek stationary points of $L(u, v, \lambda)$ constrained by the simple bounds (1.14).

In the discretized problem, we seek $u_h \in \mathcal{M}_g$, a discrete Lagrange multiplier $v_h \in \mathcal{M}_e$, and $\lambda_h \in \mathcal{M}$ that correspond to a stationary point of $L(u_h, v_h, \lambda_h)$. constrained by the simple bounds

$$\mathcal{I}(\underline{\lambda}) \leq \lambda_h \leq \mathcal{I}(\overline{\lambda}). \tag{1.16}$$

Inequalities (1.16) are imposed only at the nodes of each element in the mesh.

1.2 Main Subroutines

The software package consists of five primary subroutines. These main routines and their functions are summarized in Table 1.1. The package uses two basic data structures to specify the domain Ω: the triangulation and the skeleton. Loosely speaking, a triangulation specifies the domain Ω as the union of triangles. A skeleton specifies the domain as the union of one or more subdomains and requires only a description of the boundary of each subdomain. The user can specify the domain as either a triangulation or a skeleton. Specifying a triangulation generally requires less data only for simple domains that can be triangulated with very few triangles. If the domain has a complicated geometry or has internal interfaces that the user would like the triangulation to respect, then it is usually easier to specify the domain as a skeleton. Both data structures are documented in Chapter 2.

Subroutine	Main Function
TRIGEN	Mesh generation and modification
PLTMG	Solve partial differential equation
TRIPLT	Display solution or related function
INPLT	Display input data
GPHPLT	Display performance statistics

Table 1.1. *The main subroutines in the package.*

Subroutine *TRIGEN* is mainly concerned with transforming the data structures defining the domain. *TRIGEN* also provides a posteriori error estimates for the solution in the $\mathcal{H}^1(\Omega)$ and $\mathcal{L}_2(\Omega)$ norms. *TRIGEN* provides options for creating a triangulation from a skeleton, and adaptively modifying the triangulation data structure. Options for h, p and hp adaptive refinement and coarsening, as well as mesh moving (r adaptivity) are provided. *TRIGEN* also provides options for various tasks related to parallel processing, namely partitioning the mesh, broadcasting a given mesh to all processors, and reconciling a fine mesh distributed among several processors. *TRIGEN* is documented in Chapter 3.

Subroutine *PLTMG* uses finite element discretizations based on family of nodal C^0 piecewise polynomial spaces described above, and includes algorithms to address each of the five problem classes. In the case of parallel processing, *PLTMG* includes a domain decomposition solver for each problem class. *PLTMG* is described in detail in Chapter 4.

Subroutine *TRIPLT* provides graphical displays of the solution and other grid functions. Three-dimensional color surface/contour plots with shading and an arbitrary viewing perspective are available. Subroutine *INPLT* provides a graphical display of the mesh data (triangulation or skeleton) defining Ω. Subroutine *GPHPLT* provides a variety of graphical displays of convergence histories, statistical data, and other interesting output from *PLTMG*. These routines are described in detail in Chapter 5.

An elementary interactive test driver, *ATEST*, is described in Chapter 6. *AT-*

EST provides options for calling each of the main routines, as well as other useful functions such as writing and reading data files, resetting parameters, and executing problem specific subroutines provided by the user. Several short machine dependent routines are required for timing, graphics, and specifying the precision of the floating point number system. These are also described in Chapter 6. In Chapter 7, the example problem data sets included with the source code are briefly described.

PLTMG was originally conceived as a prototype program to study the theoretical and practical aspects of the multigrid iterative method, adaptive grid refinement and error estimation procedures, and their interaction. As such, *PLTMG* was designed to (formally) handle a wide class of elliptic operators and reasonably general domains. The boundary of the problem class has expanded as problems were encountered that required its enlargement to be solved. The problem class addressed by this version of *PLTMG* should not be interpreted as the limit of the class of problems that could be successfully solved by the techniques embodied by this package. Conversely, one should not assume that every problem (formally) within this class can be solved using the existing code.

As with other versions of the package, time efficiency is a secondary consideration to robustness, versatility, and ease of maintenance. While *PLTMG* is probably not the fastest code that could be used for any particular problem, we believe that it will deliver reasonable execution times in most environments.

1.3 Installation.

This version of *PLTMG* is provided as a single version that can be compiled in either single or double precision, depending on the machine dependent module *MTHDEF*. *MTHDEF* and other machine dependent routines are documented in detail in Section 6.12. The majority of the code is machine independent and written to the specifications of Fortran 90. In particular, it will no longer compile using Fortran 77. Several parts of the package are written to the specifications of ANSI C. The source code is contained in several files as indicated in Table 1.2. The X-Windows interface is based on the Motif widget set and can be used only on systems which support X-Windows. Certain X-Windows libraries must be loaded along with the *PLTMG* software. The OpenGL graphics program *SG* of Michael Holst has been integrated as one of several available graphics devices. *SG* is available elsewhere, and its *MALOC* library must be loaded along with the *PLTMG* software. Finally, the parallel processing options in *PLTMG* are based on MPI, and the MPI library must also be loaded in order to resolve all external names.

In MPI is not available or not desired, one can substitute the supplied *stub* interface routines. The stub routines are a set of MPI interface routines with all calls to MPI library functions and subroutines deleted. By using the stub routines in place of the regular interface, one can create an executable with no unresolved external references without loading the MPI library. In this case, however, all the parallel options of *PLTMG* are disabled.

In a similar fashion, if *SG* is not available or not desired, one can use the stub routines in place of standard interface routines. If the stub routines are used, the

File	Contents
mg0.f	sets floating point precision
pltmg.f	most source code
mgmpi.f (mgmpi_stubs.f)	MPI interface
mgvio.f (mgvio_stubs.f)	SG interface
xgui.c (xgui_stubs.c)	X-Windows interface
mgxdr.c	XDR interface
atest.f	test driver program
battery.f, box.f, burger.f, circle.f, control.f domains.f, ident.f, jcn.f, message.f mnsurf.f, naca.f, ob.f, square.f, usmap.f	test problem data sets

Table 1.2. *Files in the basic distribution.*

MALOC library is not needed, but the *SG* OpenGL and BH file graphics devices are disabled. Finally, if the X-Windows libraries are not available, one can replace the X-Windows interface with stub routines. In this case, the graphical user interface and the corresponding X-Windows graphics devices are all disabled, but the X-Windows libraries are not needed.

Chapter 2
Data Structures

2.1 Overview.

In this chapter, we define the data structures used in the *PLTMG* package. There are two basic data structures that define the domain Ω: the *skeleton* and the *triangulation*. Basic to both data structures is the concept of an *edge*. The various subregions that define a skeleton are described by a sequence of edges that traverse its boundary in a counter clockwise fashion. In the case of a triangulation, edges on the boundary $\partial\Omega$ need to be explicitly defined in order to assign boundary conditions. Additional internal edges can be defined if they have some attribute of interest; e.g., they are curved. Other internal edges are defined implicitly by the definitions of the triangles that comprise the triangulation. In the case of parallel processing, *PLTMG* explicitly defines edge data structures for all edges lying on the internal interface system generated by the partitioning of Ω among the processors. The edge related data structures are defined in Section 2.2. The triangulation and skeleton are defined in Sections 2.3 and 2.4, respectively.

The next few sections define several internal data structures used by *PLTMG*. The user is never asked to provide data for these structures; they are all computed internally by various routines in the package. However, their contents may still be of interest to the user. Data structures that track degrees of freedom associated with individual elements, as well as the solution and other finite element functions, are described in Section 2.5. The *IPATH* data structure describes relationships between the subdomains associated with different processors in a parallel adaptive calculation. It is described in Section 2.6.

The arrays *IP*, *RP*, and *SP* contain many scalar parameters, switches, control variables, flags, and pointers, some that must be specified by the user and others that are internally computed but may be of interest to the user. These are described in Section 2.7. Finally, the coefficient functions defining the differential operator and functional ρ in (1.1)–(1.3), and the optional function *QXY* used by *TRIGEN* and *TRIPLT*, are described in Section 2.8.

2.2 Edge Definitions

In this section, we define geometry data structures common to both the triangulation and the skeleton. In both cases, the domain is described by a list of vertices v_i, $1 \le i \le NVF$, and edges b_i, $1 \le i \le NBF$. In the case of of a triangulation, the v_i enumerate all vertices of all triangles that comprise the triangulation. In the case of a skeleton, the v_i enumerate the vertices of all regions that comprise the skeleton. In both cases, the (x, y) coordinates of the vertices are given in the arrays *VX* and *VY*. In particular,

$$v_I = (x_I, y_I) = (VX(I), VY(I)), \qquad 1 \le I \le NVF.$$

Edges are defined in terms of the integer array *IBNDRY* of size $7 \times NBF$ and the real array *SF* of size $2 \times NBF$. The latter is used only for curved edges. Curved edges can be most easily be defined by circular arcs (as in early versions of *PLTMG*) or parametrically through the function *SXY* provided by the user. The definitions of *IBNDRY* is given in Table 2.1.

Column I of the *IBNDRY* array contains information about edge b_I. The first two entries a pointers to the *VX* and *VY* arrays and denote the two vertices that form the endpoints of the edge. The third entry is used to indicate if the edge is curved, and is described more fully below.

Entry *IBNDRY(4,I)* describes the type of boundary conditions to be applied, or if the edge is internal to Ω. A fourth type of edge is a linked edge. Linked edges occur only in pairs. If b_I and b_J are a pair of linked edges, then *IBNDRY(4,I)* $= -J$ and *IBNDRY(4,J)* $= -I$. Linked edges b_I and b_J must be geometrically congruent. That is, b_I must be mapped to b_J using a translation and orthogonal rotation. Continuity of the solution u_h and weak continuity of $a \cdot n$ is imposed on linked edge pairs. Thus if b_I and b_J are boundary edges, this is equivalent to imposing periodic boundary conditions. In the course of parallel processing, *PLTMG* creates edges of types $3-5$. Entries *IBNDRY(5,I)* and *IBNDRY(6,I)* are used internally by *PLTMG* for parallel processing.

Entry *IBNDRY(7,I)* contains an integer label for the edge; this user defined label can be used to uniquely identify a particular edge, or to associate some property with the edge.

2.2.1 Curved Edges – Circular Arcs

If a triangle has a curved edge, it can be specified as a circular arc or given a parametric definition. In the case of a circular arc, one should set *IBNDRY(3,I)* $= 1$. The arc passes through the edge endpoints specified in *IBNDRY(1,I)* and *IBNDRY(2,I)* and its center (x_c, y_c) is specified in the array *SF* as

$$(x_c, y_c) = (SF(1,I), SF(2,I)).$$

Because there are generally two such arcs for every pair of endpoints, the shorter arc is taken to be the correct edge; therefore, one must specify arcs that subtend (strictly) less than π of arc; $\pi/4$ is a reasonable upper bound.

array entry	definition
IBNDRY(1,I)	first endpoint number
IBNDRY(2,I)	second endpoint number
IBNDRY(3,I)	curved edge switch
IBNDRY(4,I)	edge type
IBNDRY(5,I)	reserved for parallel processing
IBNDRY(6,I)	reserved for parallel processing
IBNDRY(7,I)	edge label

IBNDRY definition.

IBNDRY(3,I)	edge type
0	Straight edge
1	Curved edge – circular arc
$-K$	Curved edge – parametric

Curved edge types.

IBNDRY(4,I)	curved edge type
2	Dirichlet boundary
1	natural boundary
0	internal
$-K$	linked with edge K
3, 4, 5	reserved for parallel processing

Edge type definitions.

Table 2.1. *Boundary definitions and data structures.*

To simplify data entry, we provide the routine *CENTRE* for computing the center of a circle given three points on its boundary. *CENTRE* is called using the statement

Call CENTRE(X1, Y1, X2, Y2, X3, Y3, XC, YC)

Here *(X1,Y1)* and *(X2,Y2)* are the endpoints of an arc of the circle, and *(X3,Y3)* is a third point on the arc (e.g., the midpoint). *CENTRE* returns the center of the circle in *(XC,YC)*.

2.2.2 Curved Edges – Parametric

A second way to specify a curved edge is through a parametric representation. Since there may be several parametric curves, they are indexed by the user. In particular,

if *IBNDRY(3,I)* $= -K$, then the parametric function (q_K, r_K) is used to define the edge, where

$$\begin{pmatrix} x(s) \\ y(s) \end{pmatrix} = \begin{pmatrix} q_K(s) \\ r_K(s) \end{pmatrix}, \qquad s_1 \le s \le s_2.$$

The point $s = s_1$ corresponds to the first endpoint and $s = s_2$ corresponds to the second. In this case, the values in column I of the array *SF* are given by

$$(s_1, s_2) = (SF(1,I), SF(2,I)).$$

The parameterization itself is defined by the user in routine *SXY*. Subroutines *SXY*, has calling sequence

Call SXY(RL, S, ITAG, VALUES)

Here $RL = \lambda$ is an input array of size *NRL* giving the current value of the parameters λ. $1 \le NRL \le 10$ for parameter identification problems, while $NRL = 1$ for the other classes of problems. The parameter $s_1 \le S \le s_2$ is input specifying the point where $(q_K(S), r_K(S))$ is required. $ITAG = K$, where K is the input index of the functional, originally provided by the the user as *BNDRY(3,I)* $= -K$.

The output is provided in the array *VALUES*, a two dimensional array with 2 rows and $NRL + 2$ columns. To simplify this process, *PLTMG* supplies a labeled common block

common /VAL4/ J0, JS, JL

containing a predefined list of integer pointers mapping function and derivative values to particular entries in the *VALUES* array. The details of this mapping are given in Table 2.2.

pointer	index	$VALUES(1,\cdot)$	$VALUES(2,\cdot)$
$J0 = 1$	$J0$	q_K	r_K
$JS = 2$	JS	$q_{K,s}$	$r_{K,s}$
$JL = 3$	$JL + J - 1$	q_{K,λ_J}	r_{K,λ_J}
	$1 \le J \le NRL$		

Table 2.2. *VALUES array for subroutine SXY.*

It is important to emphasize that the parameterization is assumed to roughly correspond to arc length along the curved edge. For example, when the edge is bisected, the "midpoint" (x_m, y_m) is computed from

$$\begin{pmatrix} x_m \\ y_m \end{pmatrix} = \begin{pmatrix} q_K((s_1 + s_2)/2) \\ r_K((s_1 + s_2)/2) \end{pmatrix}.$$

Nodes for isoparametric basis functions are computed using a similar formula. The

quality of such calculations is thus dependent on these user defined parameterizations.

2.3 The Triangulation.

In this section, we define the triangulation data structure. Let $\mathcal{T}$ denote the triangulation consisting of triangles t_i, $1 \le i \le NTF$, vertices v_i, $1 \le i \le NVF$, and edges b_i, $1 \le i \le NBF$. Triangles may have curved edges, as described in Section 2.2. Curved edges may be on the boundary or in the interior of the region Ω. The *ITNODE* data structure is a $5 \times NTF$ integer array that defines triangles that comprise $\mathcal{T}$. The details of this data structure are given in Table 2.3.

array entry	definition
ITNODE(1,I)	first vertex number
ITNODE(2,I)	second vertex number
ITNODE(3,I)	third vertex number
ITNODE(4,I)	reserved for parallel processing
ITNODE(5,I)	element label

Table 2.3. *ITNODE definition for a triangulation.*

A given triangle $t_I \in \mathcal{T}$ is specified by giving an accounting of its three vertices and by specifying an integer label or tag. The Ith column of the *ITNODE* array contains information about t_I. The first three entries of *ITNODE* contain the three vertex numbers of triangle t_I. *ITNODE(J,I)* $= K$, for $1 \le J \le 3$, means *(VX(K),VY(K))* is the Jth vertex of t_I. The ordering of the vertices of a given triangle is arbitrary and independent of the other triangles.[2] Entry *ITNODE(4,I)* is used internally by *PLTMG* in parallel processing, denoting the processor that "owns" t_I; one can simply initialize *ITNODE(4,I)* $= 0$. Entry *ITNODE(5,I)* contains any user provided label for t_I. Such labels are provided strictly for the convenience of the user and can be used to identify differing regions or material properties associated with the element.

For example, consider the circle of radius one with a crack along the positive x-axis. This domain can be triangulated using $NTF = 8$ triangles, $NVF = 10$ vertices, and $NBF = 10$ boundary edges, 8 of which are curved, as illustrated in Figure 2.1. Vertices v_2 and v_{10} have the same (x, y) coordinates, but v_2 is "above" the crack and v_{10} is "below." Similarly, edge b_1 is the top of the crack, while edge b_{10} is the bottom. The ordering of vertices, triangles, and edges is arbitrary. In this example, we will define the curved edges using the parameterization

$$\begin{pmatrix} x \\ y \end{pmatrix} = \begin{pmatrix} q_1(s) \\ r_1(s) \end{pmatrix} = \begin{pmatrix} \cos(s) \\ \sin(s) \end{pmatrix}.$$

[2] *PLTMG* reorders vertices as necessary to ensure a counterclockwise orientation for elements.

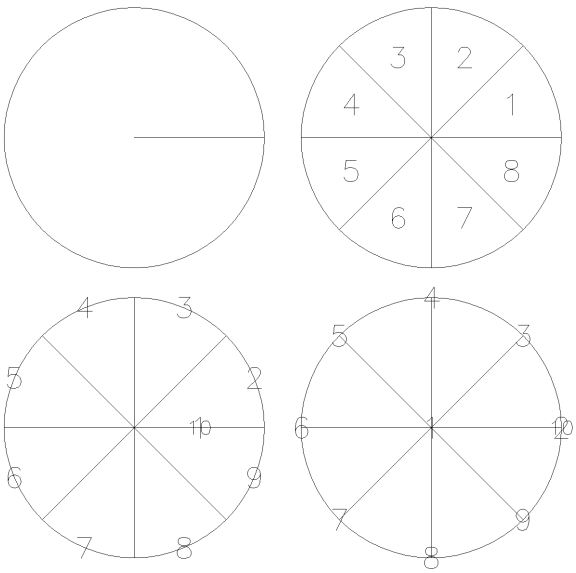

Figure 2.1. *Clockwise, from upper left: example domain; triangle numbers; vertex numbers; edge numbers.*

The data for our example is shown in Table 2.4. In this example, we have chose to label the triangles in *ITNODE(5,I)* by the quadrant in the Euclidean plane in which they lie. In our example, we impose Dirichlet boundary conditions on the outer boundary of the circle, and also along the top of the crack, and Neumann boundary conditions on the bottom of the crack. The outer boundary of the circle is labeled 0, the top of the crack 2, and the bottom of the crack 1.

Several routines in the package check triangulation data structures for common errors in the data. If found, such errors are reported by setting the parameter *IFLAG* as described in Table 2.9.

2.4 The Skeleton.

The skeleton data structure is often the easiest data structure for the user to specify by hand, especially if the domain has complicated geometry, symmetry, or internal interfaces. In the skeleton data structure, the domain Ω is viewed as the union of NTF simply connected subregions Ω_i, $1 \le i \le NTF$. The regions need not be convex, and the case $NTF = 1$ is not excluded. A shared boundary between two subregions (an internal interface) will be respected by the triangulation process in *TRIGEN*; that is, the interface will be represented as one or more triangle edges in the triangulation.

The boundary of each Ω_i should be a simple closed curve that does not intersect itself. Thus, for example, if Ω has a hole, adding a single cut between the outer boundary and the hole will not be adequate. At least two subregions will be

I	1	2	3	4	5	6	7	8	9	10
$VX(I)$	0	1	$1/\sqrt{2}$	0	$-1/\sqrt{2}$	-1	$-1/\sqrt{2}$	0	$1/\sqrt{2}$	1
$VY(I)$	0	0	$1/\sqrt{2}$	1	$1/\sqrt{2}$	0	$-1/\sqrt{2}$	-1	$-1/\sqrt{2}$	0

The VX and VY arrays. $NVF = 10$.

I	1	2	3	4	5	6	7	8	9	10
$IBNDRY(1,I)$	1	2	3	4	5	6	7	8	9	10
$IBNDRY(2,I)$	2	3	4	5	6	7	8	9	10	1
$IBNDRY(3,I)$	0	-1	-1	-1	-1	-1	-1	-1	-1	0
$IBNDRY(4,I)$	2	2	2	2	2	2	2	2	2	1
$IBNDRY(5,I)$	0	0	0	0	0	0	0	0	0	0
$IBNDRY(6,I)$	0	0	0	0	0	0	0	0	0	0
$IBNDRY(7,I)$	2	0	0	0	0	0	0	0	0	1
$SF(1,I)$	–	0	$\pi/4$	$\pi/2$	$3\pi/4$	π	$5\pi/4$	$3\pi/2$	$7\pi/4$	–
$SF(2,I)$	–	$\pi/4$	$\pi/2$	$3\pi/4$	π	$5\pi/4$	$3\pi/2$	$7\pi/4$	2π	–

The IBNDRY and SF arrays. $NBF = 10$.

I	1	2	3	4	5	6	7	8
$ITNODE(1,I)$	1	1	1	1	1	1	1	1
$ITNODE(2,I)$	2	3	4	5	6	7	8	9
$ITNODE(3,I)$	3	4	5	6	7	8	9	10
$ITNODE(4,I)$	0	0	0	0	0	0	0	0
$ITNODE(5,I)$	1	1	2	2	3	3	4	4

The ITNODE array. $NTF = 8$.

Table 2.4. *Data structures for a triangulation.*

required in this case.

Having decomposed the domain into NTF subregions, we decompose the boundaries of the subregions into NBF edges b_i, $1 \le i \le NBF$. Each edge has two endpoints ν_i^j, $1 \le j \le 2$, and if it is a curved edge, it will have a circle center or some parameterization. Globally, the vertices are labeled v_k, $1 \le k \le NVF$, and curved edges are indicated as described in Section 2.2. The intersection of any two edges should be at most one common endpoint.

As an example, we consider the square region with a hole illustrated in Figure 2.2. In this example, we decompose the region into 2 subregions ($NTF = 2$), using 10 vertices ($NVF = 10$), and 12 edges ($NBF = 12$) as shown.

Global numbering of the subregions, edges, and vertices is arbitrary. These arrays for our example domain are shown in Table 2.6. Edges are specified in $IBNDRY$ as in the case of the triangulation. Descendants of Dirichlet, natural, and

array entry	definition
ITNODE(1,I)	first vertex number
ITNODE(2,I)	first edge number
ITNODE(3,I)	congruent region number
ITNODE(4,I)	reserved for parallel processing
ITNODE(5,I)	region label

Table 2.5. *ITNODE definition for a skeleton.*

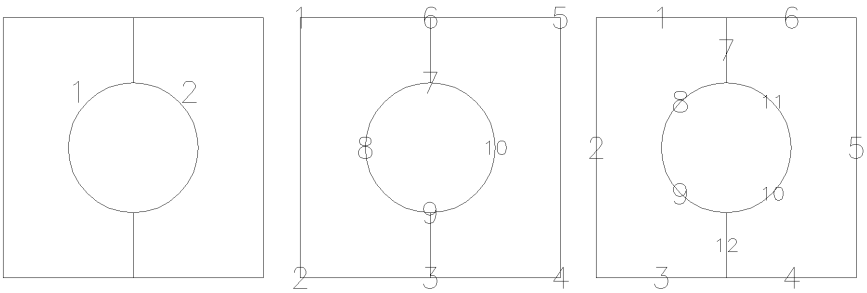

Figure 2.2. *Example domain decomposed into two subregions (left); vertex numbers (middle); edge numbers (right).*

linked edges are included in the output *IBNDRY* array when Ω is triangulated using *TRIGEN*. Descendants of internal edges are retained only if they separate regions with different labels. Descendant edges inherit the label of the original edge. In our example, we will assign Dirichlet boundary conditions to the left and right sides and the bottom of the domain, and natural boundary conditions elsewhere. The four curved edges are defined by circular arcs of a circle with its center at the origin. The *IBNDRY* and *SF* arrays then have the form given in Table 2.6.

A subregion Ω_i, $1 \le i \le NTF$, is defined by an ordered sequence of edges (at least three) that form its boundary. The sequence is ordered such that the boundary of Ω_i is traversed in a counterclockwise direction (thus providing notions of "inside" and "outside"). Each edge in the sequence shares exactly one endpoint with the edge that precedes it and the edge that follows it in the sequence; the first and last edges in the sequence also share one endpoint. A particular edge can appear only once in the sequence.

The array *ITNODE* is used to define the subregions. Column I of *ITNODE* corresponds to the region Ω_I. Entry *ITNODE(1,I)* is a global vertex number for one of the vertices on the boundary of Ω_I. Unless *ITNODE(3,I)* $\neq 0$ (see below) the choice of vertex is arbitrary. The second entry, *ITNODE(2,I)*, is the global edge number of the first edge in a counterclockwise traversal of Ω_I, beginning at vertex v_K, where *ITNODE(1,I)* $= K$.

Entry *ITNODE(3,I)* is used to specify certain symmetries the user may wish to

I	1	2	3	4	5	6	7	8	9	10
VX(I)	-2	-2	0	2	2	0	0	-1	0	1
VY(I)	2	-2	-2	-2	2	2	1	0	-1	0

The VX and VY arrays. NVF = 10.

I	1	2	3	4	5	6	7	8	9	10	11	12
IBNDRY(1,I)	6	1	2	3	4	5	6	7	8	9	7	9
IBNDRY(2,I)	1	2	3	4	5	6	7	8	9	10	10	3
IBNDRY(3,I)	0	0	0	0	0	0	0	1	1	1	1	0
IBNDRY(4,I)	1	2	2	2	2	1	0	1	1	1	1	0
IBNDRY(5,I)	0	0	0	0	0	0	0	0	0	0	0	0
IBNDRY(6,I)	0	0	0	0	0	0	0	0	0	0	0	0
IBNDRY(7,I)	2	1	3	3	1	2	0	4	4	4	4	0
SF(1,I)	–	–	–	–	–	–	–	0	0	0	0	–
SF(2,I)	–	–	–	–	–	–	–	0	0	0	0	–

The IBNDRY and SF arrays. NBF = 12.

I	1	2
ITNODE(1,I)	1	4
ITNODE(2,I)	2	5
ITNODE(3,I)	0	1
ITNODE(4,I)	0	0
ITNODE(5,I)	1	2

I	1	2
ITNODE(1,I)	1	5
ITNODE(2,I)	2	6
ITNODE(3,I)	0	-1
ITNODE(4,I)	0	0
ITNODE(5,I)	1	2

The ITNODE array for mapping by rotation (left) and by reflection (right). $NTF = 2$.

Table 2.6. *Skeleton data structures.*

impose on the triangulation. Two subregions are congruent if one can be mapped onto the other using an affine transformation consisting of a translation, an orthogonal rotation, and perhaps a simple reflection. If this mapping also induces one-to-one correspondences between the edges and vertices used to define the regions, then the user can specify that the two regions be triangulated in a similar fashion.

ITNODE(3,I) $= 0$ specifies that Ω_I can be triangulated independently of other regions. *ITNODE(3,I)* $= J$, $0 < J < I$, specifies that Ω_I can be mapped onto Ω_J using just a translation and rotation. *ITNODE(3,I)* $= -J$, $0 < J < I$, specifies that Ω_I can be mapped onto Ω_J using a translation, rotation, and a reflection. If *ITNODE(3,I)* $= \pm J$, then *ITNODE(1,I)* must correspond to the vertex on $\partial\Omega_I$ which is mapped to the vertex corresponding to *ITNODE(1,J)* on $\partial\Omega_J$. If

ITNODE(3,I) $\neq 0$, *TRIGEN* will map the triangulation generated for Ω_J onto Ω_I, ensuring the desired symmetry properties of the overall triangulation. Note that this is not a symmetric relation; *ITNODE(3,I)* $= J$ does not mean *ITNODE(3,J)* $= I$. In particular, if $|$ *ITNODE(3,I)* $| \geq I$, *TRIGEN* will return in an error condition.

In our example, Ω_2 can be mapped onto Ω_1 by either rotation or reflection. We can ensure the triangulation for Ω_2 will be similar to that for Ω_1, either under rotation or reflection. The resulting triangulations may be different in the two cases.[3] *ITNODE* arrays for the two situations are illustrated in Table 2.6. Entry *ITNODE(4,I)* is used by *PLTMG* in parallel processing. Entry *ITNODE(5,I)* is a label for the region; all the triangles created in Ω_I inherit this label.

We provide the utility subroutine *SKLUTL* to aid in the creation of the skeleton data structures. Subroutine *SKLUTL* is called using the statement

Call SKLUTL(ISW, VX, VY, SF, ITNODE, IBNDRY, IP,
RP, IFLAG, SXY)

This routine takes as input a skeleton data structure defined *VX*, *VY*, *SF*, *IBNDRY*, (except when *ISW* $= 0$) *ITNODE*, and the routine *SXY*, called if curved edges are defined by a parameterization. The integers *NTF*, *NBF*, and (except when *ISW* $= 0$) *NTF* should be specified in the *IP* array, and $\lambda =$ *RL* should be specified in *RP* if *SXY* is to be called. The integer *ISW* specifies the task, as indicated in Table 2.7.

ISW	task
0	create *ITNODE* array
1	refine long circular arcs
2	determine congruent regions

Table 2.7. *The values of ISW.*

If *ISW* $= 0$, *SKLUTL* computes all entries of the *ITNODE* array, given the remaining arrays in the skeleton data structure (*VX*, *VY*, *SF*, and *IBNDRY*), and the parameters *NVF*, and *NBF* in the *IP* array. The value of *NTF* is returned in the *IP* array. The regions are labeled with *ITNODE(5,I)* $= I$ for $1 \leq I \leq$ *NTF*, although these labels can subsequently be reset by the user. Also *ITNODE(3,I)* $= 0$ for $1 \leq I \leq$ *NTF*. If *ISW* $= 1$, *SKLUTL* accepts as input a complete skeleton description, and divides curved edges defined as circular arcs as necessary to ensure that all such edges subtend less than $\pi/4$ of arc. New edges and vertices are added as necessary, and the relevant skeleton parameters updated. New values of *NBF* and *NVF* are returned in the *IP* array. If *ISW* $= 2$, *SKLUTL* accepts as input a complete skeleton description, and finds congruent regions. The values of *ITNODE(3,I)* (and possibly *ITNODE(1,I)* and *ITNODE(2,I)*) are reset as necessary. If two regions are

[3] We could ensure greater symmetry in the triangulation by decomposing Ω into 4 or 8 congruent regions instead of 2 and then setting *ITNODE(3,I)* appropriately.

congruent but the congruence is not unique, as in our example, an arbitrary choice is made from among the possibilities. Errors are returned in the integer *IFLAG* as described in Table 2.9.

Several other routines in the package check skeleton data structures for common errors in the data. If found, such errors are reported by setting the parameter *IFLAG* as described in Table 2.9.

2.5 Finite Element Data Structures.

Several data structures in *PLTMG* define and maintain the finite element functions associated with a particular problem. In particular, the $8 \times NTF$ integer array *ITDOF* contains information about polynomial spaces on each element, the real array *GF* contains the numerical values of the solution and other finite element functions, and the real array E contains information about the a posteriori error estimates in each element. These data structures are not defined or initialized by the user, but it may be of interest for a user to understand their contents.

PLTMG uses local notation to define certain quantities related to a given element in the mesh. See Figure 2.3. For example, each element locally has vertices labeled ν_k, $1 \le k \le 3$. From this viewpoint, the *ITNODE* array contains a mapping for these locally defined vertices to globally defined vertices, with ν_K corresponding to $ITNODE(K, \cdot)$ for $1 \le K \le 3$. Edges are locally labeled as in Figure 2.3, with edge ϵ_k opposite vertex ν_k, $1 \le k \le 3$.

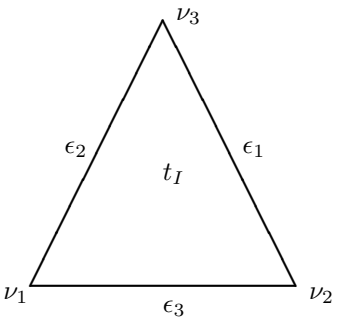

Figure 2.3. *Local notation for element t_I.*

In the *ITDOF* array, column I contains information related to element t_I. The first three entries give the global indices for the degrees of freedom associated with the three vertices of the the element. If the element has an edge with degree $p \ge 2$ there are $p - 1$ degrees of freedom (bump functions) associated with that edge. In *PLTMG* these degrees of freedom are given consecutive global indices, that either increase or decrease with a counter clockwise traversal of that edge. Entries 4–6 in column I provide the starting degree of freedom for each edge, with a sign that indicates whether they increase or decrease. If the element has degree $p \ge 3$ there are $(p - 1)(p - 2)/2$ degrees of freedom (bubble functions) associated

array entry	definition
ITDOF(1,I)	degree of freedom for vertex ν_1
ITDOF(2,I)	degree of freedom for vertex ν_2
ITDOF(3,I)	degree of freedom for vertex ν_3
ITDOF(4,I)	$\pm$ first degree of freedom for edge ϵ_1
ITDOF(5,I)	$\pm$ first degree of freedom for edge ϵ_2
ITDOF(6,I)	$\pm$ first degree of freedom for edge ϵ_3
ITDOF(7,I)	first interior degree of freedom for element t_I
ITDOF(8,I)	polynomial degrees for element t_I

Table 2.8. *ITDOF definition.*

with the element interior. These are also given consecutive global indices. The lowest numbered corresponds to the interior node closest to vertex ν_1; subsequently they are numbered "row-by-row;" within each row, degrees of freedom are numbered "left-to-right" with the lowest number for that row corresponding to the node closest to edge ϵ_3. The global index for the lowest numbered interior degree of freedom is given in *ITDOF(7,I)*.

Entry *ITDOF(8,I)* contains information about the degree of the polynomials associated with element t_I. Let the element itself have degree p_0. Each edge ϵ_k can have a different degree $p_k \geq p_0$, $1 \leq k \leq 3$. In *PLTMG*, elements and edges can have degree at most nine.[4] These degrees are encoded in *ITDOF(8,I)* as

$$ITDOF(8,I) = p_0 + 16p_1 + 16^2 p_2 + 16^3 p_3.$$

The total number of degrees of freedom associated with the finite element space is *NDF*. Values for finite element functions are stored in the array *GF*, with $MAXD \geq NDF$ rows and $1 \leq I \leq 13$ columns, depending on the problem, with each column associated with a specific finite element function. The definitions for each problem are given in Table 2.9.

The first column of *GF* always contains the finite element solution u. If the problem is solved via parallel computation, then the last column of *GF* contains the function ω, which is a locally computed dual function that indicates the influence of the regions outside of the given processor's assigned domain on that domain. For simple pde equations, the user can also specify a functional computed from the user supplied function ρ. For continuation problems, the tangent vector $\dot{u}$, as well as u_0 and $\dot{u}_0$ from the previous step, are stored. The vectors ψ_r and ψ_ℓ are the right and left singular vectors, respectively, associated with the smallest singular value of the Jacobian (stiffness) matrix; these are used in the determination of limit and bifurcation points, among other things. Parameter identification and optimal control problems require a Lagrange multiplier function v. The optimal

[4] This constraint is due to limitations of available quadrature rules, given by Zhang, Cui, and Liu in [64], and not to any intrinsic constraint on the spaces themselves.

problem	1	2	3	4	5	6	7
simple pde	u	(u_d)	(ω)				
obstacle problem	u	(ω)					
continuation problem	u	u_0	$\dot{u}$	$\dot{u}_0$	ψ_r	ψ_ℓ	(ω)
parameter identification	u	v	u_{λ_1}	(ω)			
distributed control	u	v	λ	(ω)			

Table 2.9. *GF data structure definitions. Columns labeled I, $1 \le I \le 7$, refer to the function stored in $GF(\cdot, I)$. Functions appearing within parentheses are computed only in certain situations. For the parameter identification problem, columns $2 + J$, $1 \le J \le NRL$, contain u_{λ_J} and column $3 + NRL$ contains ω if present.*

control problem also requires the distributed control function λ, and the parameter identification problem requires NRL vectors u_{λ_k} for $1 \le k \le NRL$.

The array E contains information about a posteriori error estimates. It has $MAXT \ge NTF$ rows and two columns. The first column contains the local error indicator η_I for element t_I, and the second column contains a normalization constant used in the decision process in *hp* refinement. We note that information in the E array is typically modified by various adaptive algorithms in *TRIGEN*, and the output from *TRIGEN* in the E array should be considered unreliable except in the case when *TRIGEN* is called to *only* compute error estimates.

2.6 Parallel Processing Data Structure.

When *PLTMG* solves a problem using parallel processing, it partitions the domain Ω into $NPROC$ subdomains Ω_I if $NPROC$ processors are used. This creates an internal interface system Γ; *PLTMG* creates internal edges as needed such that every edge in the internal interface system is represented in the *IBNDRY* array. At the conclusion of the adaptive process, the global conforming finite element space needs to be created, and corresponding edges and degrees of freedom on different processors need to be linked in order to carry out the domain decomposition solve that computes the final finite element solution on the global mesh.

The integer array *IPATH* is a data structure jointly computed by all of the processors; each processor provides a block of data within the *IPATH* array that describes its part of the global interface system. In particular, each processor begins its adaptive enrichment starting from the same interface system, consisting of so-called *root* edges. Root edges my be bisected (h-refined) or have their degree increased (p-refined) in potentially arbitrary combinations. The data in the *IPATH* array provides a binary tree for each root edge, as well as pointers that indicate the global edge numbers and degrees of freedom for that edge in that processors own data structures. Data for different types of nodes in the tree is given in Table 2.10.

The *IPATH* array has six rows. For all edges in the tree, the first entry

array entry	root	root/leaf	internal	leaf
IPATH(1,I)	neighbor	neighbor	neighbor	neighbor
IPATH(2,I)	child	-edge	child	-edge
IPATH(3,I)	–	vertex 1	–	vertex 1
IPATH(4,I)	–	vertex 2	–	vertex 2
IPATH(5,I)	–	± edge	–	± edge
IPATH(6,I)	–	degree	–	degree

Table 2.10. *IPATH definition – tree section.*

(neighbor) is a pointer to the column in *IPATH* that contains the same edge, but for the neighbor processor; this is the key that identifies the same physical edge on different processors. The second entry identifies the (first) child for non-leaf edges in the tree; these are just pointers to other columns in the *IPATH* array. The two children of a bisected edge appear in consecutive columns in *IPATH*. Leaf entries have a pointer (-edge) that points to the column corresponding to that edge in the given processors *IBNDRY* array; the negative sign is to distinguish it from a child pointer.

In the domain decomposition solve, interface information corresponding to all nodes lying on the global interface system must be exchanged via *MPI*. This is done using a transient interface data structure, with blocks of data provided by each processor. Entries 3–6 in the *IPATH* array for leaf edges provide pointers that indicate the location in the transient data structure for data corresponding to the two endpoints, and if the edge degree $p \geq 2$, the edge data. The fifth location is stored as ±edge, with the sign indicating a increase or decrease in index with a counter clockwise traversal.

The first $NPROC + 2$ columns of the *IPATH* data structure contain pointers, one column for each processor, one column for the global mesh and one column for the coarse part of the interface of the given processor. These pointers indicate the blocks of the *IPATH* array and the shared array for the domain decomposition solver that are used by the given processor. Note that after the basic *IPATH* array is computed jointly by all of the processors, each processor appends a tree section for the coarse part of its interface to the end of the *IPATH* array. This information is different on every processor and is used by the domain decomposition solver.

2.7 Parameter Arrays.

IP, *RP*, and *SP* are integer, real, and *CHARACTER*80* arrays, respectively, of length 100 containing various user specified parameters, and internally generated parameters, switches, flags, and pointers. A list of the currently used locations, their names, and brief definitions appears in Tables 2.12–2.14. Parameters marked "u" should be supplied by the user.

The parameter *IFIRST* is an initialization switch specifying the degree of the

IFIRST	option
0	no initialization
1	initialize for piecewise linear elements
2	initialize for piecewise quadratic elements
3	initialize for piecewise cubic elements
4	initialize for piecewise quartic elements
5	initialize for piecewise quintic elements
6	initialize for piecewise polynomials of degree 6
7	initialize for piecewise polynomials of degree 7
8	initialize for piecewise polynomials of degree 8
9	initialize for piecewise polynomials of degree 9

Table 2.11. *The values of IFIRST.*

finite element space to be used, as indicated in Table 2.11. If $IFIRST = 0$, no initialization takes place. If $IFIRST = p$, $1 \leq p \leq 9$, triangulation data structures are checked, and various arrays are initialized for piecewise polynomial elements of degree p. Array entry *IP(25)* is the error flag *IFLAG*. A summary of the possible values for *IFLAG* is given in Table 2.15.

I	*IP(I)*	u	definition
1	*NTF*	u	number of triangles / regions
2	*NVF*	u	number of vertices
3	*NBF*	u	number of edges
4	*NDF*	u	number of degrees of freedom
5	*IFIRST*	u	initialization switch
6	*IPROB*	u	problem type
7	*ITASK*	u	problem task
8	*ISPD*	u	symmetric / nonsymmetric switch
9	*METHOD*	u	preconditioner options
10	*MXCG*	u	maximum conjugate gradient iterations
11	*MXNWTT*	u	maximum damped Newton iterations
12	*ISING*	u	switch for singular Neumann problem
13	*NRL*	u	number of parameters λ
17	*IRTYPE*	u	refinement / coarsening options
18	*MXORD*	u	maximum polynomial degree
19	*IERRSW*	u	error recovery switch
20	*IADAPT*	u	mesh generation option switch
21	*IREFN*	u	uniform refinement control
22	*NDTRGT*	u	target value for number of vertices
24	*MFLAG*		parallel error flag

Table 2.12: *IP* array definitions. (Continued next page.)

I	*IP(I)*	u	definition
25	*IFLAG*		error flag
27	*NEWNTF*		number of elements owned by processor
28	*NEWNVF*		number of vertices owned by processor
29	*NEWNBF*		number of edges owned by processor
30	*NEWNDF*		number of degrees of freedom owned by processor
31	*NVV*		number of interface vertices
32	*NBB*		number of interface edges
33	*NDD*		number of interface degrees of freedom
34	*NVI*		number of coarse interface vertices
35	*NBI*		number of coarse interface edges
36	*NDI*		number of coarse degrees of freedom
37	*NTG*		global number of elements
38	*NVG*		global number of vertices
39	*NBG*		global number of edges
40	*NDG*		global number of degrees of freedom
41	*IUSRSW*	u	*USRCMD* switch
42	*MODE*	u	*ATEST* mode switch
43	*NGRAPH*	u	number of graphics windows
44	*FDEVCE*	u	*TRIPLT* graphics device
45	*GDEVCE*	u	*GPHPLT* graphics device
46	*JDEVCE*	u	*INPLT* graphics device
47	*MPIRGN*	u	region for printing and graphics
48	*MPISW*	u	MPI switch
49	*NPROC*		number of processes
50	*IRGN*		individual process number
51	*MXCOLR*	u	maximum number of colors
52	*IFUN*	u	alternate function switch for *TRIPLT*
53	*INPLSW*	u	alternate graph switch for *INPLT*
54	*IGRSW*	u	alternate graph switch for *GPHPLT*
56	*NCON*	u	number of contours
57	*ICONT*	u	continuity switch
58	*ISCALE*	u	scale option switch
59	*LINES*	u	line drawing option switch
60	*NUMBRS*	u	numbering option switch
61	*NX*	u	
62	*NY*	u	*(NX,NY,NZ)*
63	*NZ*	u	is the viewing perspective for *TRIPLT*
64	*MX*	u	
65	*MY*	u	*(MX,MY,MZ)*
66	*MZ*	u	is the viewing perspective for *GPHPLT*
68	*ICRSN*	u	graphics coarsening switch

Table 2.12: *IP* array definitions. (Continued next page.)

I	*IP(I)*	u	definition
69	*ITRGT*	u	target size of graphics mesh
71	*NVDD*		total number of interface vertices
72	*LIPATH*		length of *IPATH* array
76	*NEF*		number of error functions
77	*NGF*		number of grid functions
78	*NDL*		order of error recovery systems
79	*IEVALS*		number of function evaluations on last call
80	*ITNUM*		number of Newton iterations on last call
82	*MAXPTH*	u	number of columns in the array *IPATH*
83	*MAXT*	u	number of columns in the array *ITNODE*
84	*MAXV*	u	length of the arrays *VX* and *VY*
85	*MAXD*	u	length of grid function arrays
86	*MAXB*	u	number of columns in the array *IBNDRY*
90	*NDF*		order of the linear system
91	*NB*		number of blocks in the linear system
92	*LENJA*		length of *JA* array
93	*LENAD*		length of diagonal part *A* array
94	*LENAOD*		length of upper / lower triangular *A* array
95	*LENJU*		maximum length of *JU* array
96	*LENUOD*		maximum length of upper / lower triangular *U* array
97	*LENJU0*		length of *JU* array
98	*LENU0*		length of *U* array
99	*LENJA0*		length of *JA* for HB decomposition
100	*LENJUC*		length of *JU* for HB decomposition

Table 2.12: *IP* array definitions.

I	*RP(I)*	u	definition
1	*RLTRGT*	u	target value for λ
2	*RTRGT*	u	target value for $\rho(u, \lambda)$
3	*RMTRGT*	u	target value for μ
4	*DTOL*	u	drop tolerance for incomplete factorization
6	*SMIN*	u	lower limit for contour colors
7	*SMAX*	u	upper limit for contour colors
8	*RMAG*	u	window magnification factor
9	*CENX*	u	*(CENX,CENY)* are the window center coordinates
10	*CENY*	u	
12	*HMAX*	u	approximate largest element size
13	*GRADE*	u	largest growth factor for adjacent elements

Table 2.13: *RP* array definitions. (Continued next page.)

I	*RP(I)*	u	definition
14	*HMIN*	u	approximate smallest edge length
16	*XMIN*		$\Omega \subset (XMIN, XMAX) \times (YMIN, YMAX)$
17	*XMAX*		
18	*YMIN*		
19	*YMAX*		
21	*RL*		current value of λ_h
22	*R*		current value of $\rho(u_h, \lambda_h) = \rho_h$
23	*RLDOT*		current value of $\dot{\lambda}_h$
24	*RDOT*		current value of $\dot{\rho}_h$
25	*SVAL*		current value of smallest singular value
26	*RLSTRT*		starting value for λ_h
27	*RSTRT*		starting value for $\rho(u_h, \lambda_h)$
31	*RL0*		previous value of λ_h
32	*R0*		previous value of $\rho(u_h, \lambda_h) = \rho_h$
33	*RL0DOT*		previous value of $\dot{\lambda}_h$
34	*R0DOT*		previous value of $\dot{\rho}_h$
35	*SVAL0*		previous value of smallest singular value
37	*ENORM1*		estimate for $\|u - u_h\|_{\mathcal{H}^1(\Omega)}$
38	*UNORM1*		the norm $\|u_h\|_{\mathcal{H}^1(\Omega)}$
39	*ENORM2*		estimate for $\|u - u_h\|_{\mathcal{L}_2(\Omega)}$
40	*UNORM2*		the norm $\|u_h\|_{\mathcal{L}_2(\Omega)}$
41	*N0*		degrees of freedom for region Ω_I
42	*E0*		error for region Ω_I
43	*NF*		global degrees of freedom
44	*EF*		global error
52	*STEP*		damping step s for Newton's method
53	*RELER0*		relative size of solution error $\|e_h\|_{\mathcal{H}^1(\Omega)}/\|u_h\|_{\mathcal{H}^1(\Omega)}$
54	*RELERR*		relative size of Newton update $\|\delta U\|/\|U\|$
55	*ANORM*		maximum diagonal entry in Jacobian matrix
56	*RELRES*		the relative residual $\|\mathcal{G}_k\|/\|\mathcal{G}_0\|$
57	*BRATIO*		the relative residual $\|\mathcal{G}_k\|/\|\mathcal{G}_{k-1}\|$
58	*DNEW*		the discrete inner product $-\langle G_u \delta U, G\rangle$
59	*BNORM0*		scaling factor $\|\mathcal{G}_0\|$
60	*BMNRM0*		scaling factor for ρ
63	*RMU*		current value of μ
64	*REG4*		internal regularization parameter
65	*REG5*		internal regularization parameter
67	*SCLEQN*		current value of scalar equation $N - \sigma$
68	*SCALE*		scaling factor for scalar equation
69	*THETAL*		$(2 - \theta)\dot{\lambda}_h$ in scalar equation

Table 2.13: *RP* array definitions. (Continued next page.)

I	*RP(I)*	u	definition
70	*THETAR*		$\theta\dot{\rho}_h$ in scalar equation
71	*SIGMA*		the step σ for scalar equation
72	*DELTA*		Newton update for λ_h
73	*DRDRL*		the value of $\partial\rho/\partial\lambda$
74	*SEQDOT*		the value of $\dot{N}$
76	*QUAL*		target element quality
77	*ANGMN*		target minimum angle
78	*DIAM*		approximate diameter of Ω
79	*BEST*		value of *TRIGEN* quality function
80	*AREA*		area of Ω
82	*SFAVE*		average scale factor
83	*SFVAR*		scale factor variance
84	*SFMIN*		minimum scale factor
85	*SFMAX*		maximum scale factor
86	*RELERP*		relative size of solution error $\|e_h\|_{\mathcal{H}^1(\Omega_I)}/\|u_h\|_{\mathcal{H}^1(\Omega_I)}$
87	*EAVE2*		arithmetic average of $\|e_h\|^2_{\mathcal{H}^1(t)}$
88	*EAVEG*		geometric average of $\|e_h\|^2_{\mathcal{H}^1(t)}$
91	*RL1*		value of λ_1
92	*RL2*		value of λ_2
93	*RL3*		value of λ_3
94	*RL4*		value of λ_4
95	*RL5*		value of λ_5
96	*RL6*		value of λ_6
97	*RL7*		value of λ_7
98	*RL8*		value of λ_8
99	*RL9*		value of λ_9
100	*RL10*		value of λ_{10}

Table 2.13: *RP* array definitions.

I	*SP(I)*	u	definition
1	*ITITLE*	u	title for *INPLT*
2	*FTITLE*	u	title for *TRIPLT*
3	*GTITLE*	u	title for *GPHPLT*
5	*SHCMD*	u	string for shell command
6	*RWFILE*	u	save file for read/write commands
7	*JRFILE*	u	read file for journal command
8	*JWFILE*	u	write file for journal command
9	*BFILE*	u	output file

Table 2.14: *SP* array definitions. (Continued next page.)

I	*SP(I)*	u	definition
10	*JTFILE*	u	temporary file for journal command
11	*IOMSG*		error message string
12	*CMD*		current command string
13	*LOGO*	u	logo for X-Windows display
14	*BGCLR*	u	background color for X-Windows display
15	*BTNBG*	u	button background color for X-Windows display
18	*PSFILE*	u	root name for PostScript files
19	*XPFILE*	u	root name for xpm files
20	*BHFILE*	u	root name for bh files
21	*SGHOST*	u	host name for *SG* display

Table 2.14: *SP* array definitions.

PLTMG has seven labeled *common* blocks:

```
common /pltmg1/ic(3,363),jc(12)
common /pltmg2/c(2,78),wt(78),np1(13)
common /pltmg3/c(3,746),wt(746),np2(22)
common /pltmg4/fc(2541),ishift(7)
common /pltmg5/cb(65,65),cd(12,65),cs(12,45),iptr(12),jptr(12)
common /pltmg6/path(101,6)
common /pltmg7/time(3,50),hist(22,30)
```

Common block *PLTMG1* contains basic definitions of the family of finite elements. Blocks *PLTMG2* and *PLTMG3* contain definitions of quadrature rules for one dimensional integrals on intervals (Gauss Quadrature), and two dimensional integrals on triangles, from Zhang, Cui, and Liu, [64]. Block *PLTMG4* contains information used in the two level *HB* solver described in Section 4.3. Block *PLTMG5* contains information used in the evaluation of basis functions on transition elements. Block *PLTMG6* collects data on various aspects of continuation problems, $IPROB = 3$ (See Section 4.6). Block *PLTMG7* collects statistical data on various aspects of the calculation.

2.8 Coefficient Functions.

Several routines in the package require knowledge of the partial differential equation (1.1), the boundary conditions (1.2), the functional ρ in (1.3), and, on occasion, an alternate function of the solution. This information is provided by the user through subroutines *A1XY*, *A2XY*, *FXY*, *GNXY*, *GDXY*, *P1XY*, *P2XY*, and *QXY*.

Subroutines *A1XY*, *A2XY*, *FXY*, and *P1XY* have identical argument lists.

Call A1XY(X, Y, U, UX, UY, RL, ITAG, VALUES),
Call A2XY(X, Y, U, UX, UY, RL, ITAG, VALUES),

IFLAG	general return codes
0	normal return
25	wrong input data structure
IFLAG	*PLTMG* and *TRIGEN* errors
1	zero pivot in sparse factorization
2	Newton method line search failed
6	illegal problem type
7	continuation procedure failed
10	multigraph iteration failed to converge
11	Newton (Newton/DD) iteration failed to converge
24	Error on one or more MPI processes
48	MPI was off for a command needing MPI
49	$NPROC > NTF$ in load balance
71	no interface unknowns in DD solver
72	*IPATH* array not created
IFLAG	storage errors
82	storage exhausted in array *IPATH*
83	storage exhausted in arrays *ITNODE* and *ITDOF*
84	storage exhausted in arrays *VX* and *VY*
85	storage exhausted in array *GF*
86	storage exhausted in arrays *IBNDRY* and *SF*
IFLAG	data errors for triangulation
-31	illegal *ITNODE(K,*)* $K = 1, 2, 3$
-32	overlapping triangles in *ITNODE*
IFLAG	data errors for triangulation and skeleton
-40	illegal value for *NVF*, *NTF*, or *NBF*
-41	illegal *IBNDRY(K,*)* $K = 1, 2$
-42	illegal *IBNDRY(3,*)*
-43	illegal *IBNDRY(4,*)*
-44	incorrect circle center coordinates
-45	arc greater than $\pi/2$ in length
-46	error in linked edges
-47	boundary vertex without two boundary edges
-48	*ITNODE* and *IBNDRY* are not consistent
IFLAG	data errors for skeleton
-51	illegal *ITNODE(1,*)*
-52	illegal *ITNODE(2,*)*
-53	skeleton tracing error
-54	region specified in clockwise order
-55	illegal *ITNODE(3,*)*

Table 2.15. *Error flag values.*

Call P1XY(X, Y, U, UX, UY, RL, ITAG, VALUES),
Call FXY(X, Y, U, UX, UY, RL, ITAG, VALUES).

In these subroutines, all of the arguments except *VALUES* are provided as input. In particular $(X, Y) \in \Omega$ is the evaluation (quadrature) point, and

$$\begin{aligned} U &= u_h(X, Y), \\ UX &= \frac{\partial u_h}{\partial x}(X, Y), \\ UY &= \frac{\partial u_h}{\partial y}(X, Y), \\ RL &= \lambda_h, \end{aligned}$$

For the parameter identification problem, *RL* is an array for size *NRL* with the value of the vector λ_h, and for the distributed control problem, $RL = \lambda_h(X, Y)$. The parameter *ITAG=ITNODE(5,I)* is the user specified label associated with element $\tau_I \in \mathcal{T}$ containing (X, Y). From this input data, the user provides values of the given function and its derivatives in the array *VALUES*. This array is of size 4+*NRL*. All entries are initially set to zero by the calling routine; thus the user need supply only nonzero values.

To simplify this process, *PLTMG* supplies a labeled common block

common /VAL0/ K0, KU, KX, KY, KL

containing a predefined list of integer pointers mapping function and derivative values to particular entries in the *VALUES* array. The details of this mapping are given in Table 2.16 for the case of f; the identical mapping is used for a_1, a_2 and p_1.

pointer	index	$VALUES(\cdot)$
$K0 = 1$	$K0$	f
$KU = 2$	KU	f_u
$KX = 3$	KX	f_{u_x}
$KY = 4$	KY	f_{u_y}
$KL = 5$	$KL + J - 1$	f_{λ_J}
	$1 \le J \le NRL$	

Table 2.16. *VALUES array for subroutine FXY.*

For example, if

$$f = \lambda \frac{\partial u}{\partial x} + u^2,$$

then the following code fragment would be included in *Subroutine FXY*.

*VALUES(K0)= RL * UX + U**2*
VALUES(KX)= RL
*VALUES(KU)= 2 * U*
VALUES(KL)= UX

The subroutine corresponding to p_2 is *P2XY* and is called using

Call P2XY(X, Y, DX, DY, U, UX, UY, RL, ITAG, JTAG, VALUES).

The arguments are a superset of those of the previous subroutines, and all arguments with the same name serve the same purpose. This routine is called only with points (X, Y) lying on some edge $e_J \in \Gamma$. The additional arguments (DX, DY) are the unit normal direction for the edge, and *JTAG=IBNDRY(7,J)* is the user specified label for the given edge. The mapping given in Table 2.16 is used here as well.

The subroutine corresponding to g_1 is *GNXY* and is called using

Call GNXY(X, Y, U, RL, ITAG, VALUES).

This routine is called only for points $(X, Y) \in \partial\Omega_1$, and as in the previous cases, all arguments except the array *VALUES* are input. In this case *ITAG=IBNDRY(7,I)* is the user supplied label for the edge, and *VALUES* is an array of size $2 + NRL$. Here the labeled common block

common /VAL1/ K0, KU, KL

assists in mapping function and derivative values to particular entries in the *VALUES* array. The details of the mapping are given in Table 2.17.

pointer	index	*VALUES*$(\cdot)$
$K0 = 1$	$K0$	g
$KU = 2$	KU	g_u
$KL = 3$	$KL + J - 1$	g_{λ_J}
	$1 \le J \le NRL$	

Table 2.17. *VALUES array for subroutine GNXY.*

The subroutine corresponding to g_2 is *GDXY* and is called using

Call GDXY(X, Y, RL, ITAG, VALUES).

This routine also supplies the upper and lower bounds for the inequality constraints on u_h for the obstacle problem, bounds on λ_h in the case that $\lambda = \lambda(x, y)$, and the initial guess u_0, for the solution u_h. For parameter identification problems, the

Lagrange multiplier can be initialized using v_0, and for optimal control problems the Lagrange multiplier can be initialized with v_0 and $\lambda(x,y)$ can be initialized with λ_0. When called to supply a Dirichlet boundary condition, $(X,Y) \in \partial\Omega_2$ and *ITAG=IBNDRY(7,I)* is an edge label. When called in regard to inequality constraints and the initial guess, $(X,Y) \in \Omega$ and *ITAG=ITNODE(5,I)* is the element label supplied by the user. Similar to the other routines, *VALUES* is an output array of size $3 + 4\,NRL$. It's entries can be conveniently accessed through pointers provided in the labeled common block

common /VAL2/ K0, KL, KLB, KUB, KIC, KIM, KIL

The details are provided in Table 2.18.

pointer	index	$VALUES(\cdot)$
$K0 = 1$	$K0$	g
$KL = 2$	$KL + J - 1$	g_{λ_J}
$KLB = 2 + NRL$	$KLB + J - 1$	$\underline{u}$, $\underline{\lambda}_J$
$KUB = 2 + 2\,NRL$	$KUB + J - 1$	$\overline{u}$, $\overline{\lambda}_J$
$KIC = 2 + 3\,NRL$	KIC	u_0
$KIM = 3 + 3\,NRL$	KIM	v_0
$KIL = 4 + 3\,NRL$	$KIL + J - 1$	$\lambda_{0,J}$
	$1 \le J \le NRL$	

Table 2.18. *VALUES array for subroutine GDXY.*

Subroutine *QXY* is

Call QXY(X, Y, U, UX, UY, RL, ITAG, VALUES)

This routine provides the alternate function to display in *TRIPLT* and the alternate function for adaptive algorithms in *TRIGEN*. The arguments are defined as in the other coefficient functions. The output array *VALUES* has dimension 4; It's entries can be conveniently accessed through pointers provided in the labeled common block

common /VAL3/ KF, KF1, KF2, KAD

whose entries are documents in Table 2.19.

In the case of a singular Neumann problem (e.g., $a_1 \equiv u_x$, $a_2 \equiv u_y$, $f \equiv 0$, and $\partial\Omega_1 = 0$ in (1.1)), the solution u is determined only up to an arbitrary constant. In this situation, the solution is not unique, and is determined only up to an additive constant. Setting the switch $ISING = 1$ causes both right hand sides and solutions in all linear systems to be orthogonalized with respect to constants, in effect computing least squares solutions in the orthogonal complement subspace. In other situations, one should set $ISING = 0$.

pointer	index	*VALUES*(·)
$K0 = 1$	*K0*	alternate scalar function for *TRIPLT*
$KF1 = 2$	*KF1*	first component of vector function for *TRIPLT*
$KF2 = 3$	*KF2*	second component of vector function for *TRIPLT*
$KAD = 4$	*KAD*	alternate function for adaptive algorithms in *TRIGEN*

Table 2.19. *VALUES array for subroutine QXY*

2.9 Sparse Matrix Storage.

Although sparse matrices are presently generated internally within *PLTMG*, it may still be of interest to understand the data structures involved. This version of *PLTMG* uses two variants of a basic sparse matrix data structure – a point version, where matrix elements are simple scalar values, and a block version where matrix elements are allowed to be blocks of arbitrary size. The block version is of interest, since the degrees of freedom associated with a single edge or element interior form a so-called clique within the graph of the matrix. These correspond to dense blocks within the sparse matrix if all members of a clique are ordered consecutively, which is the case here. Taking advantage of these dense blocks can reduce the integer overhead and indirect addressing associated with processing those cliques.

We begin discussion with the point version of the data structure. Here matrices are stored in the sparse matrix format described in [3] using an integer array *JA* and a real array *A*. As an example, consider the 4×4 matrix given by

$$A = \begin{pmatrix} a_{11} & a_{12} & & a_{14} \\ a_{21} & a_{22} & a_{23} & a_{24} \\ & a_{32} & a_{33} & \\ a_{41} & a_{42} & & a_{44} \end{pmatrix}. \tag{2.1}$$

This matrix is stored in *JA* and *A* as illustrated in Table 2.20. All nonzeros are stored in the array *A*. First the diagonal entries are stored, followed by the upper triangular entries, stored row by row. If the matrix is nonsymmetric, this is followed by the lower triangular entries, stored column by column. Symmetric and nonsymmetric storage is governed by the parameter *ISPD* as indicated in Table 2.20.

ISPD	storage/iteration options
0	nonsymmetric/biconjugate gradient
1	symmetric/conjugate gradient

Table 2.20. *The values of ISPD.*

The first $NDF + 1$ entries of *JA* are pointers. In particular, entries *JA(I)* to *JA(I+1)* $- 1$ of the *JA* array contain column indices for nonzeros in row *I* of

the strict upper triangle. As illustrated in Table 2.21, the column indices stand in correspondence to the nonzeros of the upper triangle stored in the array A. If nonsymmetric storage is used, entries of the *transposed* lower triangle are stored in the same order as the upper triangle.

I	1	2	3	4	5	6	7	8	9	10	11	12	13
$JA(I)$	6	8	10	10	10	2	4	3	4				
$A(I)$	a_{11}	a_{22}	a_{33}	a_{44}	$-$	a_{12}	a_{14}	a_{23}	a_{24}	a_{21}	a_{41}	a_{32}	a_{42}

Table 2.21. *Sparse matrix data structures. JA has 9 entries. A has 9 entries if* $ISPD = 1$ *or 13 entries if* $ISPD = 0$.

Now suppose the elements a_{ii} in (2.1) are $k_i \times k_i$ square matrices. Then the off-diagonal blocks $a_{i,j}$ are $k_i \times k_j$ rectangular blocks. Suppose that there are NB blocks, where

$$NDF = \sum_{i=1}^{NB} k_i$$

The JA array for the block case is identical to the point case, except that now entries refer to block rows and columns rather than individual elements. This could be much smaller that the point version of the JA array. For example, a mesh with NVF vertices and all elements of degree p will have approximately $NDF \approx p^2 NVF$ degrees of freedom and a point JA array with $O(p^4 NVF)$ entries. On the other hand, for this case $NB \approx 6 \times NVF$, and the corresponding block JA array will have about $39 \times NVF$ entries.

Additionally we need an array IBS of size NB to indicate the sizes of the diagonal blocks

$$IBS(I) = k_I \qquad\qquad 1 \le I \le NB.$$

The A array in this case is more complicated. Following the pattern of the scalar case, we store the diagonal blocks first, followed by the upper triangular blocks, stored (block) row-wise. If $ISPD = 0$, the upper triangle is followed by the lower triangular block, stored (block) column-wise. The individual diagonal blocks are stored in the same pattern; the diagonal stored first, followed by the upper triangle, stored row-wise, and if $ISPD = 0$, this is followed by the lower triangle stored column-wise. The upper triangular blocks are stored row-wise, and the lower triangular blocks, if present, are stored column-wise.

To access this data, we need an additional integer array JAP of pointers, where $JAP(I)$ indicates the location in the A array where the block corresponding to $JA(I)$ begins. This array is the same size as JA (plus one for convenience).

For the case $ISPD = 1$, $JAP(1) = 1$ and

$$JAP(I+1) = JAP(I) + \{IBS(I) \times (IBS(I) + 1)\}/2,$$

while for $ISPD = 0$

$$JAP(I+1) = JAP(I) + IBS(I)^2,$$

for $1 \leq I \leq NB$. Note that the value of *JAP(NB+1)* is defined. For the upper triangle, we have *JAP(NB+2)* = *JAP(NB+1)*. For $I = 1, 2, \ldots NB$ and *JA(I)* $\leq K \leq$ *JA(I+1)* $- 1$, we have

$$JAP(K+1) = JAP(K) + IBS(I) \times IBS(JA(K)).$$

The array *JAP* can be computed once and saved, but we prefer to compute it as needed from the *IBS* and *JA* arrays. Some of our problem classes involve several sparse matrices, some symmetric and some nonsymmetric. For this case, one instance of the *IBS* and *JA* arrays can be used for all sparse matrices, independent of their symmetry, and routines that need *JAP* (e.g, a routine to compute a matrix-vector multiply) can compute it based on the symmetry status of the particular matrix involved.

Data structures *JU* and *U* are analogous to *JA* and *A*, respectively, and contain the (incomplete) $A \approx LDU$ factorization, where D is (block) diagonal, U is unit (block) upper triangular, and L is unit (block) lower triangular, with $L^t = U$ if $A^t = A$.

Chapter 3
Mesh Generation

3.1 Overview.

Subroutine *TRIGEN* creates or adaptively modifies the data structures defining the region Ω. There are options to generate a triangulation from a skeleton, adaptively refine or unrefine a triangulation, uniformly refine a triangulation, and adaptively smooth the vertices of a triangulation. *TRIGEN* also has several options for partitioning and mesh management in parallel computation environments. The parameter *IADAPT* specifies various options for *TRIGEN*, summarized in Table 3.1.

TRIGEN is called using the statement

Call TRIGEN(VX, VY, SF, ITNODE, IBNDRY, ITDOF, IPATH,
E, IP, RP, SP, IU, RU, SU, GF, QXY, SXY)

Except for the case $IADAPT = 5$, on input the arrays *VX*, *VY*, *SF*, *ITNODE*, and *IBNDRY* should define a triangulation. For $IADAPT = 5$, the input should be a skeleton. The arrays *IU*, *RU*, and *SU* are broadcast and received in MPI communication steps, but are not directly used in *TRIGEN*. When *TRIGEN* is used to adaptively modify an existing triangulation the procedures generally rely on local a posteriori error estimates for the finite element approximation, although some options are provided for adaptation based on other functions.

If $IADAPT = -K$ for $1 \leq k \leq 3$, the refinement and/or unrefinement or adaptive mesh smoothing processes are carried out using interpolation errors for the function *QXY* in place of the a posteriori error estimates. In particular, for a given element t of degree p, let q_{p+1} denote the interpolating polynomial for *QXY* of degree $p+1$, characterized by nodes at the usual Lagrange lattice points of t. In this situation, we can use the (constant) derivatives of order $p+1$ of q_{p+1} in place of the corresponding recovered derivatives for u_h. Once this substitution is made, the adaptive algorithms proceed in the usual fashion.

We do not anticipate that this option will be used much; it was originally implemented to allow subroutine *TRIGEN* to be debugged independently of subrou-

IADAPT	mesh generation option
0	error estimates only
1	refine *or* unrefine mesh using u_h
-1	refine *or* unrefine mesh using QXY
2	unrefine *and* refine mesh using u_h
-2	unrefine *and* refine mesh using QXY
3	smooth mesh points using u_h
-3	smooth mesh points using QXY
4	uniform mesh refinement
-4	uniform degree refinement
5	skeleton $\rightarrow$ triangulation
6	load balance (MPI)
7	reconcile mesh (MPI)

Table 3.1. *Some options use a posteriori error estimates for the computed solution u_h or interpolation errors for the alternative function QXY. Other options require MPI for parallel communication.*

tine *PLTMG*. On the other hand, there may be special cases where some functional other than the a posterior error estimate for $\|\nabla(u-u_h)\|_{\mathcal{L}_2(t)}$ should be optimized. Note that if *TRIGEN* is called before a solution u_h is computed by *PLTMG*, values of the arguments U, UX, UY, and RL provided by *TRIGEN* to QXY are arbitrary and should be ignored.

3.2 Creating a Triangulation from a Skeleton.

When $IADAPT = 5$, on input the arrays *VX*, *VY*, *SF*, *ITNODE*, and *IBNDRY* should define a skeleton as described in Section 2.4. *TRIGEN* triangulates the subregions defining the skeleton in the order that they are given in *ITNODE*, taking into account shared internal boundaries and the symmetry requirements.

Let t be a triangle with area a and side lengths h_1, h_2, and h_3. The quality of t, $q(t)$, is measured using the formula

$$q(t) = 4\sqrt{3}a/(h_1^2 + h_2^2 + h_3^2). \tag{3.1}$$

The function $q(t)$ is normalized to equal one for an equilateral triangle and to approach zero for triangles with small angles. In attempting to compute a high quality triangulation, *TRIGEN* uses

$$q(t) \geq .6 \tag{3.2}$$

as a test for acceptability of a triangle (sufficiently small interior angles on the boundaries of the subregions Ω_i could cause (3.2) to be violated).

The triangulation process for those regions for which $ITNODE(3, I) \neq 0$ is simple and is carried out by generating the appropriate affine mapping. The triangulation process for subregions with $ITNODE(3, I) = 0$ is somewhat complicated but embodies three straightforward heuristics.

Given a subregion viewed as a polygon (possibly with curved edges, and interior angles of size π or greater), *TRIGEN* first tries to reduce the order of the polygon by one by "chopping" off a triangle using a vertex with small interior angle. Inequality (3.2) and several less obvious conditions must be satisfied for a successful chop. When the chopping strategy is no longer successful, *TRIGEN* checks to see if the remaining polygon is convex with six or fewer sides. If it is, *TRIGEN* tries to triangulate the entire remaining subregion by adding the centroid as a vertex and connecting it to each boundary vertex. All the resulting triangles must satisfy (3.2) and some other conditions for this strategy to be successful.

If the second strategy fails or is inapplicable, *TRIGEN* tries to break the polygon into two smaller polygons by connecting two nonadjacent vertices by a straight line. *TRIGEN* excludes many potential cuts as geometrically infeasible or otherwise undesirable. From the remaining possibilities *TRIGEN* picks the cut that maximizes the minimum of the four interior angles the cut creates. *TRIGEN* then applies the three strategies to the two newly created polygons in recursive fashion. After the region has been successfully triangulated, *TRIGEN* tries to improve the triangulation by (locally) rearranging edges and adjusting vertex locations such that the criterion (3.2) is optimized.

The user can control the triangulation process to some extent through the parameters *HMAX* and *GRADE*. Element size is controlled by *HMAX*. Normally, one should choose $0 < HMAX \leq 1$. *TRIGEN* then attempts to create triangles with edges shorter than $HMAX \cdot \text{diam}(\Omega)$. If $HMAX \leq 0$ or $HMAX > 1$, *TRIGEN* will reset $HMAX = 1$. Setting *HMAX* only places an upper bound on triangle sizes; the sizes of the triangles actually generated depend strongly on the geometry of the Ω_i and may not achieve the bound.

GRADE is (approximately) the largest ratio of sizes of elements sharing a common edge ($1/GRADE$ is the smallest ratio). *GRADE* should be set on the interval $1.5 \leq GRADE \leq 2.5$; values outside this interval are set to the appropriate end point. Generally speaking, smaller values of *GRADE* result in smoother transitions from regions of large elements to those of small elements, and a higher overall quality measured by (3.1). On the other hand, larger values of *GRADE* tend to produce meshes with fewer elements, more rapid transitions in element size, and lower overall quality. One may have to experiment to achieve the proper balance between these conflicting objectives.

For example, consider the domain pictured in Figure 3.1, top left. The remaining pictures in Figure 3.1 show triangulations generated by *TRIGEN* for various values of *HMAX* and *GRADE*, illustrating their effect on the resulting triangulation.

The pictures are made by *INPLT* (see Section 5.3), which draws the mesh with elements colored according to the quality measure $q(t)$ in (3.1). In the pictures, an element is "good" if $q(t) \geq \sqrt{3}/2$, "fair" if $.6 \leq q(t) < \sqrt{3}/2$, and "poor" if $q(t) < .6$. This is an interesting region to triangulate because the two narrow subregions at

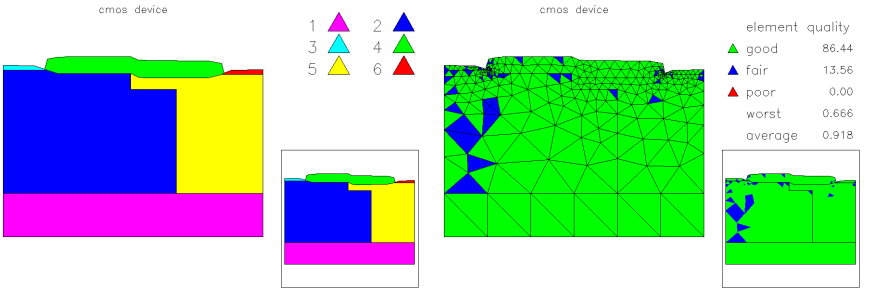

A skeleton with NTF = 6, NVF = 30, NBF = 35 (left). The triangulation for HMAX = 0, GRADE = 1.5 has NTF = 509, NVF = 292 (right).

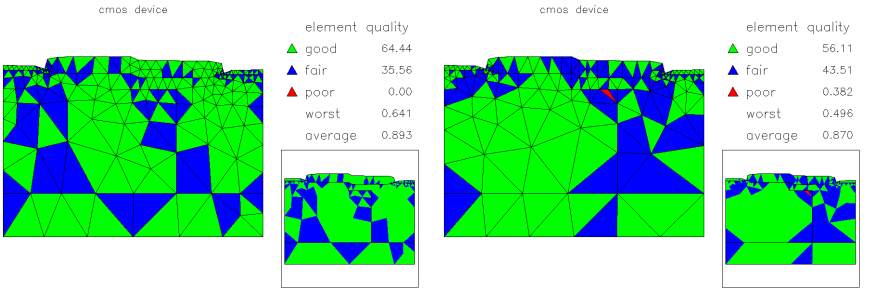

The triangulation for HMAX = 0, GRADE = 2.0 has NTF = 329, NVF = 199 (left). The triangulation for HMAX = 0, GRADE = 2.5 has NTF = 262, NVF = 163 (right).

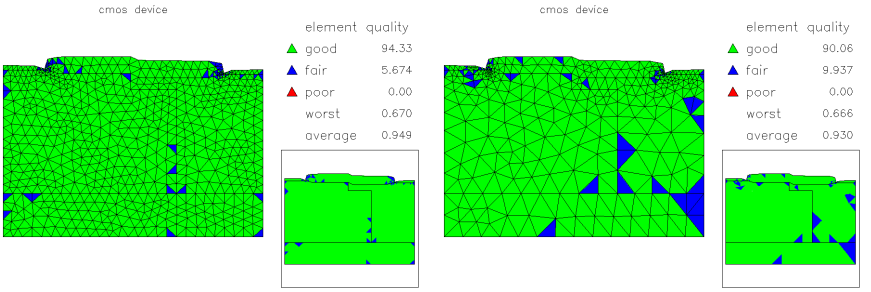

The triangulation for HMAX = .03, GRADE = 1.5 has NTF = 1269, NVF = 695 (left). The triangulation for HMAX = .06, GRADE = 1.5 has NTF = 634, NVF = 361 (right).

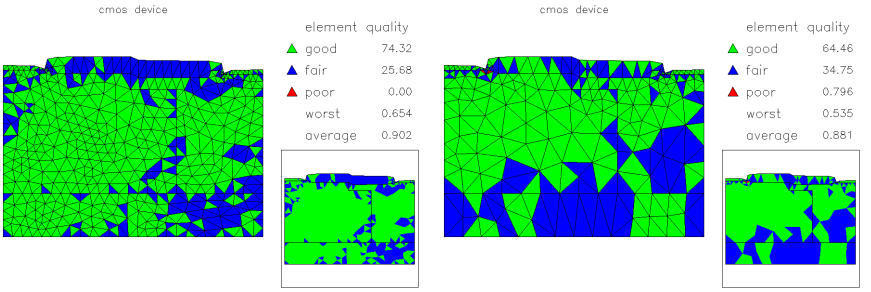

The triangulation for HMAX = .03, GRADE = 2.5 has NTF = 849, NVF = 480 (left). The triangulation for HMAX = .06, GRADE = 2.5 has NTF = 377, NVF = 227 (right).

Figure 3.1.

the top require small elements. *TRIGEN* tries to use larger elements in the larger subregions, but is constrained by the choices of *HMAX* and *GRADE*. Decreasing *HMAX* or *GRADE* tends to improve the overall quality of the triangulation, at the expense of introducing more elements.

3.3 A Posteriori Error Estimates.

Of central importance to the adaptive procedures is the computation of a posteriori local error estimates [2, 1, 61, 63]. In the case of piecewise polynomials of degree p, our a posteriori error estimate is based on a superconvergent approximation of the derivatives of u of order p [35, 36, 37]. In particular, given the finite element function u_h, we compute the piecewise linear vector functions $S_h^m Q_h \partial_x^k \partial_y^{p-k} u_h$, for $0 \le k \le p$. where Q_h is the $\mathcal{L}_2$ projection from the space of discontinuous piecewise constant functions into the space of continuous piecewise linear polynomials, and S_h is a smoothing operator based on the discrete Laplace operator; in *PLTMG*, we take $m \le 1$. See [35, 36, 37] for details. For meshes with variable p, we recover derivatives patchwise, processing all elements of the same degree in the same patch.

The switch *IERRSW* allows the user to control the continuity of the recovered derivatives. The options are specified in 3.2. In some problems, one expects the gradient or higher derivatives of the solution to be discontinuous, typically due to discontinuities in the coefficient functions. If $IERRSW = 1$, a patchwise continuous recovery is made. The user defines the patch boundaries by specifying different values of *ITNODE(5,*)* for different patches. The parameter *NDL* is the combined order of the (block diagonal) linear systems that are used in the recovery.

IERRSW	error recovery option
0	globally continuous recovery
1	patchwise continuous recovery

Table 3.2. *Patches are defined using element labels ITNODE(5,*).*

Using these recovered derivatives, we compute a local error estimate ϵ_t for $t \in \mathcal{T}$. Suppose the finite element space consists of continuous piecewise polynomials of degree p, and denote by u_p the usual Lagrange interpolant. In [39], it is shown that in many cases interpolation error is both an upper and lower bound on the finite element error,

$$C_1 \|\nabla(u - u_p)\|_{\mathcal{L}_2(\Omega)} \le \|\nabla(u - u_h)\|_{\mathcal{L}_2(\Omega)} \le C_2 \|\nabla(u - u_p)\|_{\mathcal{L}_2(\Omega)},$$

implying that error indicators based on interpolation error are both reliable and efficient. In [26], constants involved in such estimates are numerically computed for a variety of finite element spaces, including the Lagrange triangular elements used in *PLTMG*.

Our estimate is motivated by noting that under certain circumstances, $\|\nabla(u_{p+1} - u_p)\|_{\mathcal{L}_2(\Omega)}$ is an asymptotically exact estimate of $\|\nabla(u - u_h)\|_{\mathcal{L}_2(\Omega)}$. This is known

for the cases $p = 1$ and $p = 2$ [36, 37]. Since the usual interpolation points for u_p and generally not a subset of those for u_{p+1}, on each individual element t, we replace u_{p+1} by $\hat{u}_{p+1} = u_p + e_{p+1}$, where e_{p+1} is a locally defined polynomial of degree $p+1$ that is zero at the interpolation points for the polynomial of degree p and has the same (constant) derivatives of order $p+1$ as u_{p+1} (see Figure 1.1). Such polynomials form a (local) vector space of dimension $p+2$. For example, e_2 is a locally defined quadratic polynomial with value zero at all vertices of the mesh. On a given element t, e_2 can be expressed as a linear combination of three quadratic "bump functions" q_k associated with the edge midpoints of t,

$$e_2 = \sum_{k=1}^{3} \ell_k^2 \boldsymbol{t}_k^t M_t \boldsymbol{t}_k \, q_k(x,y) \tag{3.3}$$

where ℓ_k is the length of edge k, $\boldsymbol{t}_k$ is the unit tangent, and

$$M_t = -\frac{1}{2} \begin{pmatrix} \partial_{xx} u_2 & \partial_{xy} u_2 \\ \partial_{yx} u_2 & \partial_{yy} u_2 \end{pmatrix}.$$

is the Hessian matrix. All terms on the right hand side of (3.3) are known except for the second derivatives appearing in the Hessian matrix M_t. In our local error indicator, we simply approximate the second derivatives in the Hessian matrix M_t using derivatives of $S^m Q_h \nabla u_h$. In particular, let

$$\begin{aligned} \tilde{M}_t &= -\frac{1}{2} \begin{pmatrix} \partial_x S^m Q_h \partial_x u_h & \partial_x S^m Q_h \partial_y u_h \\ \partial_y S^m Q_h \partial_x u_h & \partial_y S^m Q_h \partial_y u_h \end{pmatrix}, \\ \bar{M}_t &= \frac{\alpha_t}{2} (\tilde{M}_t + \tilde{M}_t^t), \\ \epsilon_t &= \sum_{k=1}^{3} \ell_k^2 \boldsymbol{t}_k^t \bar{M}_t \boldsymbol{t}_k \, q_k(x,y). \end{aligned} \tag{3.4}$$

The normalization constant α_t is chosen such that the local error indicator η_t satisfies

$$\eta_t \equiv \|\nabla \epsilon_t\|_{\mathcal{L}_2(t)} = \|(I - S^m Q_h) \nabla u_h\|_{\mathcal{L}_2(t)}.$$

Normally we expect that $\alpha_t \approx 1$, which is likely to be the case in regions where the Hessian matrix for the true solution is well defined. Near singularities, u is not smooth and we anticipate difficulties in estimating the Hessian. For elements near such singularities, α_t provides a heuristic for partly compensating for poor approximation. For the cases e_{p+1}, $p > 1$, more complicated formulas of similar nature are used. In particular, ϵ_t is expressed in terms of parameters describing the geometry of t, and the derivatives of order $p+1$ in t, which are obtained from $\partial_x S_h^m Q_h \partial_x^k \partial_y^{p-k} u_h$, and $\partial_y S_h^m Q_h \partial_x^k \partial_y^{p-k} u_h$, for $0 \le k \le p$, in a fashion analogous to the case $p = 1$ described above. Global a posteriori estimates $\|\epsilon_t\|_{\mathcal{L}_2(\Omega)}$ and $\|\nabla \epsilon_t\|_{\mathcal{L}_2(\Omega)}$ are stored as the parameters *ENORM2* and *ENORM1*, respectively.

In the case of parameter identification problems, the error in the Lagrange multiplier $\tilde{\epsilon}_t$ is computed by the a similar procedure to that described above. The

local error indicator is given by

$$\eta_t = \left\{ \|\nabla \epsilon_t\|^2_{\mathcal{L}_2(t)} + \|\nabla \tilde{\epsilon}_t\|^2_{\mathcal{L}_2(t)} \right\}^{1/2}.$$

In the case of optimal control problems, errors in both the Lagrange multiplier $\tilde{\epsilon}_t$ and the control $\hat{\epsilon}_t$ are computed, and the local error indicator is given by

$$\eta_t = \left\{ \|\nabla \epsilon_t\|^2_{\mathcal{L}_2(t)} + \|\nabla \tilde{\epsilon}_t\|^2_{\mathcal{L}_2(t)} + \|\nabla \hat{\epsilon}_t\|^2_{\mathcal{L}_2(t)} \right\}^{1/2}.$$

In both the cases, the definitions of *ENORM1* and *ENORM2* are similarly modified.

Local error estimates are stored in the array E. This array has $MAXT$ rows and two columns. Row I of E corresponds to element t_I, with entry $E(I,1) = \eta^2_{t_I}$, and $E(I,2) = \alpha_{t_I}$. The contents of the E array can be graphically displayed using *TRIPLT* (see Section 5.2). The E array is typically updated in *TRIGEN* as part of adaptive algorithms that make use of the error estimates. Thus if one is interested in viewing uncorrupted versions of these quantities, plot them after calling *TRIGEN* with $IADAPT = 0$.

3.4 Adaptive Mesh Refinement and Unrefinement.

Our adaptive algorithms are based on work described in Nguyen [54], Bank and Nguyen [21, 23, 22, 24], and Bank and Deotte [12]. When $IADAPT = 1$, the current mesh is adaptively refined or unrefined. When $NDTRGT > NDF$, the mesh is refined, while if $NDTRGT < NDF$, the mesh is unrefined. In either case, the goal is to achieve the best possible mesh using (approximately) $NDTRGT$ degrees of freedom. The switch *IRTYPE* specifies the type of adaptivity to be used – h, p, or hp as indicated in Table 3.3.

IRTYPE	adaptivity option
0	hp refinement / unrefinement
1	h refinement / unrefinement
-1	p refinement / unrefinement

Table 3.3. *Adaptivity options using IRTYPE.*

When $IADAPT = 2$, both refinement and unrefinement are employed. First, the mesh is unrefined to obtained a mesh with approximately $NDTRGT < NDF$ degrees of freedom. The mesh is then refined to obtain a mesh with approximately NDF degrees of freedom. The output triangulation thus has approximately the same number of degrees of freedom as the input triangulation, but the topology of the mesh and the distribution of degrees of freedom can be quite different.

3.4.1 Procedure Refine

Our *hp* refinement procedure is summarized in Figure 3.2. We initialize a heap data structure where all elements are placed in the heap according to the size of η_t, with the element with largest error indicator at the root.

Procedure Refine

R1 Create a heap with respect to η_t with the largest error estimate η_{tmax} at the root;
R2 If $NDF \approx NDTRGT_0$, then go to **R6**.
If $\eta^2_{tmax} \le \eta^2_{ave}/3$, then go to **R6**.
R3 Execute case specific tests for h, p, and hp refinement of element $tmax$.
R4 Refine element $tmax$, and possibly others as required.
R5 Update error indicators for affected elements.
Add new elements as needed. Remake the heap.
Go to **R2**.
R6 Smooth the mesh based on geometry ((3.1)–(3.2)).
Clean up data structures as needed.

Figure 3.2.

When $IADAPT = \pm 1$ and $NDTRGT > NDF$, the target number of degrees of freedom for the new mesh, denoted by $NDTRGT_0$, is given by

$$NDTRGT_0 = \min(NDTRGT, NDF \times 4). \tag{3.5}$$

The use of (3.5) tries to force a geometric increase in the number of degrees of freedom in each refinement step. For the the case $IADAPT = \pm 2$, $NDTRGT_0 = NDF_0$, where NDF_0 was the value of NDF when *TRIGEN* was entered.

While we normally expect the refinement loop to exit when the target number of degrees of freedom is approximately achieved in line **R2** of Procedure Refine, we can also exit if the largest error in the current mesh is sufficiently small. In particular,

$$\eta^2_{ave} = \frac{1}{N} \sum_{t \in \Omega_I} \eta^2_t \equiv EAVE2, \tag{3.6}$$

where Ω_I is the fine subregion associated with processor I in the case of parallel computation, and $\Omega_I \equiv \Omega$ otherwise; N is the number of triangles in Ω_I.

For *hp*-refinement, the critical test is to decide between between *h*-refinement and *p*-refinement for element $tmax$. The main test is to use *h*-refinement if

$$E(tmax, 2) \equiv \alpha_{tmax} \ge 2 \times SFAVE. \tag{3.7}$$

If the scaling factor $\alpha_t \approx 1$, then the recovered derivatives and the error estimate are consistent, and we assume that the solution is locally smooth, which in turn justifies *p*-refinement. Large values of α_t empirically correspond to locally non-smooth behavior of the solution, and this in turn suggests *h*-refinement. See [24, 12]

for more detailed explanations and numerical experiments, and Bank, Parsania and Sauter [27] for some convergence analysis.

While (3.7) is the main test for *hp*-refinement, we also make some case specific tests on line **R3** of Procedure Refine. In the case of *h*-refinement, we test for potential round-off error problems if *h*-refined elements become too small in size. In the case of *p*-refinement, we check to be sure the *p*-refined element will have degree less than *MXORD*. We require that $MXORD \leq 9$ due to limits on the order of accuracy for the suite of numerical quadrature rules implemented in *PLTMG*. These quadrature formulas were provided by Zhang, Cui, and Liu in [64]. Failure of these case specific tests could reverse the decision suggested by (3.7). Finally, if element *tmax* has degree k, and

$$RELERP \leq \frac{1}{5 \times 3^{k-1}} \tag{3.8}$$

then *h*-refinement is selected. The thresholds (3.8) are based on the empirical observation that it is efficient to require sufficiently many elements in the mesh (as measured by (3.8)) before allowing increasingly higher degree elements.

At the conclusion of the main refinement loop, in **R6** we smooth the mesh, locally "flipping" edges and adjusting the location of vertices to locally optimize the geometric quality measure $q(t)$ given in (3.1).[5]

3.4.2 Procedure Unrefine

Our unrefinement procedure is complementary to the refinement procedure, as summarized Figure 3.3. In many details, it implements the opposite rules of Procedure Refine. For example, we initialize a heap data structure where all elements are placed in the heap according to the size of η_t, but now with the element *tmin* with the smallest error error indicator at the root.

If $IADAPT = \pm 1$ or $IADAPT = \pm 2$, then $NDTRGT_0$ is given by

$$NDTRGT_0 = \max(NDTRGT, NDF/4).$$

This generally provides a geometric decrease in the number of degrees of freedom. The parameter η_{ave} in **U2** is computed as in (3.7).

For *hp*-unrefinement, the main test is based on (3.7). If (3.7) and

$$RELERP \geq \frac{1}{5}$$

are both satisfied, then use *h*-unrefinement; otherwise use *p*-unrefinement. Our bias here is to try to preserve the largest number of elements in the mesh. The result of this test is possibly changed on the basis of the *h* and *p* specific tests mentioned below. The case specific test for *h*-unrefinement determines the best vertex of

[5] In adjusting the mesh, we take into account constraints imposed by boundary geometry, boundary conditions, and internal interfaces defined by the the user or by *PLTMG* in the context of parallel computation.

Procedure Unrefine

U1 Create a heap with respect to η_t with the smallest error estimate η_{tmin} at the root;
U2 If $NDF \approx NDTRGT_0$, then go to **U6**.
If $\eta^2_{tmin} \geq \eta^2_{ave}/2$, then go to **U6**.
U3 Execute case specific tests for h or p unrefinement of element *tmin*.
U4 Unrefine element *tmin*, and possibly others as required.
U5 Update error indicators for affected elements.
Remove elements as needed. Remake the heap.
Go to **U2**.
U6 Smooth the mesh based on geometry ((3.1)–(3.2)).
Clean up data structures.

Figure 3.3.

element *tmin* to be removed from the mesh.[6] For p-unrefinement, an element must have degree at least two.

Similar to Procedure Refine, at the conclusion of Procedure Unrefine, the final mesh is smoothed, and some edges possibly flipped in **U6** to locally optimize the geometric quality as measured by (3.1).

3.4.3 h Refinement

Our basic h-refinement algorithm uses a relaxed version of the longest edge bisection procedure of Rivara [49, 58] but does not generate a refined element tree. The element *tmax* to be refined is bisected along it longest edge. If *tmax* has a neighbor element across its longest edge, and the shared edge is longer than 0.9 times its longest edge, then it is refined. If not, the neighbor is refined along its longest edge, and the procedure described above is recursively applied to its longest-edge neighbor. An example is shown is Figure 3.4. The classic (unrelaxed) longest edge bisection process is known to have finite termination, typically in a very small number of steps. The relaxation factor 0.9 attempts to make the process terminate even sooner; it is small enough that the test is satisfied by most shape regular elements, so that only one edge is bisected in most steps of **R4** in Procedure Refine (Figure 3.2).[7]

When our relaxed longest edge bisection process finally results in a triangulation, elements are bisected, new elements created, (in reverse order to always maintain a triangulation) and the triangulation data structures updated. New elements inherit the (constant) derivative values from their parents, allowing error estimates to be computed for the refined elements, and the heap to be updated.

[6] Certain vertices lying on the boundary or on internal interfaces are not eligible to be removed from the mesh. In exceptional cases an element might be deemed ineligible for h-unrefinement.

[7] Since shape regularity is improved in step **R6** of Procedure Refine, we relax shape regularity requirements during the refinement process itself to improve efficiency.

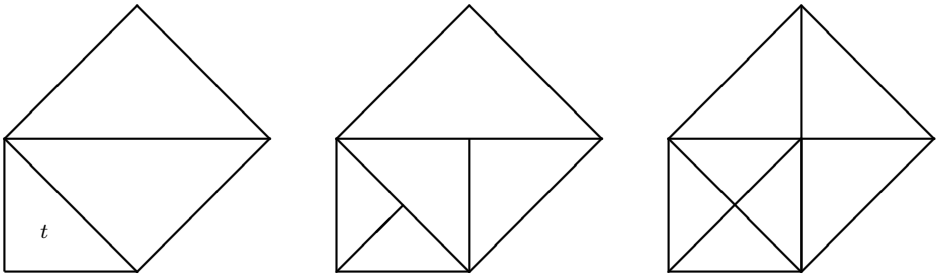

Figure 3.4. *Element t is refined by the longest edge bisection method. The original mesh is on the left. The first step of bisection (middle) does not yield a compatible triangulation. However, the second step (right) does yield a triangulation.*

3.4.4 h Unrefinement

In the case of h-unrefinement, the basic step consists of deleting vertices from the mesh; this is accomplished by merging two vertices of element *tmin* that share a common edge. This is illustrated in Figure 3.5.

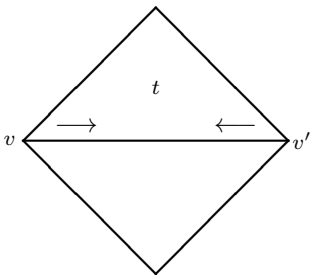

Figure 3.5. *Element t is unrefined by the merging vertices v and v', and collapsing the edge connecting them. The location of the merged vertex could be v, v', or $(v + v')/2$, depending on the shape quality of other elements having v or v' as one of their vertices.*

While this merging process tends to degrade the geometric quality of surrounding elements, it is typically restored in step **U6** of Procedure Unrefine, when element edges are flipped and vertices moved to locally optimize the quality measure (3.1).

3.4.5 p Refinement

The p-refinement algorithm is relatively straightforward. Let element $tmax$ have degree p with edges of degree $p_i \geq p$, $1 \leq i \leq 3$. The refined element has degree $p+1$ with edges of degree $\max\{p_i, p+1\}$, $1 \leq i \leq 3$. As a technical point, since we require degrees of freedom associated with element interiors and edges have consecutive global indices,[8] storage arrays (e.g., GF) have degrees of freedom for p-refined edges and interiors appended to their tails, leaving gaps where earlier edge and interiors degrees of freedom were stored. There is a global cleanup step at the end of the refinement process to compress the data structure and remove these gaps, similar to that performed at the end of unrefinement algorithms.

3.4.6 p Unrefinement

p-unrefinement is similar in structure to p-refinement. An element of degree p has it interior decreased to degree $p-1$. The edge degrees of freedom p_i, $1 \leq i \leq 3$, are reduced to $p_i - 1$ or remain at degree p_i, depending on the degree of the neighbor element (if present) that shares the given edge. In the case of degree reduction, the reduced degrees of freedom can occupy space previously used by the higher degree edges or interior degrees of freedom, leaving small gaps in these data structures that are removed at the end of the unrefinement process.

3.5 Adaptive Mesh Smoothing.

When $IADAPT = \pm 3$, subroutine *TRIGEN* does no refinement or unrefinement of the mesh but rather adjusts the (x, y) coordinates of the mesh points (VX and VY) in an attempt to optimize the mesh.

The procedure consists of a Gauss–Seidel-like iteration on the vertices in the mesh, where each vertex is locally optimized with all other vertices held fixed [30]. Four sweeps are performed in each call. Let Ω_v denote the patch of elements that share a given vertex v; an example is shown in Figure 3.6. Typically, vertex v is allowed to move within the region Ω_v. However, not all vertices in the mesh are allowed to move. Some boundary and interface vertices must remain fixed to preserve the definition of the region. These vertices are called *corners*. Corners include actual geometric corners of the region, vertices where boundary conditions change type or label, vertices where interfaces intersect the boundary, and vertices where two or more interfaces intersect. An interface here is taken as any sequence of triangle edges that separate triangles with different user defined labels. Vertices on the boundary or on interfaces that are not designated corners are allowed to move only along the boundary or interface. The remaining vertices, called *interior* vertices, are allowed to move freely within Ω_v. As in our refinement algorithms, some local mesh smoothing based on (3.1) is used to locally optimize the shape regularity of the mesh.

[8] Having consecutive indices for interior and edge degrees of freedom makes the amount of information stored in array *ITDOF* for a given element independent of its degree.

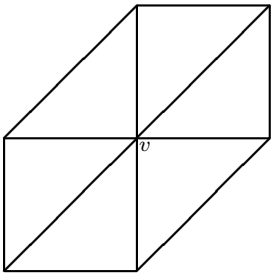

Figure 3.6. *Subregion Ω_v is associated with vertex v.*

For each vertex $v = (x, y)$ in the mesh, we solve the minimization problem

$$\min_{x,y} \|\nabla \epsilon_t\|^2_{\mathcal{L}_2(\Omega_v)} \tag{3.9}$$

of order two by a damped Newton's method. As noted above, we assume the derivatives of order $p+1$ are constant in each element t having v as a vertex, leading to an overall piecewise constant approximation of these derivatives on Ω_v. All other dependencies on $v = (x, y)$ are taken into account by Newton's method. Boundary and interface vertices have an additional constraint equation, so an appropriately constrained version of problem (3.9) is solved for those vertices. Besides its usual task of ensuring sufficient decrease, the damping strategy for Newton's method is also used to ensure that the point (x, y) remains well within Ω_v, so that all triangles are always well defined. It is interesting to note that the function $\|\nabla \epsilon_t\|_{\mathcal{L}_2(\Omega_v)}$ contains a natural barrier function that becomes infinite as (x, y) approaches $\partial\Omega_v$.

In the case $IADAPT = -3$, the adaptive smoothing procedure uses the interpolation errors for the function QXY in place of the a posteriori error estimates, in a fashion analogous to the cases of refinement and unrefinement with $IADAPT < 0$.

3.6 Uniform Refinement.

TRIGEN allows options for uniform refinement in h and p. In the standard sequential setting, the uniform refinement is standard and straightforward. In the case of parallel computation, each processor approximately uniformly refines its own subregion. If the parallel computation uses *NPROC* processors, each processor adds approximately $1/NPROC$ of the expected increase in degrees of freedom resulting from uniform refinement in the standard sequential case. Because different subregions can have widely varying numbers of elements, this can result in different levels of uniform refinement in different regions. See Section 3.8 for discussion of the mesh partitioning process.

3.6.1 h Uniform Refinement

When $IADAPT = 4$, subroutine *TRIGEN* performs uniform h-refinement of the existing triangulation. The refinement is controlled by the parameter $IREFN > 1$. Each element in the triangulation is uniformly divided into $IREFN^2$ similar triangles. Some examples are shown in Figure 3.7. If $IADAPT = 4$ and $MPISW = 1$, the situation is different. In this case, *TRIGEN* tries to increase the global dimension of the space by roughly a factor of $IREFN^2$. The target value for each processor is given by

$$NDTRGT_0 = \min\left(NDTRGT, NDF \times \left\{1 + \frac{IREFN^2 - 1}{NPROC}\right\}\right).$$

Each processor refines uniformly, restricting this refinement mainly to region *IRGN*. Rather than the uniform refinement described above, the relaxed longest edge procedure is used. Regions with relatively few elements may require several levels of refinement to achieve the target number of degrees of freedom; those with many elements may need only one partial level of refinement to achieve this target. In the case of partial levels of refinement, the elements chosen to be refined are essentially random.

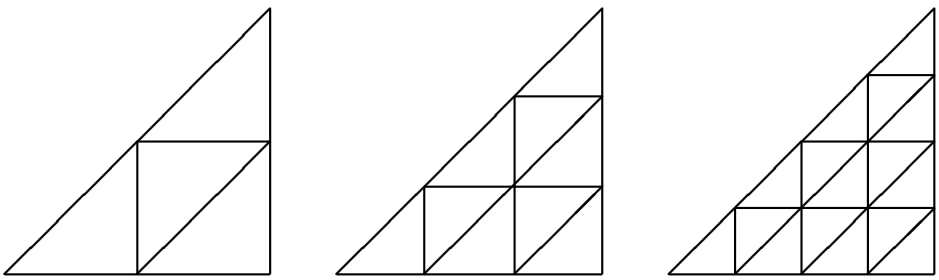

Figure 3.7. *Uniform refinement for the cases* $IREFN = 2, 3, 4$.

3.6.2 p Uniform Refinement

When $IADAPT = -4$, subroutine *TRIGEN* performs uniform p-refinement of the existing triangulation. The refinement is controlled by the parameter $IREFN > 0$. In this case, every element interior of degree p is increased to degree $\min(p + IREFN, MXORD)$, and every edge of degree p_i is increased to degree $\min(p_i + IREFN, MXORD)$. If $IADAPT = -4$ and $MPISW = 1$, *TRIGEN* does uniform p refinement, but restricts this refinement mainly to region *IRGN*. In this case, the target number of degrees of freedom is given by

$$NDTRGT_0 = \min\left(NDTRGT, NDF \times \left\{1 + \frac{[(p_{ave} + IREFN)/p_{ave}]^2 - 1}{NPROC}\right\}\right),$$

where p_{ave} estimates the average degree of elements in the mesh and is given by

$$p_{ave} = \sqrt{\frac{NDF}{NVF}}.$$

Similar to the case of $IADAPT = 4$, degrees of some elements may be increased by more than *IREFN* if few elements are present in *IRGN*. If there are many elements in *IRGN* some elements may have their degrees increased by less than *IREFN*, or even left unchanged. The elements chosen for partial levels of p refinement are essentially random, as in the case of h uniform refinement.

3.7 An Example

Some examples of our adaptive procedures are shown in Figures 3.8–3.9. In these examples, we employ the alternate function $QXY = r^{1/4}\sin(\theta/4)$ defined on the circular domain with a crack shown in Figure 2.1. The initial mesh with $NVF = 10$ is shown in Figure 3.8, top. The mesh was then refined with $IADAPT = -1$ to produce a sequence of *hp* adapted meshes. In Figure 3.8, we see the resulting mesh with $NTF = 7386$ elements and $NDF = 18362$ degrees of freedom.

In the next experiment, we begin with the same mesh with $NTF = 8$ elements and uniformly refine it using $IADAPT = 4$ and $IREFN = 8$, creating a uniform mesh of $NTF = 512$ elements. We the uniformly refine in p ($IADAPT = -4$ and $IREFN = 2$) to create a uniform mesh of piecewise cubic polynomials with a total of $NDF = 2425$ degrees of freedom.

We employ adaptive mesh smoothing ($IADAPT = -3$); in Figure 3.9 we see the results of one step and eight steps of mesh smoothing. It is visually apparent that the mesh smoothing tries to concentrate degrees of freedom near the singularity at the origin. However, mesh smoothing is limited by the constraint that the mesh topology remain invariant, and this ultimately limits its effectiveness in this setting.

Next, we call *TRIGEN* int $IADAPT = -2$ (unrefine and refine) and $NVTRGT = 1800$. The results are shown in Figure 3.9, where the mesh is colored by both polynomial degree and by element size. We see that in the unrefinement phase, most of the coarsening consisted mostly of p-unrefinement, reducing the polynomial degree from three to two in those elements most distant from the origin, when the error should be smallest. The refinement step was mostly h-refinement, where elements near the origin were refined. This seems like a reasonable outcome given that the unrefinement and refinement steps are conducted sequentially and independently. However, one could argue that a more informed strategy in this situation is to coarsen in p the elements *near* the origin, which have *larger* errors, and then h-refine those elements using lower degree polynomials. Such a strategy requires more specialized coarsening and refinement algorithms than currently exist in *PLTMG* and is a topic for future research.

3.8 Parallel Adaptive Methods.

In this section we summarize the general strategy for adaptive mesh generation that is implemented in *PLTMG*. A number of static and dynamic load balancing

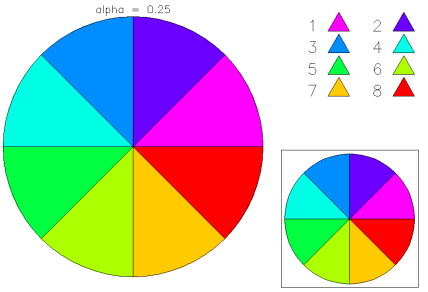

The initial triangulation with NTF = 8, NVF = 10, and NBF = 10.

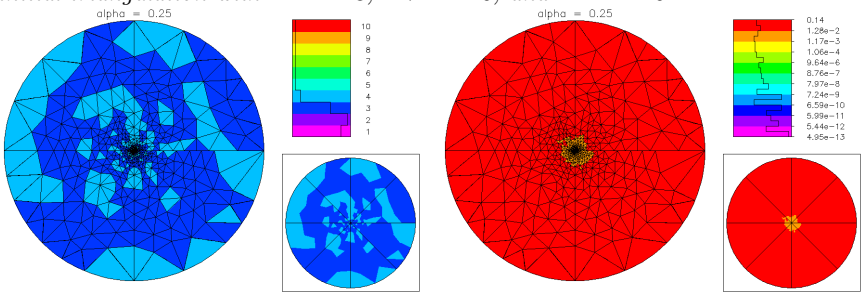

The refined triangulation with NTF = 7386, NDF = 18362. Elements are colored by polynomial degree (left) and by element size (right).

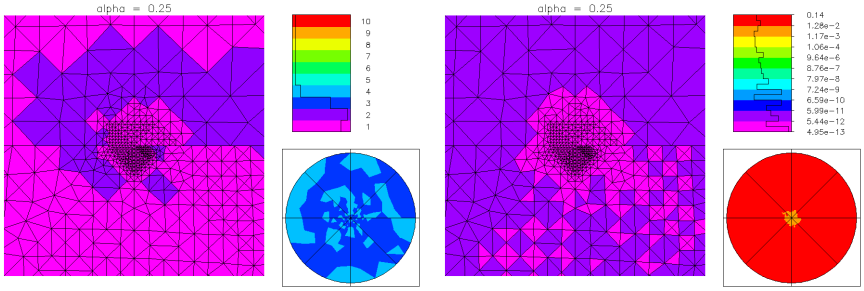

The refined triangulation with NTF = 7386, NDF = 18362. The mesh is magnified near the origin with RMAG = 10^{10}, revealing the presence of low degree polynomials (left) and very small elements (right).

Figure 3.8.

approaches for unstructured meshes have been proposed in the literature [62, 59, 43, 45, 40, 47, 41]; most of the dynamic strategies involve repeated application of a particular static strategy. One of the difficulties in all of these approaches is the amount of communication that must be performed both to assess the current load imbalance severity, and to redistribute the work among the processors once the imbalance is detected and an improved distribution is calculated.

The approach used by *PLTMG* is based upon the Bank-Holst paradigm [14, 15, 5, 25, 55, 50, 51], that addresses the load balancing problem in a new way, requiring far less communication. Another important point is that our approach

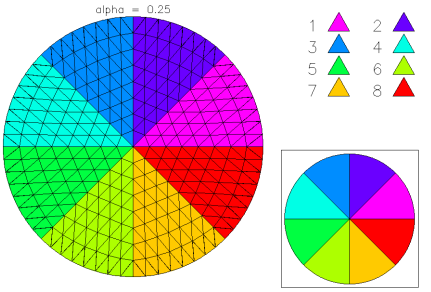

A Uniformly refined mesh with NTF = 512, NVF = 297, and NBF = 80.

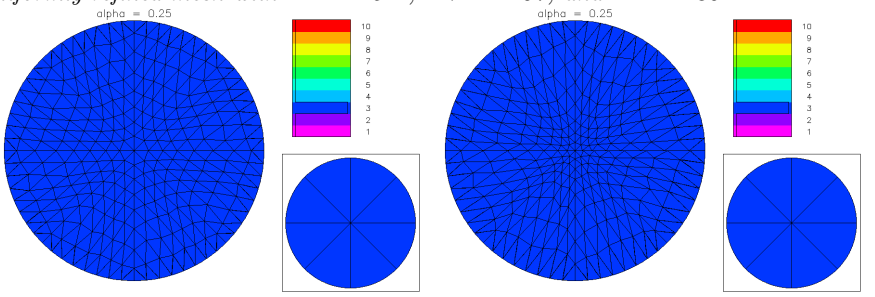

The uniformly refined mesh after one step of mesh smoothing (IADAPT = −3), with piecewise cubic elements, NDF = 2425 (left). The same mesh after eight steps of mesh smoothing (right).

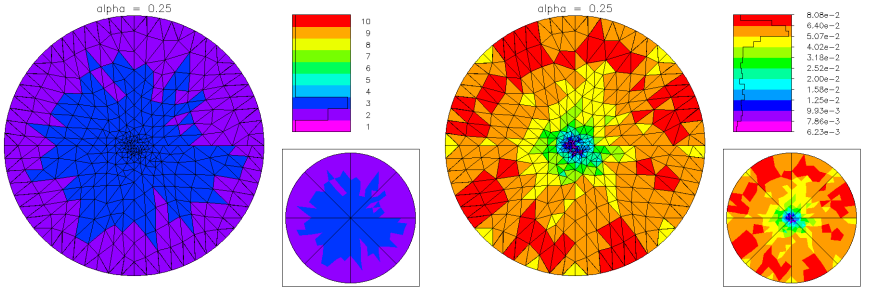

The mesh resulting from one step of unrefinement and refinement (IADAPT = −2) with NDTRGT = 1800. The resulting mesh is colored by polynomial degree (left) and element size (right) and has NTF = 648 elements with NDF = 2424 degrees of freedom.

Figure 3.9.

allows *PLTMG* to run in a parallel environment without a large investment in additional coding. This approach has three main components:

Step 1: A small (nonlinear) problem is solved on an initial coarse mesh, and *a posteriori* error estimates are computed for the coarse grid solution. The triangulation is partitioned such that each subdomain has approximately equal *error* (although they can significantly differ in size, numbers of elements and degrees of freedom).

Step 2: Each processor is provided the complete coarse mesh and solution, and instructed to solve the *entire* (nonlinear) problem, with the stipulation that its adaptive refinement should be limited largely to its own partition. Load balancing is achieved by instructing each processor to create a refined mesh with the same number of degrees of freedom.

Step 3: A final mesh is computed using the union of the refined partitions provided by each processor. This mesh is reconciled such that the (virtual) mesh made up of the union of the refined subregions would be conforming. A final solution is computed, using a domain decomposition method. An initial guess is provided by the local solutions.

The above approach has several interesting features. First, the load balancing problem (Step 1) is reduced to the numerical solution of a small problem on a single processor, without requiring any modifications to *PLTMG*. Second, the adaptive mesh generation calculation (Step 2) takes place independently on each processor, and can also be performed with no communication.

The only parts of the calculation requiring communication are

1. the initial fan-out of the mesh distribution to the processors, once the decomposition is determined by the error estimator.

2. the mesh regularization, requiring communication to produce a global conforming mesh.

3. the final solution phase. Note that a good initial guess for Step 3 is provided in Step 2 by taking the solution from each subregion restricted to its partition.

The options $6 \leq IADAPT \leq 7$ provide basic parallel mesh management tools that support this paradigm. The domain decomposition solver is implemented as an option in subroutine *PLTMG*. These options require the use of MPI library routines for communication.

3.8.1 Mesh Partitioning.

When $IADAPT = 6$, *TRIGEN* computes *a posteriori* error estimates and partitions the mesh as in the Bank-Holst paradigm. If *PLTMG* is running on *NPROC* processors, then the mesh is partitioned into *NPROC* subregions, such that each subregion has approximately equal error. Deotte [44] and Bank and Deotte [11] examine several partitioning strategies, including the one used in *PLTMG*, and in particular study their effect on the convergence rate of Domain Decomposition solvers using such partitions. The underlying algorithm employed is a variant of the recursive spectral bisection algorithm [42, 57, 60]. While this particular mesh partitioning algorithm is among the more expensive of the choices that we could make, it is typically used only once on a relatively small problem. Although this calculation is important in the parallel processing environment, it is done on a single processor and does not use the MPI library. At the conclusion of the load balancing step, *TRIGEN* creates new internal edges in *IBNDRY* at the interface between different

subregions. Then the processor corresponding to $IRGN = 1$ broadcasts its mesh, solution, and supporting data to all processors using an MPI broadcast command.

The partitioning process begins with the creation of patches of elements with small errors called macro-elements. Macro-element patches contain a minimum of one and a maximum of 100 elements and must form a geometrically connected set. Let

$$E = \frac{1}{NPROC} \sum_t \|\nabla \epsilon_t\|^2_{\mathcal{L}_2(t)}.$$

For a patch P, let

$$E_P = \sum_{t \in P} \|\nabla \epsilon_t\|^2_{\mathcal{L}_2(t)}.$$

If the patch P contains more than one element, we require $E_P \leq 10^{-2} \times E$.

Suppose the mesh is composed of N macro-elements. We define the $N \times N$ symmetric, positive semi-definite M-matrix A by

$$A_{ij} = \begin{cases} -\ell & i \neq j \text{ and patches } i \text{ and } j \text{ share } \ell \text{ common edges} \\ 0 & i \neq j \text{ and patches } i \text{ and } j \text{ share no common edge} \\ s_i & i = j,\ s_i = -\sum_{k \neq i} A_{ik} \end{cases}$$

Macro element patches are created to reduce the order of the matrix A, and thus reduce the cost of solving the eigenvalue problems described below. The matrix A corresponds to the *discrete Laplacian* for the dual graph of the macro element mesh, in which the macro elements are considered nodes, and the off-diagonal entries correspond to edges defined by the adjacency relation, weighted by the number of overlapping edges in the original triangulation.

We consider the eigenvalue problem

$$A\psi = \lambda\psi \tag{3.10}$$

Our approach is standard; by construction, the smallest eigenvalue for (3.10) is $\lambda_1 = 0$ and $\psi_1 = (1, 1, \ldots, 1)^t$. Our interest is in the second eigenvector ψ_2, known as the Fiedler vector.

We use a standard binary tree with $2\,NPROC - 1$ nodes ($NPROC$ leaves and $NPROC - 1$ internal nodes). The root is labeled $i = 1$ and node i has children $2i$ and $2i + 1$, $1 \leq i \leq NPROC - 1$. Associated with each node is a weight ω_i denoting the number of leaves contained in its subtree. In particular, $\omega_i = 1$, $i = 2\,NPROC - 1, \ldots, NPROC$ and $\omega_i = \omega_{2i} + \omega_{2i+1}$ for $i = NPROC - 1, \ldots, 1$.

The entire mesh is assigned to root, and it is partitioned among its two children as follows. We first approximately solve the eigenvalue problem (3.10) for the whole mesh, and then create a permutation of the macro-elements $\{q_i\}$ such that

$$q_i < q_j \quad \text{implies} \quad \psi_{2,i} \leq \psi_{2,j}.$$

We then find the index k which provides the best partition of the form

$$\frac{1}{\omega_2} \sum_{q_i \leq k} E_{P_{q_i}} \approx \frac{1}{\omega_3} \sum_{q_i > k} E_{P_{q_i}}.$$

The corresponding submeshes are assigned to the children nodes.

We apply this procedure recursively, at each level dividing each group of element patches into two smaller groups by solving an eigenvalue problem of the type (3.10) restricted to that group of patches. The final result is *NPROC* subregions with approximately equal error E.

We now briefly describe some details of our procedure for computing the second eigenvector of (3.10). Our procedure is essentially just a classical Rayleigh quotient iteration [56], modified both to bias convergence to λ_2, and to account for the fact that the linear systems arising in the inverse iteration substep are solved (approximately) by an iterative process. To simplify notation and avoid multiple subscripts, we let $\phi_k \approx \psi_2$, where k now denotes the iteration index.

We suppose that we have a current iterate ϕ_k which satisfies $\phi_k^t \phi_k = 1$ and $\psi_1^t \phi_k = 0$. Using ϕ_k, we compute the approximate eigenvalue $\tilde{\lambda}_{2,k} \approx \lambda_2$ from the Rayleigh quotient $\tilde{\lambda}_{2,k} = \phi_k^t A \phi_k$, and approximately solve the linear system

$$A\tilde{\delta}_k = r_k \equiv \tilde{\lambda}_{2,k}\phi_k - A\phi_k.$$

Note that by construction $\psi_1^t r_k = \phi_k^t r_k = 0$. This linear system is approximately solved using a simple Symmetric Gauss-Seidel iteration.

From $\tilde{\delta}_k$, we form the vector δ_k satisfying $\delta_k^t \delta_k = 1$ and $\psi_1^t \delta_k = \phi_k^t \delta_k = 0$. Finally, we solve the 3×3 eigenvalue problem for $\hat{A}$, where

$$\hat{A} = \begin{pmatrix} \phi_k^t \\ \delta_k^t \\ \xi_k^t \end{pmatrix} A \begin{pmatrix} \phi_k & \delta_k & \xi_k \end{pmatrix}$$

where ξ_k is defined below. If $v = (\alpha, \beta, \gamma)^t$ is an eigenvector corresponding to the smallest nonzero eigenvalue, we form $\tilde{\phi}_{k+1} = \alpha\phi_k + \beta\delta_k + \gamma\xi_k$ and $\tilde{\xi}_{k+1} = \beta\delta_k + \gamma\xi_k$ with $\xi_1 = 0$. Then ϕ_{k+1} and ξ_{k+1} are formed from $\tilde{\phi}_{k+1}$ and $\tilde{\xi}_{k+1}$, respectively, by normalization and orthogonalization to ψ_1. Solving the 3×3 eigenvalue problem rather than a 2×2 problem was motivated by the work of Knyazev [46].

3.8.2 Reconciling the Mesh.

The option *IADAPT* = 7 reconciles the mesh. This is the most complex of the MPI options in *TRIGEN*, and is typically called once, at the conclusion of the second step of the Bank-Holst paradigm. It **must** be called before the domain decomposition solution in subroutine *PLTMG*, as *PLTMG* makes use of the parallel interface data structure *IPATH* generated by this call.

In creating the *IPATH* data structure, each processor first organizes its triangulation and solution data structures. Generally, edges, vertices, and degrees of freedom on the interface between region *IRGN* and the rest of the domain appear first in their respective arrays (*IBNDRY*, *VX*, *VY*, *GF*, etc). This data is organized to correspond to counter clockwise traversal of the interface. Next in all arrays comes data corresponding to the interior of subregion *IRGN*; generally, this should be the majority of the data. Finally, at the end of each array appears data corresponding to regions other than *IRGN*. Each processor then assembles its

contributions to the preliminary *IPATH* array based on the reordered data, and this information is then exchanged among processors using MPI (see Section 2.6).

After the boundary exchange, each processor tries to match its boundary interface edges to those provided by neighboring regions, in order to establish the structure of the global mesh. Typically this mesh is not conforming. When non-matching edges are found, the region that is less refined does additional refinement until its boundary edges form a one-to-one match with those of its neighbors. An example is shown in Figure 3.10.

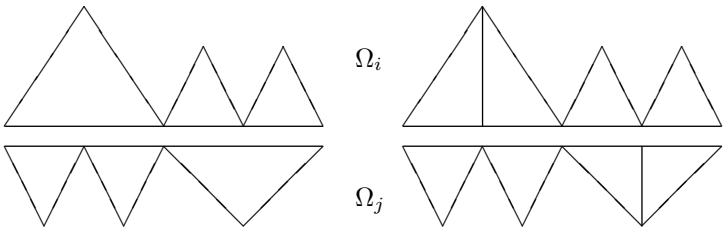

Figure 3.10. *The coarse side of a non matching interface (left) is refined to make the global mesh conforming (right).*

After the mesh is made h-conforming it is made p-conforming. When a p-nonconforming edge is found, the region containing the edge of lower degree p-refines its edge appropriately in order to resolve the nonconformity.

Each processor then reorders its data structures and communicates its contribution to the *IPATH* array a second time. This time the edge matching process concludes with no nonconforming edges found. By matching boundary edges at the interface, one also effectively matches degrees of freedom on the interface; it is this information that is needed for the domain decomposition solver.

Chapter 4
Equation Solution

4.1 Overview.

Subroutine *PLTMG* solves the problems described in Section 1.1. The solution process for each class of problems has certain unique aspects, but all make use of Newton's method. Subroutine *PLTMG* is entered using the statement

Call PLTMG(VX, VY, SF, ITNODE, IBNDRY, ITDOF, IPATH,
E, IP, RP, SP, GF, A1XY, A2XY, FXY, GNXY, GDXY,
P1XY, P2XY, SXY)

On input, the arrays *VX*, *VY*, *SF*, *ITNODE*, *ITDOF*, and *IBNDRY* define a triangulation. Arrays *IPATH E*, and *GF* are discussed in Sections 2.5 and 2.6. Fortran subroutines *A1XY*, *A2XY*, *FXY*, *GNXY*, *GDXY*, *P1XY*, and *P2XY* are documented in Section 2.8. Subroutine *SXY* is documented in Section 2.2. Parameters in the *IP*, *RP*, and *SP* arrays read and written by *PLTMG* are summarized in Tables 2.12–2.14.

The parameter *IPROB* indicates the problem class; the various options are shown in Table 4.1. The case $IPROB > 0$ indicates a standard sequential solve, either on a single processor, or on multiple processors as part of the second phase of the Bank-Holst paradigm. The case $IPROB < 0$ indicates the global parallel domain decomposition solve as part of the Bank-Holst paradigm. Because this is a global solve it involves some MPI communication at each iteration step. When $IPROB < 0$, the parallel domain decomposition solve is preceded by a local solve on each processor, in order to insure the quality of the initial guess for the global problem.

The cases $IPROB = \pm 3$ and $IPROB = \pm 4$ have various suboptions unique to their particular problem class. The available options are specified through the parameter *ITASK*. These are summarized in Table 4.2.

IPROB	problem option
1	elliptic boundary value problem
2	obstacle problem
3	continuation problem
4	parameter identification problem
5	optimal control problem
-1	DD solve for elliptic boundary value problem
-2	DD solve for obstacle problem
-3	DD solve for continuation problem
-4	DD solve for parameter identification problem
-5	DD solve for optimal control problem

Table 4.1. *The parameter IPROB.*

ITASK	*IPROB*	option
0	1	default
9		use functional
0	2	default
0	3	continue to the nearest target point
1		continue to the nearest target or singular point
2		switch branches at a bifurcation point
3		switch λ and/or ρ; initialize with λ fixed
4		switch λ and/or ρ; initialize with ρ fixed
5		solve with $\sigma = 0$, $\theta = 0$ (λ fixed)
6		solve with $\sigma = 0$, $\theta = 2$ (ρ fixed)
7		solve with $\sigma = 0$, $\theta = 1$
0	4	default
8		λ affects domain shape
0	5	default

Table 4.2. *The parameter ITASK.*

4.2 Elliptic Boundary Value Problems.

When *IPROB* = 1, *PLTMG* solves the discrete system (1.6). If the underlying boundary values problem is not self-adjoint some upwinding terms based on the Scharfetter–Gummel discretization scheme [6, 10] are added to the discretization; in this case (1.6) should be replaced by: find $u_h \in \mathcal{M}_d$ such that

$$a_h(u_h, v) = 0 \qquad \text{for all } v \in \mathcal{M}_e, \tag{4.1}$$

where $a_h(u_h, v)$ reflects the additional stabilization terms. We note that the upwinding terms are derived for the case of piecewise linear finite elements ($p = 1$). While a similar upwinding scheme is also formally applied to higher degree elements, its stability and convergence properties are not yet analyzed. In any event, (4.1) corresponds to the system of nonlinear equations

$$\mathcal{G}(\mathcal{U}) = 0, \tag{4.2}$$

where the unknown vector $\mathcal{U}$ corresponds to the values of the finite element solution u_h at the vertices of the triangulation. The Jacobian matrix

$$\mathcal{A}(\mathcal{U}) = \frac{\partial \mathcal{G}(\mathcal{U})}{\partial \mathcal{U}}$$

is a sparse stiffness matrix corresponding to a *linear* elliptic boundary value problem (linearized about $\mathcal{U}$). Even in the event the the original problem is linear, *PLTMG* solves all problems with *IPROB* = 1 as nonlinear, and formally applies Newton's method to (4.2). In Figure 4.1, we summarize our approximate Newton procedure with line search.

Procedure Newton

N1 Begin with initial guess $\mathcal{U}_0$, and a sufficient decrease parameter τ. Set $k \leftarrow 0$, $s_0 \leftarrow 1$, and compute $\mathcal{G}_0$ and $\|\mathcal{G}_0\|$.

N2 solve (approximately) $\mathcal{A}_k \delta\mathcal{U}_k = -\mathcal{G}(\mathcal{U}_k)$.

N3 compute $\mathcal{U}_{k+1} = \mathcal{U}_k + s_k \delta\mathcal{U}_k$, $\mathcal{G}_{k+1}$, $\|\mathcal{G}_{k+1}\|$, and $\xi_{k+1} = \|\mathcal{G}_{k+1}\|/\|\mathcal{G}_k\|$.

N4 if $1 - \xi_{k+1} < \tau s_k$, then decrease s_k and go to **N3**; else set $s_{k+1} \leftarrow s_k/(s_k + (1 - s_k)\xi_{k+1}/100)$ and $k \leftarrow k + 1$.

N5 if converged, then exit; else go to **N2**.

Figure 4.1.

The scalar s_k is the damping parameter. When the sufficient decrease criterion is not satisfied on line **N4** and s_k must be reduced, the next value is found through application of one step of a guarded secant/bisection algorithm to the one-dimensional minimization problem

$$\min_{s_k} \|\mathcal{G}(\mathcal{U}_k + s_k \delta\mathcal{U}_k)\|.$$

If sufficient decrease is achieved, the current s_k is used to predict s_{k+1}; this formula is designed to force rapid increase of $s_{k+1} \to 1$ when ξ_{k+1} becomes small as superlinear convergence occurs, and at the same time provide a reasonable first guess in the early stages of the Newton iteration, when damping is most important. A maximum of *MXNWTT* damped Newton iterations are allowed. *PLTMG* reports the actual number of Newton iterations used on the most recent call in the parameter *ITNUM*,

and the number of evaluations of $\mathcal{G}$ as *IEVALS*; $IEVALS \geq ITNUM$, since more than one function evaluation may be used in each line search.

As a simple example, we solve the Poisson equation

$$\begin{aligned} -\Delta u &= 1 \quad \text{in } \Omega, \\ u &= 0 \quad \text{on } \partial\Omega, \end{aligned}$$

The domain Ω was provided as a skeleton and is shown in Figure 4.2. This problem was solved using *hp* adaptive refinement using eight processors. The skeleton was triangulated, and then a mesh with $NVF = 3529$ and $NDF = 9566$, was adaptively created on one processor. The processor then did a load balance step ($IADAPT = 6$ in *TRIGEN*) and broadcast this mesh to all processors. The load balance is shown in Figure 4.2. Each processor then independently continued the refinement process on its subregion, using five *hp* adaptive refinement steps. The global refined mesh was made conforming ($IADAPT = 7$ in *TRIGEN*) and the domain decomposition solver invoked in *PLTMG* ($IPROB = -1$). The resulting global mesh had $NDF = 98115$ degrees of freedom; the global solution is shown in Figure 4.2. The global mesh colored by element size and polynomial degree is shown in Figure 4.2, along with a timing summary for the entire calculation, and a convergence history for the Domain Decomposition solver (see Section 4.4).

4.3 Linear Solvers.

All sets of linear equations involving the matrices $\mathcal{A}(\mathcal{U})$ and $\mathcal{A}(\mathcal{U})^t$ have the appearance of finite element discretizations of linear elliptic boundary value problems. These systems can be solved using a variety of preconditioners, coupled with the composite step conjugate gradient method ($ISPD = 1$) or composite step biconjugate gradient method ($ISPD = 0$). The composite step algorithms [9, 8] are similar to the standard biconjugate gradient and conjugate gradient methods, respectively, except that they occasionally proceed from the iterate for step k to the iterate for step $k+2$. Such composite steps are taken to improve the stability of the recurrence relations and smooth the behavior of the residual norm. Note in particular that the composite step conjugate gradient method can be applied to symmetric but indefinite problems. The maximum number of iterations to be used per solution is specified by the parameter *MXCG*. Note that as many as *MXCG* iterations are used each time a system of linear equations is solved.

The selection of preconditioner is governed by the parameter *METHOD* as summarized in Table 4.3. Combinations of three different matrices are used in composing these preconditioners. We remark that in all cases the matrices are ordered using a (block) minimum degree algorithm. In particular, dense blocks corresponding to element interior degrees of freedom are always ordered first, as these blocks could be eliminated through Gaussian Elimination (static condensation) without causing any fill-in.

ILU is an incomplete *LDU* factorization based on the multigraph algorithm [32, 31]. The parameter *DTOL* is the drop tolerance for this approximate factorization. Generally, smaller values of *DTOL* result in more accurate *ILU* factorizations,

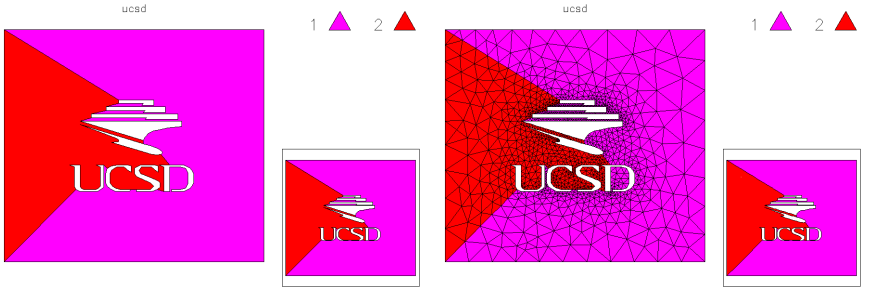

The skeleton with NVF = 135 (left) and the resulting triangulation with NVF = 1381 (right).

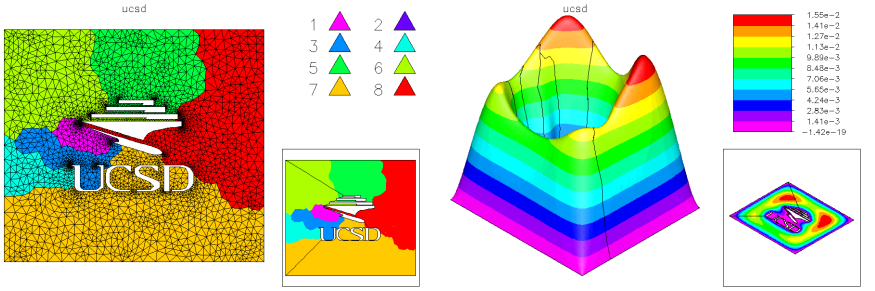

The mesh with NDF = 9566 showing the load balance (left), and the solution on the global fine mesh NDG = 98115 (right).

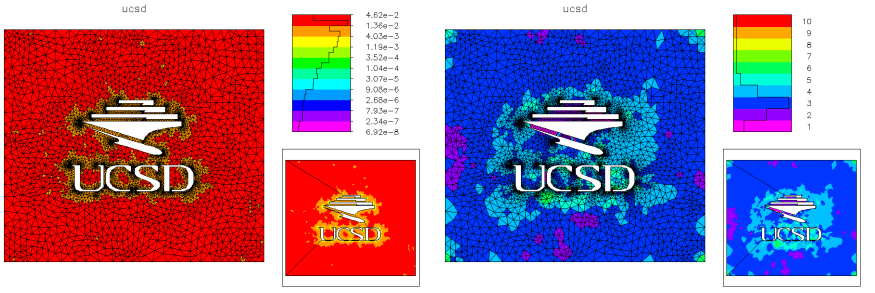

The global refined mesh colored by element size (left) and by polynomial degree (right).

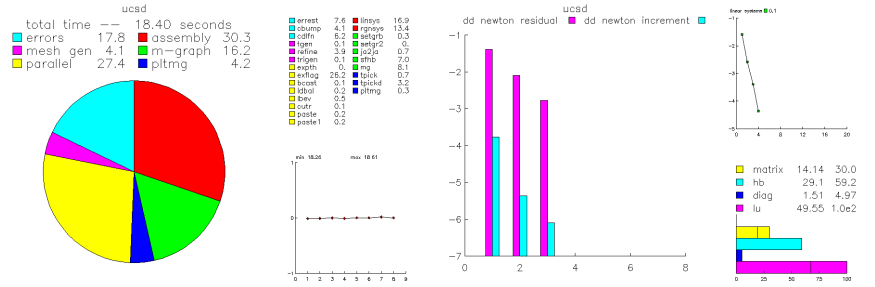

Some timing statistics (left) and convergence history for the DD solver (right).

Figure 4.2.

METHOD	preconditioner
0	Block *SGS* smoother, *HB* coarse space
1	*ILU*

Table 4.3. *The parameter METHOD.*

but higher costs in space and time per iteration. The extreme case $DTOL = 0$ results in a sparse direct factorization.

SGS is a block symmetric Gauss-Seidel preconditioner, based on the diagonal, upper and lower triangular blocks of the matrix $\mathcal{A}$. The diagonal blocks of $\mathcal{A}$ are factored using dense *LDU* factorizations. *HB* is a coarse grid correction based on hierarchical basis. Let $\mathcal{M}$ denote the *hp* finite element space used in assembling the matrix $\mathcal{A}$. Our coarse space $\mathcal{M}_c \subset \mathcal{M}$ is composed as the union of the following sets of basis functions.

1. A standard continuous piecewise linear nodal basis function is associated with each vertex in the mesh.

2. For every edge in the triangulation with $p \geq 2$, we associate a continuous piecewise quadratic nodal basis function (quadratic bump function) corresponding to the edge midpoint.

3. For every element in the triangulation with $p \geq 3$, we associate a continuous piecewise cubic nodal basis function (cubic bubble function) corresponding to the element barycenter.

The maximum dimension of $\mathcal{M}_c$ is approximately $6 \times NVF$, if every quadratic bump and cubic bubble function is present. The coarse space matrix $\mathcal{A}_c$ is computed from $\mathcal{A}$ by

$$\mathcal{A}_c = S^t \mathcal{A} S$$

for an appropriately defined rectangular change of basis matrix S. Then we compute an approximate *LDU* factorization of the matrix $\mathcal{A}_c$. The parameter *DTOL* is the drop tolerance for this approximate factorization. This approximate factorization serves as the coarse grid correction in a two-level preconditioner. One cycle of the two level iteration consists of one pre-smoothing step (*SGS*), followed by the coarse grid correction step, and one post-smoothing step (*SGS*).

As a general remark, the *SGS/HB* two-level solver typically requires less setup time but more solution time compared to *ILU*. Overall, *ILU* becomes increasingly effective when there are many high degree elements and the matrix $\mathcal{A}$ becomes increasingly dense. *ILU* also is very effective on convection dominated highly nonsymmetric problems. The *SGS/HB* two-level solver is most effective when there are many low degree elements in the mesh. Finally, note that a direct method is available using *ILU* with $DTOL = 0$.

4.4 Domain Decomposition Solver

Here we describe the domain decomposition algorithm implemented in *PLTMG* for Step 3 of the Bank-Holst paradigm (see Section 3.8). This algorithm is described in detail in [18, 4, 48, 34]. It is motivated by and similar to the domain decomposition algorithms described in [17, 16]. In the case $IPROB = -1$, this solver is used in place of the simple linear solver in line **N2** of Procedure Newton given in Figure 4.1.

For simplicity in our discussion here, we restrict attention to the case of just two subdomains. In our scheme, each subregion contributes equations corresponding all fine degrees of freedom, including its interface. Thus in general there will be multiple unknowns and equations in the global system corresponding to the interface degrees of freedom. This is handled by equality constraints that impose continuity at all degrees of freedom on the interface. The result is a mortar-element like formulation, using Dirac δ functions for the mortar element space. In any event, with a proper ordering of unknowns, the global system of equations has the block 5×5 form

$$\begin{pmatrix} A_{11} & A_{1\gamma} & & & \\ A_{\gamma 1} & A_{\gamma\gamma} & & & I \\ & & A_{\nu\nu} & A_{\nu 2} & -I \\ & & A_{2\nu} & A_{22} & \\ & I & -I & & \end{pmatrix} \begin{pmatrix} \delta U_1 \\ \delta U_\gamma \\ \delta U_\nu \\ \delta U_2 \\ \Lambda \end{pmatrix} = \begin{pmatrix} R_1 \\ R_\gamma \\ R_\nu \\ R_2 \\ U_\nu - U_\gamma \end{pmatrix}. \tag{4.3}$$

Here A_{11} and A_{22} correspond to the fine degrees of freedom on processors 1 and 2, respectively, that are not on the interface, while $A_{\gamma\gamma}$ and $A_{\nu\nu}$ correspond to interface points. The fifth block equation imposes continuity, and its corresponding Lagrange multiplier is Λ. The identity matrix appears because the global fine mesh is conforming. The introduction of the Lagrange multiplier and the saddle point formulation (4.3) are only for expository purposes; indeed, Λ is never computed or updated.

On processor 1, we develop a similar but "local" saddle point formulation. That is, the fine mesh subregion on processor 1 is "mortared" to the remaining course mesh on processor 1. This leads to a linear system of the form

$$\begin{pmatrix} A_{11} & A_{1\gamma} & & & \\ A_{\gamma 1} & A_{\gamma\gamma} & & & I \\ & & \bar{A}_{\nu\nu} & \bar{A}_{\nu 2} & -I \\ & & \bar{A}_{2\nu} & \bar{A}_{22} & \\ & I & -I & & \end{pmatrix} \begin{pmatrix} \delta U_1 \\ \delta U_\gamma \\ \delta \bar{U}_\nu \\ \delta \bar{U}_2 \\ \Lambda \end{pmatrix} = \begin{pmatrix} R_1 \\ R_\gamma \\ R_\nu \\ 0 \\ U_\nu - U_\gamma \end{pmatrix}, \tag{4.4}$$

where quantities with a bar (e.g., $\bar{A}_{22}$) refer to the coarse mesh. A system similar to (4.4) can be derived for processor 2. With respect to the right hand side of (4.4), the interior residual R_1 and the interface residual R_γ are locally computed on processor 1. We obtain the boundary residual R_ν, and boundary solution U_ν from processor 2; processor 2 in turn must be sent R_γ and U_γ. The residual for the coarse grid interior points is set to zero. This avoids the need to obtain R_2 via communication, and to implement a procedure to restrict R_2 to the coarse mesh on

processor 1. Given our initial guess, we expect $R_1 \approx 0$ and $R_2 \approx 0$ at all iteration steps. R_γ and R_ν are not generally small, but $R_\gamma + R_\nu \to 0$ at convergence.

As with the global formulation (4.3), equation (4.4) is introduced mainly for exposition. The goal of the calculation on processor 1 is to compute the updates δU_1 and δU_γ, which contribute to the global conforming solution. To this end, we formally reorder (4.4) as

$$\begin{pmatrix} & -I & & I & \\ -I & \bar{A}_{\nu\nu} & & & \bar{A}_{\nu 2} \\ & & A_{11} & A_{1\gamma} & \\ I & & A_{\gamma 1} & A_{\gamma\gamma} & \\ & \bar{A}_{2\nu} & & & \bar{A}_{22} \end{pmatrix} \begin{pmatrix} \Lambda \\ \delta\bar{U}_\nu \\ \delta U_1 \\ \delta U_\gamma \\ \delta\bar{U}_2 \end{pmatrix} = \begin{pmatrix} U_\nu - U_\gamma \\ R_\nu \\ R_1 \\ R_\gamma \\ 0 \end{pmatrix}. \tag{4.5}$$

Block elimination of the Lagrange multiplier Λ and $\delta\bar{U}_\nu$ in (4.5) leads to the block 3×3 Schur complement system

$$\begin{pmatrix} A_{11} & A_{1\gamma} & \\ A_{\gamma 1} & A_{\gamma\gamma} + \bar{A}_{\nu\nu} & \bar{A}_{\nu 2} \\ & \bar{A}_{2\nu} & \bar{A}_{22} \end{pmatrix} \begin{pmatrix} \delta U_1 \\ \delta U_\gamma \\ \delta\bar{U}_2 \end{pmatrix} = \begin{pmatrix} R_1 \\ R_\gamma + R_\nu + \bar{A}_{\nu\nu}(U_\nu - U_\gamma) \\ \bar{A}_{2\nu}(U_\nu - U_\gamma) \end{pmatrix}. \tag{4.6}$$

The system matrix in (4.6) corresponds to the final adaptive refinement step on processor 1, with possible modifications due to global fine mesh regularization. It is exactly the matrix used in the preliminary local solve to generate the initial guess for the global domain decomposition iteration. In the solution of (4.6), the components δU_1 and δU_γ contribute to the global solution update, while $\delta\bar{U}_2$ is discarded. We remark that the global iteration matrix corresponding to this formulation is not symmetric, even if all local system matrices are symmetric.

The domain decomposition algorithm is incorporated as the solver for the approximate Newton iteration described in Figure 4.1. In particular, only one domain decomposition iteration (a so-called *inner iteration*) is used in each approximate Newton step. Thus, loosely speaking, each solve of (4.6) alternates with a line search step in which the global solution is updated. The Newton line search procedure requires global communication to form some norms and inner products, as well as the boundary exchange described above.

4.5 Obstacle Problems.

When *IPROB* = 2, *PLTMG* solves the obstacle problem (1.8). The inequality constraints are treated via an interior point procedure [13]. In particular, we consider the Lagrange function

$$L(u_h) = \rho(u_h) - \mu \sum_{i=1}^{NDF} d_i \left\{ \log(u_h(p_i) - \underline{u}(p_i)) + \log(\overline{u}(p_i) - u_h(p_i)) \right\} \tag{4.7}$$

where $\mu > 0$ is a small barrier parameter; the user specifies the target value in *RMTRGT*. Vertices of the triangulation are denoted by $p_i = (x_i, y_i)$, and d_i is the

diagonal entry of the mass matrix corresponding to p_i. The weights $d_i = O(h_i^2)$ scale the barrier terms in a fashion similar to $\rho(u_h)$, and make μ independent of the mesh.

The overall solution strategy is to compute stationary points of the Lagrange function (4.7) for a decreasing sequence of $RMTRGT = \mu > 0$ values, following a smooth trajectory moving towards the boundary of the feasible region. This has much in common with the more general path following procedures used in the case $IPROB = 3$.

The assembly and solution procedures are quite similar to the case $IPROB = 1$. In particular, the right hand side is modified by terms of the form

$$-\mu d_i \left\{ (u_h(p_i) - \underline{u}(p_i))^{-1} + (u_h(p_i) - \overline{u}(p_i))^{-1} \right\},$$

and the diagonal of the stiffness matrix (Hessian matrix of the functional $\rho(u_h)$) is modified by terms of the form

$$\mu d_i \left\{ (u_h(p_i) - \underline{u}(p_i))^{-2} + (u_h(p_i) - \overline{u}(p_i))^{-2} \right\}.$$

With these modifications, the approximate Newton strategy described in Section 4.2 is used here.

When $IPROB = -2$, the domain decomposition algorithm outlined in Section 4.4 is used, with appropriate modifications to the stiffness matrix and right hand sides. As in the case $IPROB = -1$, only one domain decomposition solve (inner iteration) is used in each approximate Newton iteration.

As an example, we use *PLTMG* to solve the variational inequality

$$\min_{u \in K} \int_\Omega \{ |\nabla u|^2 - 2f(x,y)u \} dx\, dy$$

where the domain $\Omega = (0,1) \times (0,1)$, and

$$K = \left\{ u \in \mathcal{H}_0^1(\Omega) : |u| \le \frac{1}{4} - \frac{1}{10} \sin(\pi x) \sin(\pi y) \right\},$$
$$f(x,y) = -\Delta(\sin(3\pi x) \sin(3\pi y)).$$

In the absence of the obstacle, this is a simple elliptic equation with exact solution $u = \sin(3\pi x) \sin(3\pi y)$.

In this example, we compare h-refinement using piecewise linear elements with hp-refinement. In both cases, we begin with linear elements on a uniform 9×9 mesh, as illustrated in Figure 4.3. In both cases, we went through eight adaptive loops, followed by solving the problem with $\mu = 1$. Then we made three additional solutions with $\mu = 10^{-k}$ for $1 \le k \le 3$.

In the case of piecewise linear elements, the final mesh had $NTF = 31285$ elements and $NDF = 15831$ degrees of freedom. The solution, the mesh colored by element size, and the a posterior error estimate for the final solution are shown in Figure 4.3. In the case of hp-refinement, the final mesh had $NTF = 4413$ elements and $NDF = 12650$ degrees of freedom. The solution, the mesh colored by element size and element degree, and the error estimate are shown in Figure 4.3.

We note that in the *hp*-adaptive case, the mesh is coarser and more uniform. In the *h*-refinement case, there was more refinement near the boundaries where the inequality constraint was satisfied as equality, and much less refinement in the interior of those regions. The *hp* mesh used mostly quadratic and cubic elements, and was much more uniform. In the regions where the inequality constraint was satisfied as equality, one sees the effect of imposing the inequalities just at the nodes; one observes small oscillations in these regions due to the higher degree polynomials.

4.6 Continuation Problems.

In the case of continuation problems ($IPROB = 3$), the parameter *ITASK* specifies the the continuation option. Available options are summarized in Table 4.2. For convenience in notation, we will systematically drop the subscript h from all variables in this section (e.g., λ_h will be denoted λ).

When the continuation process is used, we use a normalization equation of the form

$$N(u, \lambda) = \sigma.$$

The scalar $\sigma = SIGMA$ is the steplength. *PLTMG* uses then the normalization equation described in [7, 53],

$$N(u, \lambda) = \theta\dot{\rho}_0(\rho - \rho_0) + (2 - \theta)\dot{\lambda}_0(\lambda - \lambda_0). \tag{4.8}$$

Here $\theta = THETA$ is a parameter selected by *PLTMG*; by choosing θ and σ properly, it is possible to achieve target values in either ρ or λ. The vector (u_0^t, λ_0) is the current solution point and $(\dot{u}_0^t, \dot{\lambda}_0)$ the current unit tangent vector. The scalar $\dot{\rho}$ is defined formally using the chain rule for differentiation:

$$\dot{\rho} = \rho_u \dot{u} + \rho_\lambda \dot{\lambda}.$$

The values $0 \le ITASK \le 4$ embody the basic continuation path following options available in *PLTMG*. The values $5 \le ITASK \le 7$ are designed for updating the solution at a fixed point when the mesh has been changed by a call to *TRIGEN*.

An initial solution is provided by the user through subroutine *GDXY*. Thereafter, the continuation proceeds from the last successfully computed point. A brief outline of the basic continuation process ($ITASK = 0$ or $ITASK = 1$) is given in Figure 4.4.

PLTMG always returns with $(RLTRGT, RTRGT) = (RL, R) \equiv (\lambda, \rho)$. To continue with $ITASK = 0$ or $ITASK = 1$, the user specifies a target value for either *RTRGT* or *RLTRGT*. If $RLTRGT \neq RL$, then *PLTMG* seeks a solution with $\lambda = RLTRGT$. Similarly, if $RTRGT \neq R$, then *PLTMG* seeks a solution with $\rho = RTRGT$.

A step σ and a predicted solution are computed on line **C2**. The predictor is a standard Euler type commonly used in continuation procedures. The step size calculation is influenced not only by the user request but also by imposed requirements that the predicted solution be sufficiently accurate. The procedures used in this portion of the calculation are described in detail in [20]. The solution

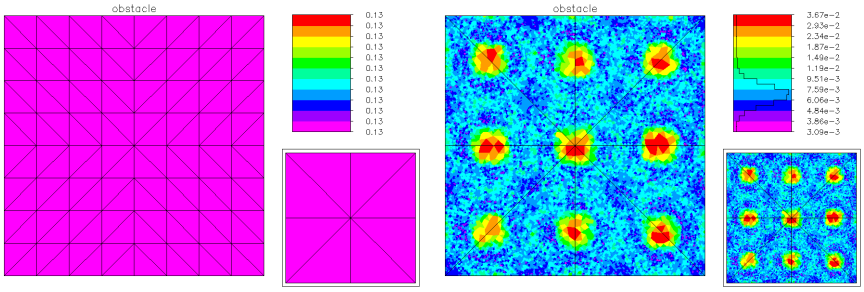

The initial uniform mesh (left), and the final mesh for the case of h-refinement, colored by element size (right).

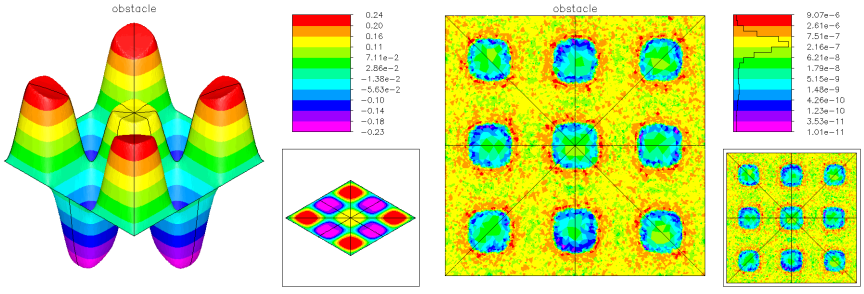

The piecewise linear solution (left) and corresponding error estimate (right).

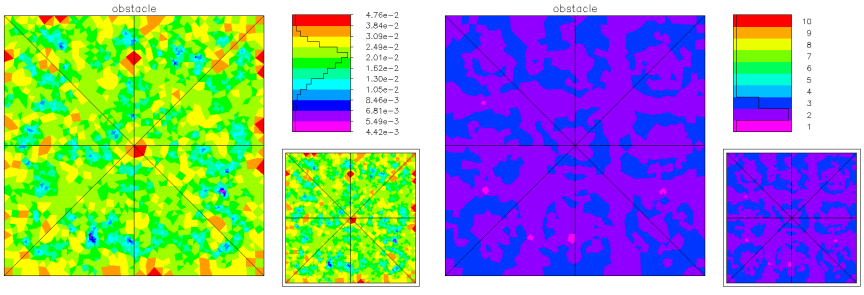

The final adaptive mesh for hp-refinement, colored by element size (left) and polynomial degree (right).

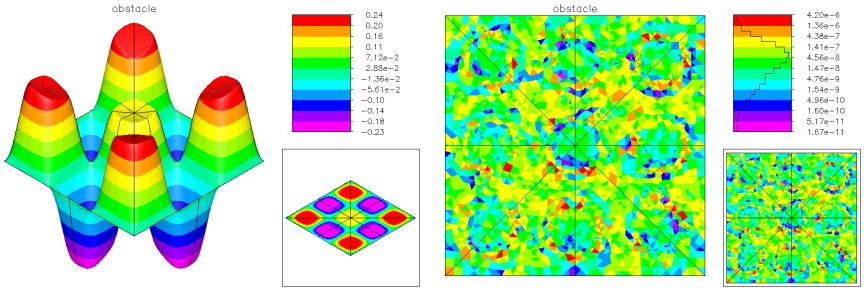

The hp-adaptive solution (left) and corresponding error estimate (right).

Figure 4.3.

Procedure Continue

C1 Begin with initial solution (u_0^t, λ_0) and tangent vector $(\dot{u}_0^t, \dot{\lambda}_0)$.
C2 compute the step σ for the normalization equation; predict $(u^t, \lambda) \leftarrow (u_0^t, \lambda_0) + \alpha(\dot{u}_0^t, \dot{\lambda}_0)$.
C3 correct $(u^t, \lambda) \leftarrow NWT(u^t, \lambda)$; compute ψ_ℓ, ψ_r, and ν; compute tentative $\dot{u}$ and $\dot{\lambda}$.
C4 if a singular point was detected and $ITASK = 1$, then go to **C7**.
C5 set $(u_0^t, \lambda_0) \leftarrow (u^t, \lambda)$ and $(\dot{u}_0^t, \dot{\lambda}_0) \leftarrow (\dot{u}^t, \dot{\lambda})$.
C6 if (u_0^t, λ_0) is a target point, then exit; else go to **C2**.
C7 compute the singular point using secant/bisection algorithm on $\nu(\sigma) = 0$; exit.

Figure 4.4.

is corrected on line **C3**. The correction process symbolized by the operator NWT involves the solution of a set of nonlinear equations, and is discussed in greater detail below.

PLTMG locates singular points by computing the smallest singular value ν of the Jacobian matrix. A modified inverse iteration procedure computes the left and right singular vectors ψ_ℓ and ψ_r corresponding to ν as part of each correction step **C3**. If the matrix is symmetric ($ISPD = 1$), then $\psi_\ell \equiv \psi_r$. In a somewhat nonstandard fashion for singular values, we normalize the singular vectors to have unit length and satisfy

$$\int_\Omega \psi_\ell \psi_r \, dx > 0.$$

Requiring the sign of the inner product of ψ_ℓ and ψ_r to be positive forces the singular value ν to change sign at a singular point (normally one requires $\nu \geq 0$ and then the inner product changes sign at singular points). Unfortunately, while ν changes sign in a continuous fashion at singular points, it can also change sign *discontinuously* at regular points. For example, in the self-adjoint linear eigenvalue problem, along the trivial branch ν will continuously pass through zero at each eigenvalue and will discontinuously change sign at some point *between* each consecutive pair of eigenvalues where the smallest singular value of the Jacobian changes from the preceding to the following eigenvalue.

If *PLTMG* detects a change in sign in ν along the solution curve between the starting point and target point, and if $ITASK = 1$, the computation of the target point is abandoned in favor of computation of the possible singular point. A secant/bisection algorithm for the equation $\nu(\sigma) = 0$ is used. More details of these procedures can be found in Bank and Chan [7] and the references therein. At the conclusion of this iteration, some tests are made to determine if the point is a bifurcation point, a limit point, or a regular point.

The algorithms in *PLTMG* were designed to handle only simple limit and bifurcation points, although on occasion we have observed them to work on some higher degree singular points as well. When a target or singular point has been successfully computed, *PLTMG* returns with $(RLTRGT, RTRGT)$ set to the current values of (λ, ρ).

If *PLTMG* is called with $ITASK = 2$ at a bifurcation point, parameters relevant for the continuation procedure are initialized for the bifurcating branch, but the solution itself remains unchanged. In the next call to *PLTMG* with $ITASK = 0$ or $ITASK = 1$, the continuation procedure will follow the bifurcating branch.

If *PLTMG* is called with $ITASK = 3$ or $ITASK = 4$, parameters relevant for the continuation procedure are reinitialized using the new parameter or functional; the solution itself remains unchanged. The two cases differ in that either λ or ρ can be held fixed during the reinitialization; for either case it is possible to specify either a new continuation parameter λ, a new functional ρ, or both.

The successful use of the continuation procedure requires guidance from the user. For example, it is possible to specify target values that cannot be reached. Also, since singular points are detected by changes in sign of ν, one can fool the singular-point detection algorithm by specifying target values sufficiently far away that two sign changes are passed on one step.

We now consider the cases $5 \le ITASK \le 7$. We begin by noting that the discretization process can introduce spurious solution curves or cause significant distortions in the solution curves of the continuous problem (1.1); one must therefore be cautious in interpreting the numerical results [52]. As the mesh is refined or the mesh points are smoothed, the solution curves generally will move; the assumption of *PLTMG* is that, as a function of the discretization, the solution curves converge in some uniform fashion to those of the continuous problem, and that the mesh is sufficiently fine to capture the qualitative features of the continuous problem's solution curves in the regions of interest [7, 19]. Typically, for each point on the current grid, there are three natural points on a nearby new grid solution curve that can be associated with it: the point with the same λ value ($ITASK = 5$), the point with the same ρ value ($ITASK = 6$), and the point of intersection with the perpendicular hyperplane passing through the current solution point ($ITASK = 7$). Some typical examples are illustrated in Figure 4.5.

In some situations, all three points may not exist, or they may not be distinct. This is illustrated in Figure 4.5, right, where $ITASK = 6$ and $ITASK = 7$ correspond to the same fine grid point, while no (nearby) solution exists for $ITASK = 5$.

We now consider the linear algebraic aspects of the problem. As with other problem types, the nonlinear systems for $IPROB = 3$ are solved by the approximate Newton iteration [29, 28] described in Figure 4.1. The nonlinear system to be solved has the form

$$G(u, \lambda) = 0,$$
$$N(u, \lambda) = \sigma.$$

Here the operator G represents the finite element equations of order *NDF*, and N the normalizing equation used in the continuation process; σ is the steplength. At

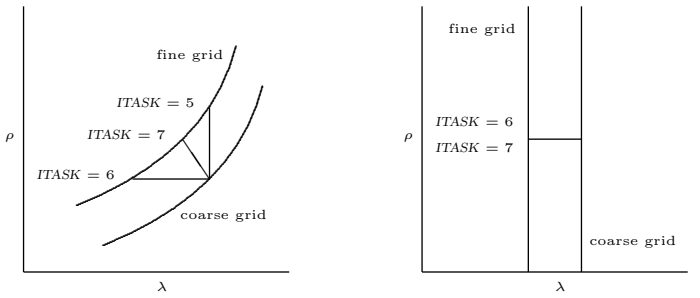

Figure 4.5. *The effect of ITASK in the case of mesh refinement.*

each step of the Newton process, the linear system to be solved has the form

$$\begin{pmatrix} G_u & G_\lambda \\ N_u & N_\lambda \end{pmatrix} \begin{pmatrix} \delta u \\ \delta\lambda \end{pmatrix} = - \begin{pmatrix} G(u,\lambda) \\ N(u,\lambda) - \sigma \end{pmatrix}, \tag{4.9}$$

where δu is a vector of length *NDF* and $\delta\lambda$ is a scalar. The solution is constructed by solving

$$\begin{aligned} G_u v &= -G, \\ G_u w &= -G_\lambda - G_u \bar{u}_\lambda, \\ \bar{u}_\lambda &\leftarrow \bar{u}_\lambda + w, \\ \delta\lambda &= -\frac{N_u v + N - \sigma}{N_u \bar{u}_\lambda + N_\lambda}, \\ \delta u &= v + \delta\lambda\, \bar{u}_\lambda. \end{aligned}$$

The vector $\bar{u}_\lambda$, initially set to zero, is updated at every step. Thus the right-hand side $G_\lambda + G_u \bar{u}_\lambda$ has the appearance of a residual, and w may be viewed as an incremental update. At convergence, $\bar{u}_\lambda \dot{\lambda} = \dot{u}$, so $\dot{u}$ is known at every Newton step. The linear systems involving G_u are solved by the one of the linear solvers described in Section 4.3.

The block elimination process is embedded in the overall damped Newton process [20, 28] given in Figure 4.1. Here $\mathcal{U}_k^t = (u^t, \lambda)$ is the kth Newton iterate, $\delta\mathcal{U}_k^t = (\delta u^t, \delta\lambda)$, and $\mathcal{G}_k^t = (G^t, N - \sigma)$. The norm $\|\mathcal{G}_k\|$ is given by

$$\|\mathcal{G}_k\|^2 = \|G\|^2 + c|N - \sigma|^2,$$

where c is a scaling parameter (*SCALE* in the *RP* array) chosen to balance the two terms appropriately.

The case $IPROB = -3$ corresponds to a parallel solve of the block linear system (4.9), embedded in the overall Newton iteration. It is defined only for the cases $ITASK = 5, 6, 7$; at present there is no parallel implementation of the basic path following options. Thus we assume that the continuation is done on a coarse mesh on a single processor, and parallel computation is used only in the context of computing a highly refined solution at a particular point.

For continuation problems, *PLTMG* provides a limited amount of written output summarizing the state of the computation. All formats are designed for output devices having a minimum of 80 characters per line. All output is directed to the subroutine $FILUTL$, which is responsible for creating the files *BFILE* and *JWFILE*.

For each call to *PLTMG* a banner is printed. Each continuation step results in a single line of output containing seven numbers. A typical example of such output is illustrated below:

```
pltmg:     lambda        rho       lambda dot    rho dot     eigenvalue
  0  3  0.99004E+01  0.39814E+01 -0.80768E-02  0.39890E+01 -0.94673E-04
```

The first column contains the current value of *IFLAG* (in this example, $IFLAG = 0$). The second contains the value of *ITNUM*, the actual number of approximate Newton iterations used. The next four columns contain the current values of the parameter λ, the functional ρ, and their derivatives with respect to arclength along the current solution manifold $\dot{\lambda}$ and $\dot{\rho}$. The column labeled "eigenvalue" gives an approximation to the smallest singular value ν of the Jacobian matrix $\mathcal{G}_u$.

As an example, we consider the nonlinear eigenvalue problem

$$\begin{aligned} -\Delta u &= \lambda \sin u \quad \text{in } \Omega \equiv (0,1) \times (0,1), \\ u &= 0 \qquad\quad \text{on } \partial\Omega, \end{aligned}$$

with the functional given by

$$\rho(u, \lambda) = \int_\Omega u^2 \, dx \, dy.$$

This problem has bifurcation points at the eigenvalues of the linear eigenvalue problem, $-\Delta u = \lambda u$, which are given by $\lambda_{k\ell} = (k^2 + \ell^2)\pi^2$, $k = 1, 2, \ldots$, $\ell = 1, 2, \ldots$. We chose as our coarse mesh a 17×17 uniform mesh, and will employ piecewise linear elements.

Our goal is to compute the first four eigenvalues and eigenfunctions. The first and third eigenvalues have multiplicity one. The second and fourth eigenvalues have multiplicity two. While the algorithms in *PLTMG* are not designed to handle multiplicities greater than one, the code performed in a satisfactory fashion and computed all four eigenvalues without difficulty. As a cautionary remark, one should not assume that the situation in this respect will always be so favorable.

We initialize at $\lambda = 0$ and continue to $\lambda = 10$ with $ITASK = 0$ and then to $\lambda = 22$ with $ITASK = 1$. At $\lambda = 22$, the sign of ν (eigenvalue) has changed, so *PLTMG* computes the singular point, in this case the first eigenvalue. These basic continuation steps were done on a uniform 17×17 mesh, using piecewise linear finite elements.

```
pltmg:     lambda        rho       lambda dot    rho dot     eigenvalue
  0  1  0.00000E+00  0.00000E+00  0.10000E+01  0.00000E+00  0.78964E-01
  0  1  0.10000E+02  0.00000E+00  0.10000E+01  0.00000E+00  0.38375E-01
  0  1  0.22000E+02  0.00000E+00  0.10000E+01  0.00000E+00 -0.81464E-02
```

```
pltmg: find limit / bifurcation point
  0  1  0.19899E+02  0.00000E+00  0.10000E+01  0.00000E+00 -0.86933E-04
  0  1  0.19876E+02  0.00000E+00  0.10000E+01  0.00000E+00  0.71791E-06
  0  1  0.19876E+02  0.00000E+00  0.10000E+01  0.00000E+00 -0.36357E-11
pltmg: probable bifurcation point
  0  0  0.19876E+02  0.00000E+00  0.10000E+01  0.00000E+00 -0.36357E-11
```

Note that the secant/bisection algorithm converged in three steps. After determining that the singular point was a bifurcation point, *PLTMG* makes an additional calculation to ensure that the tangent vector $\dot{u}_h$ corresponds to the current branch (in this case, the trivial branch).

We save the solution in a file in order to continue from this point to the second eigenvalue in a convenient manner (see Section 6.7), and switch branches ($ITASK = 2$). We then routinely continue on the bifurcating branch in several steps ($\rho = .01, \lambda = 25, 50, 100, 150, 300, 500$). At $\lambda = 500$, we *hp*-refine the mesh with a three calls to *TRIGEN* with $IADAPT = 1$, alternating with calls to *PLTMG* with $ITASK = 7$. The eigenfunction and mesh are shown in Figure 4.6.

We restore the solution at the bifurcation point and continue along the trivial branch to the second eigenvalue. We save the solution, switch branches and explore the bifurcating branch in a fashion similar to the first eigenvalue. A similar procedure is repeated for the third and fourth eigenvalues. The eigenfunctions computed on *hp*-refined meshes are shown in Figure 4.6. In Figure 4.7, we show the complete history of the calculation in terms of the continuation path.

4.7 Parameter Identification Problems.

When $IPROB = 4$, *PLTMG* solves the parameter identification problem (1.9)-(1.12). Up to ten scalar parameters are allowed; $1 \le NRL \le 10$ denotes the number of parameters. If one or more of the parameters influences the shape of Ω through *SXY*, then one should set $ITASK = 8$. This signals *PLTMG* to invoke certain additional procedures within the basic Newton iteration that modify the shape of Ω.

The simple bounds on λ_h are treated in a fashion analogous to the case $IPROB = 2$. In particular, we consider the Lagrangian

$$L(u_h, v_h, \lambda_h) = \rho(u_h, \lambda_h) + a(u_h, v_h) - \mu \left\{ \sum_{k=1}^{NRL} \log(\lambda_{h,k} - \underline{\lambda}_k) - \log(\overline{\lambda}_k - \lambda_{h,k}) \right\} \quad (4.10)$$

where $\mu > 0$ is the barrier parameter and v_h is the Lagrange multiplier (a member of the finite element subspace). Our procedure computes a stationary point of the Lagrangian (4.10) using an approximate Newton method.

The linear algebra problem at each Newton iteration is of the form

$$\begin{pmatrix} H & A^t & C_u \\ A & 0 & C_v \\ C_u^t & C_v^t & D \end{pmatrix} \begin{pmatrix} \delta u \\ \delta v \\ \delta \lambda \end{pmatrix} = \begin{pmatrix} b_u \\ b_v \\ b_\lambda \end{pmatrix}. \quad (4.11)$$

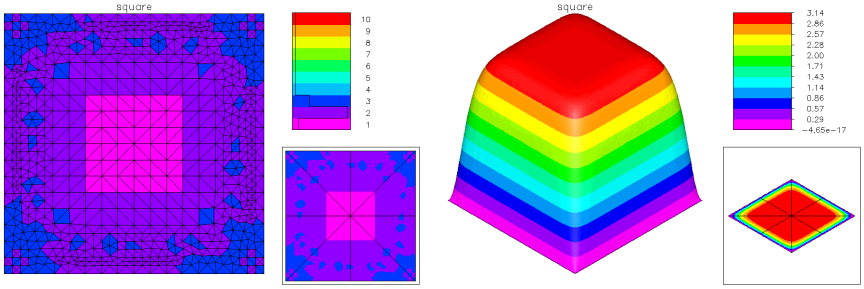

The first eigenfunction; NTF = 1490 *and NDF* = 3868.

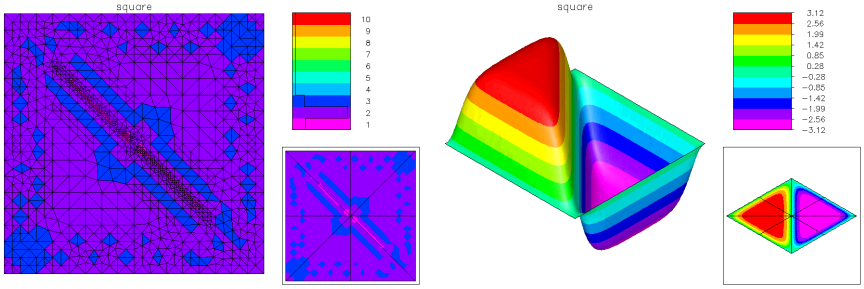

The second eigenfunction; NTF = 2150 *and NDF* = 4820.

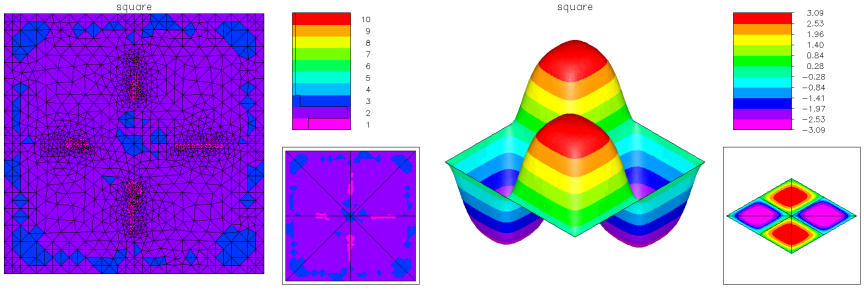

The third eigenfunction; NTF = 2506 *and NDF* = 4999.

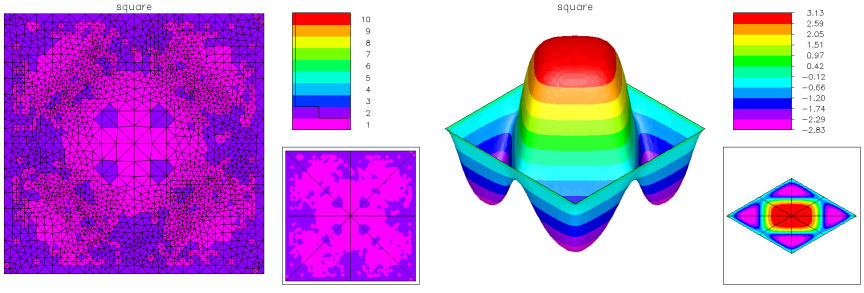

The fourth eigenfunction; NTF = 4684 *and NDF* = 4999.

Figure 4.6.

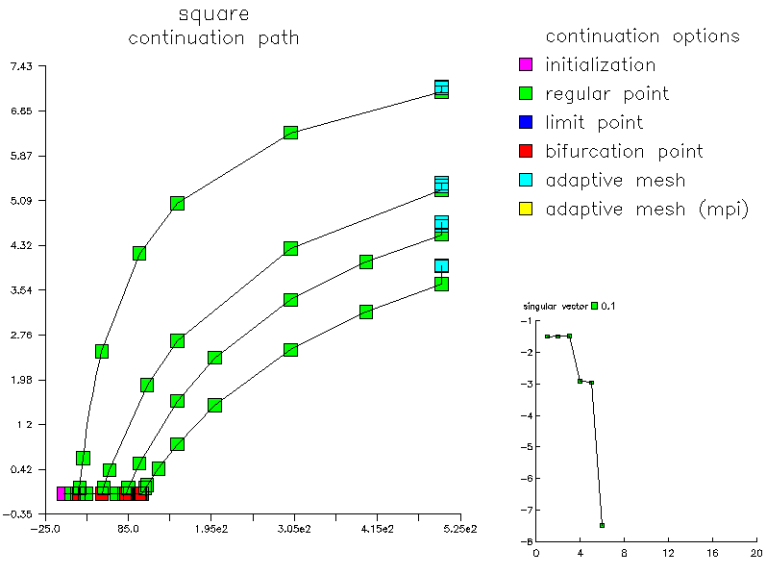

Figure 4.7. *The continuation path.*

Here the matrix A is the Jacobian matrix corresponding the the bilinear form $a(u_h, v_h)$. In particular, linear systems involving A (or A^t) are solved using the the linear solver specified by *METHOD*. The matrix H is symmetric and has the same sparsity pattern as A; other characteristics strongly depend on the particular problem. C_u and C_v are $NDF \times NRL$ rectangular matrices, generally composed of NRL dense column vectors, and D is a $NRL \times NRL$ symmetric matrix. The vectors δu and δv are the (Newton) updates for u_h and the Lagrange multiplier v_h, respectively, and $\delta\lambda$ is the update for λ_h. b_u, b_v and b_λ correspond to the appropriate Newton residuals.

To describe the solution process for 4.11, we begin with the block factorization

$$\begin{pmatrix} H & A^t & C_u \\ A & 0 & C_v \\ C_u^t & C_v^t & D \end{pmatrix} = \begin{pmatrix} I & 0 & 0 \\ 0 & A & 0 \\ 0 & 0 & I \end{pmatrix} \begin{pmatrix} H & I & 0 \\ I & 0 & 0 \\ C_u^t & \bar{C}_v^t & \bar{D} \end{pmatrix} \begin{pmatrix} I & 0 & \bar{C}_v \\ 0 & I & \bar{C}_u \\ 0 & 0 & I \end{pmatrix} \begin{pmatrix} I & 0 & 0 \\ 0 & A^t & 0 \\ 0 & 0 & I \end{pmatrix}$$

where

$$\begin{aligned} A\bar{C}_v &= C_v, \\ \bar{C}_u &= C_u - H\bar{C}_v, \\ \bar{D} &= D - C_u^t\bar{C}_v - \bar{C}_v^t\bar{C}_u. \end{aligned}$$

Computing $\bar{C}_v$ requires solving NRL linear systems with A. The two block diagonal matrices each require solution of one linear system with A or A^t. Thus a total of $2 + NRL$ elliptic pde systems need to be solved in each Newton step. The block

lower triangular system requires solving one dense linear system with the symmetric $NRL \times NRL$ matrix $\bar{D}$.

The overall solution procedure is summarized below. Since the linear systems involving A are generally solved only approximately by iteration, we introduce the matrix $\bar{u}_\lambda \approx \bar{C}_v$, that is generally the approximate $\bar{C}_v$ saved from the previous Newton step. This allows the computation of the current $\bar{C}_v$ to be done as an update with a residual-like right hand side. $\bar{u}_\lambda$ is initially set to zero, and updated with the solution of every linear system.

First we solve

$$\begin{aligned} A\bar{b}_v &= b_v, \\ Aw &= C_v - A\bar{u}_\lambda, \\ \bar{u}_\lambda &\leftarrow \bar{u}_\lambda + w, \\ \bar{C}_v &= \bar{u}_\lambda. \end{aligned}$$

All linear systems involving A are (approximately) solved using the linear solver specified by *METHOD*. Then we form

$$\begin{aligned} \bar{b}_u &= b_u - H\bar{b}_v, \\ \bar{C}_u &= C_u - H\bar{C}_v, \end{aligned}$$

which requires sparse matrix multiplications with H. Next we compute $\delta\lambda$ using the Schur complement

$$\begin{aligned} \bar{D} &= D - C_u^t\bar{C}_v - \bar{C}_v^t\bar{C}_u, \\ \bar{D}\delta\lambda &= b_\lambda - C_u^t\bar{b}_v - \bar{C}_v^t\bar{b}_u. \end{aligned}$$

Finally, we form δu and δv from

$$\begin{aligned} \delta u &= \bar{b}_v - \bar{C}_v\delta\lambda, \\ A^t\delta v &= \bar{b}_u - \bar{C}_u\delta\lambda. \end{aligned}$$

The latter requires the use of the linear solver for A^t. The basic Newton iteration is again that given in Figure 4.1 with the interpretation $\mathcal{U}^t = (u_h^t, v_h^t, \lambda_h^t)$ and $\mathcal{G}^t = (b_u^t, b_v^t, b_\lambda^t)$.

When $IPROB = -4$, a parallel Newton algorithm is implemented, similar in structure to the case $IPROB = -1$. A domain decomposition solver analogous to that described in Section 4.4 is incorporated into the block elimination algorithm defined above.

As an example, we consider the problem

$$\min \int_\Omega \nabla u^2 + \delta \sum_{i=1}^{3} \lambda_i^2 \, dx,$$

subject to the boundary value problem and inequality constraints

$$\begin{aligned} -\Delta u &= 1 && \text{in } \Omega \\ u &= 0 && \text{on } \partial\Omega \\ \underline{\lambda}_i \le \lambda_i &\le \overline{\lambda}_i, && \text{for } 1 \le i \le 3. \end{aligned}$$

The domain Ω is shown in Figure 4.8. The interior box is free to move within the domain, with its position governed by three parameters. (λ_1, λ_2) are the (x, y) coordinates of the center of the box and λ_3 is its angle of rotation. This is the special case $IPROB = 4$ and $ITASK = 8$ allowing parameters to control the geometry of the domain.

The domain was provided as a skeleton and the initial mesh generated by *TRIGEN*. Both are shown in Figure 4.8. The optimization problem was then solved on this mesh using piecewise linear elements. This first optimization step involved substantial movement of the boundary, but the number of degrees of freedom was relatively small. Next, using alternating refinement and optimization steps, we created a final mesh with $NDF = 22483$ degrees of freedom. In each optimization step, the interior point parameter *RMTRGT* was reduced by a factor of 2 starting from its initial value of 1. While the boundary was allowed to move on all these additional optimization steps, it moved very little. In Figure 4.8, we also show the final solution, Lagrange multiplier, and the a posteriori error estimate computed on the final mesh.

4.8 Optimal Control Problems.

When $IPROB = 5$, *PLTMG* solves the control problem (1.13)-(1.16). This problem is similar to the case $IPROB = 4$ except that now λ_h is a finite element function rather than a scalar. Here we consider the Lagrangian

$$L(u_h, v_h, \lambda_h) = \rho(u_h, \lambda_h) + a(u_h, v_h) \\ - \mu \sum_{i=1}^{NDF} d_i \left\{ \log(\lambda_h(p_i) - \underline{\lambda}(p_i)) + \log(\overline{\lambda}(p_i) - \lambda_h(p_i)) \right\} \quad (4.12)$$

where $\mu > 0$ is the barrier parameter, d_i is the diagonal of the mass matrix corresponding to vertex p_i, and v_h is the Lagrange multiplier. As usual, our algorithm seeks a stationary point of the Lagrangian (4.12) using an approximate Newton method.

The linear algebra problem at each Newton step is of the form

$$\begin{pmatrix} H & A^t & S_u \\ A & 0 & S_v \\ S_u^t & S_v^t & G \end{pmatrix} \begin{pmatrix} \delta u \\ \delta v \\ \delta \lambda \end{pmatrix} = \begin{pmatrix} b_u \\ b_v \\ b_\lambda \end{pmatrix}. \quad (4.13)$$

Here H and A are defined as before. In typical problems G is a symmetric, positive definite matrix, corresponding the regularization terms in (4.12). The matrix G also has a nonnegative diagonal term arising from the inequality constraints for λ_h. As before, linear systems involving A and A^t are easily solved using the linear solver specified by *METHOD*. Additionally, since G formally has the same sparsity as the stiffness matrix A, linear systems involving G are solved using a similar preconditioning strategy. The matrices S_u and S_v have the same symmetric sparsity structure as G and A, but are generally not symmetric.

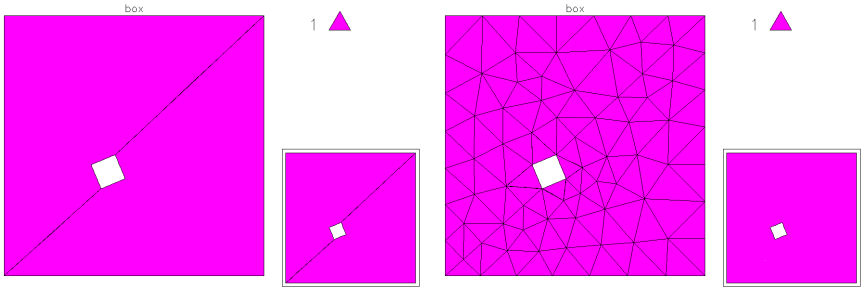

The skeleton (left) and initial mesh with $NTF = 132$ *and* $NDF = 82$ *(right).*

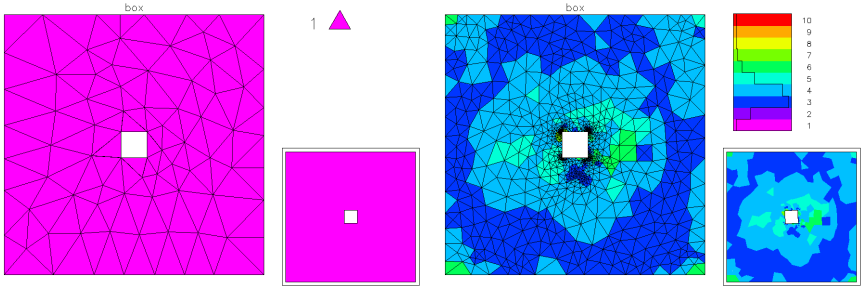

The mesh after the first optimization step (left) and the final mesh with $NTF = 2981$ *and* $NDF = 22483$ *colored by polynomial degree (right).*

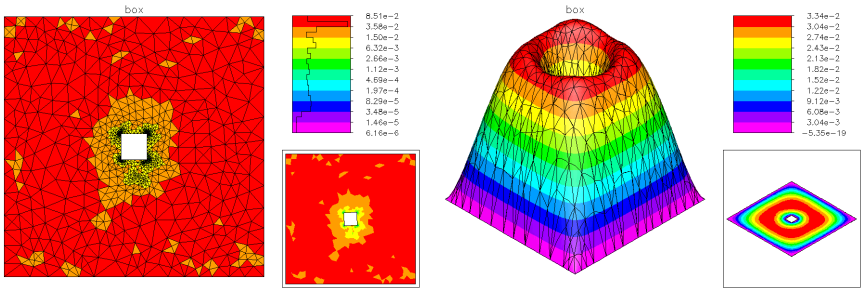

The final mesh colored by element size (left) and the solution (right).

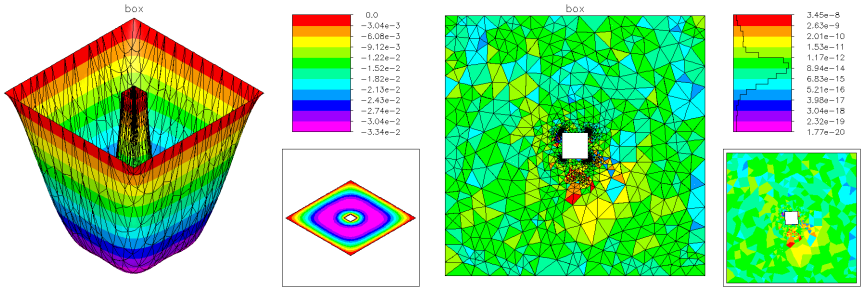

The Lagrange multiplier (left), and the error estimate for the final mesh (right).

Figure 4.8.

Our solver is based on block Gaussian elimination, similar to the case $IPROB = 4$. However, in the case of (4.13), it is too expensive to compute an exact Schur complement for the $3,3$ block; instead we approximate the Schur complement by G itself. Thus, our solution algorithm is just a preconditioner. In particular, it is one step of a block symmetric Gauss-Seidel iteration. This is realized as follows:

$$\begin{aligned} A\tilde{c}_u &= b_v, \\ A^t\tilde{c}_v &= b_u - H\tilde{c}_u, \\ G\delta\lambda &= b_\lambda - S_u^t\tilde{c}_u - S_v^t\tilde{c}_v, \\ A\delta u &= b_v - S_v\delta\lambda, \\ A^t\delta v &= b_u - H\delta u - S_u\delta\lambda. \end{aligned}$$

Linear systems involving A, A^t, and G are solved using the appropriate linear solver. If G were replaced by the Schur complement and all linear systems solved exactly, this would yield the exact solution. This approximate solver is used a the preconditioner for the composite step conjugate gradient iteration.

When $IPROB = -5$, a parallel Newton algorithm is implemented, similar in structure to the case $IPROB = -1$. A domain decomposition solver analogous to that described in Section 4.4 is incorporated into the block preconditioner defined above.

As an example, we solve the optimal control problem

$$\min \int_\Omega (u - u_0)^2 + \beta(\nabla u - \nabla u_0)^2 + \gamma\lambda^2 \, dx$$

subject to the constraint equation

$$\begin{aligned} -\Delta u &= \lambda \quad \text{in } \Omega \equiv (0,1) \times (0,1), \\ u &= 0 \quad \text{on } \partial\Omega, \end{aligned}$$

and the inequalities

$$1 \le \lambda \le 10.$$

The target function u_0 was

$$u_0 = \sin(3\pi x)\sin(3\pi y),$$

$\beta = 10^{-2}$, and the regularization parameter $\gamma = 10^{-4}$.

This problem was solved in parallel using 16 processors, starting from an initial uniform 17×17 mesh and piecewise linear elements. This mesh was adaptively refined to $NTF = 13241$ elements and $NDF = 6700$, and partitioned, as illustrated in Figure 4.9. Each processor went through five iterations of adaptive refinement, with $MXORD = 1$, so that only piecewise linear polynomials were used. This produced a global mesh with $NDG = 330269$ and block 3×3 linear systems of order 990807. The interior point parameter $\mu = \mu_0 = 10^{-2}$ on the 17×17 mesh, and thereafter was reduced by a factor of 2 in each refinement step, for a final size of $\mu \approx 1.4 \times 10^{-4}$.

The final global mesh, colored by element size, is shown in Figure 4.9. In Figure 4.9, the solution (state variable), the Lagrange multiplier, the control λ, and the error estimate are also shown. Note that *PLTMG* chooses only one approximation space that is used for all three functions. Also all three functions contribute to the error estimate used in the adaptive procedure. The fact that the control λ is essentially a piecewise constant, while the other two functions are relatively smooth is likely responsible for the observed refinement pattern.

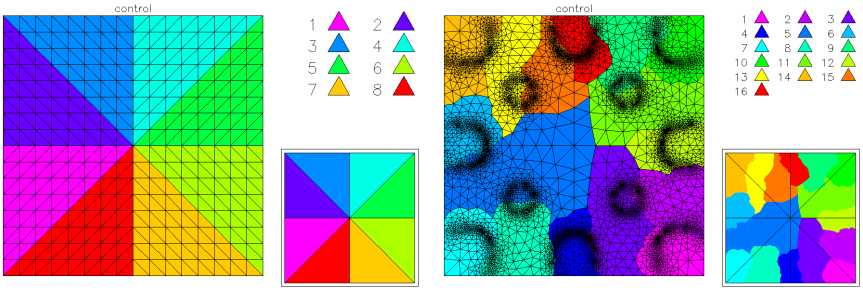

The initial 17×17 *mesh (left) and the load balance with* $NTF = 13241$ *(right).*

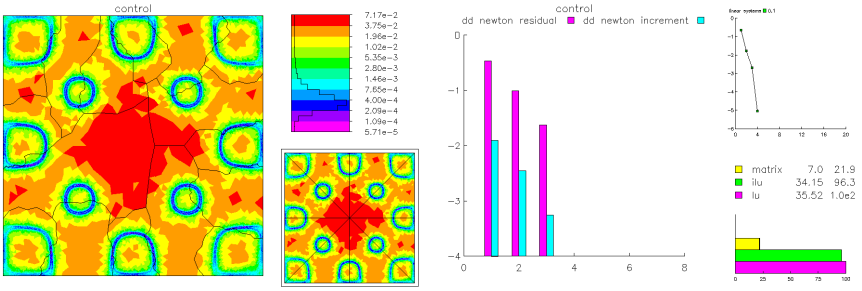

The global refined mesh with $NDG = 330269$ *colored by size (left) and the convergence history of the Domain Decomposition solver (right).*

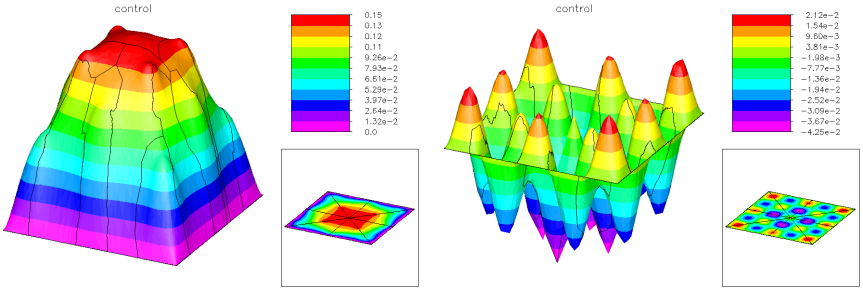

The solution u *(left) and the Lagrange multiplier* v *(right).*

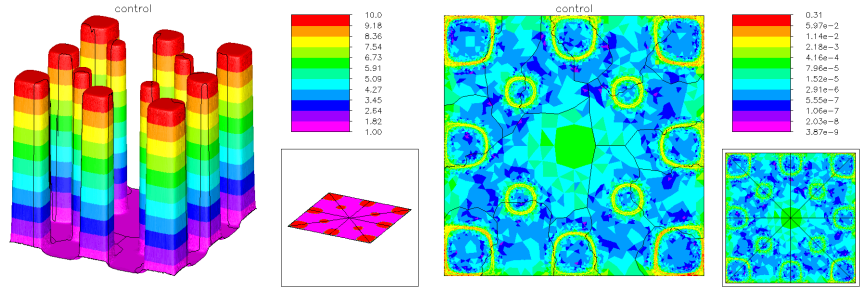

The control λ *(left) and the error estimate on the final mesh (right).*

Figure 4.9.

Chapter 5
Graphics

5.1 Overview.

The graphics package associated with *PLTMG* is composed of subroutines *TRIPLT*, *INPLT*, and *GPHPLT*. These routines are written in self-contained, portable Fortran, addressing the graphics output device through subroutines *PLINE*, *PFILL*, *PFRAME*, and *PLTUTL*. The specifications for these routines are given in Section 6.12.

Typical graphics output consists of three windows or frames. There is a large square window on the left, and two smaller square windows on the right. The main image typically appears in the large frame, and other useful information (for example, a legend matching colors to function values) appears in the smaller frames. The graphics interface provides z-buffer information, for use in three dimensional imaging systems such as OpenGL. All the graphics routines are written such that the image appearing in the main window can be animated using such graphics systems when appropriate.

Subroutine *TRIPLT* graphs the solution and various associated functions (e.g., $\dot{u}$, ψ_r, ϵ_t). *TRIPLT* also has options for plotting vector functions (e.g., ∇u_h). Subroutine *INPLT* can display either a triangulation or a skeleton, with elements or regions colored according to various attributes such as the quality of the elements in a triangulation. Subroutine *GPHPLT* displays various graphs and charts containing timings, convergence histories, and other items of interest.

The parameter *MXCOLR* is a device dependent constant, stating the maximum number of colors available for use by the graphics package. We assume that $2 \leq MXCOLR$. While it is possible to make some interesting plots and contour maps with *TRIPLT* using only monochrome devices ($MXCOLR = 2$), *TRIPLT* makes extensive use of available color facilities in producing (shaded) three-dimensional surface plots and vector plots. *GPHPLT* and *INPLT* also use color, but in less critical ways.

Subroutines *TRIPLT*, *INPLT* and *GPHPLT* offer some capabilities for parallel processing. In the parallel processing environment, only the master process (corre-

sponding to $IRGN = 1$) makes calls to the graphics interface routines (*PLTUTL*, *PFRAME*, *LINE*, and *PFILL*. However, in the case of *TRIPLT* or *INPLT*, one may wish to plot the solution, error, or some other function in situations where the data is distributed among the processors. If MPI is turned on ($MPISW = 1$), and $MPIRGN = 0$, then *TRIPLT* and *INPLT* collect data from all other processors, and draw a composite picture consisting of the union of the refined regions for each processor. If the problem is sufficiently large that it is impossible or inefficient to collect all the data on a single processor, each processor can coarsen its data before sending it to the master process. This coarsening process is controlled by the parameters *ICRSN* and *ITRGT*. If MPI is turned off ($MPISW = -1$), then *TRIPLT* and *INPLT* draw the function on processor one (refined in region one and coarse elsewhere). If one wishes to see the complete image as its exists on some other processor, say processor I, set $MPISW = 1$, $MPIRGN = I$, and call *TRIPLT* or *INPLT*. For some options, *GPHPLT* collects data from all processors when MPI is turned on, for example in presenting timing and load balancing data.

For most of the examples of graphics output, we solved Laplace's equation in a circle of radius one with a crack along the positive x axis. This domain was used to illustrate the triangulation data structure in Section 2.3. Nonhomogeneous Dirichlet boundary conditions were imposed on the circular boundary such that the true solution is $u = r^{1/4}\sin(\theta/4)$, the leading term in the singularity due to the crack tip. Some example output in Section 5.4 came from other problems, in cases where it could not be provided by our simple example.

5.2 Subroutine TRIPLT.

TRIPLT is called using the statement

Call TRIPLT(VX, VY, SF, ITNODE, IBNDRY, ITDOF, E,
IP, RP, SP, GF, QXY, SXY)

The arrays *VX*, *VY*, *SF*, *ITNODE*, *IBNDRY*, and *ITDOF* should define a triangulation. *GF* and *E* contain functions for potential display. *TRIPLT* uses several variables from the *IP*, *RP*, and *SP* arrays, as shown in Tables 2.6–2.8. The string variable *FTITLE* is the character string displayed as a label above the graph. Additionally, *TRIPLT* can use the Fortran subroutine *QXY*. Subroutine *QXY* is documented in Section 2.8. The error flag *IFLAG* is set as in Table 2.9.

The parameter *IFUN* specifies the function to be plotted. The available options are summarized in Table 5.1. Some of these functions are not defined for all problem types. Although there are many possibilities for *IFUN*, they may be classified as *surface plots* and *vector plots*.

For surface plots, all functions are continuous with the (possible) exceptions of the error and scaling factors, which are piecewise constant on triangles, and *QXY*, which can be multivalued along element boundaries due to discontinuities in ∇u_h. If desired, a discontinuous function can be mapped to a continuous function using a local averaging technique. This is invoked by setting the switch $ICONT = 1$.

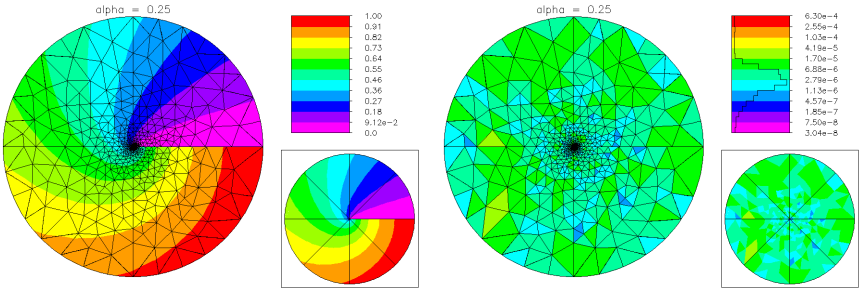

Figure 5.1. *The solution* $IFUN = 0$ *and the error* $IFUN = 5$.

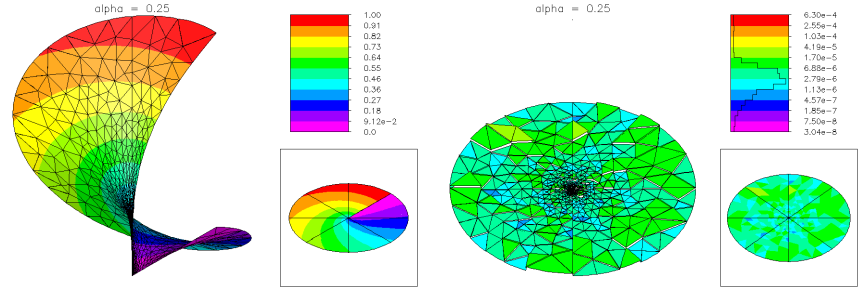

Figure 5.2. *The case* $IFUN = 0$, $(NX, NY, NZ) = (1, -1, -1)$, *and* $IFUN = 5$, $(NX, NY, NZ) = (1, 1, 1)$.

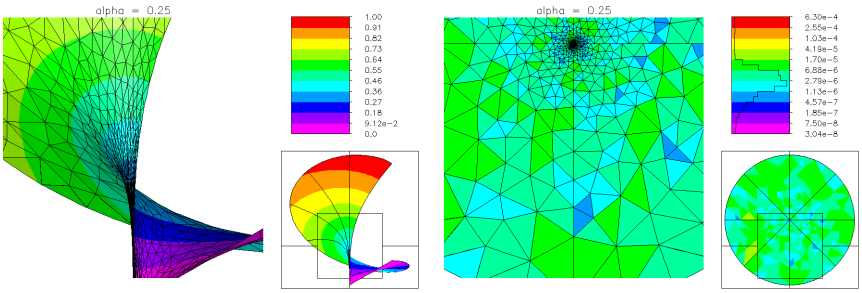

Figure 5.3. *The case* $IFUN = 0$, $(NX, NY, NZ) = (1, -1, -1)$, $RMAG = 2$, $CENX = .5$, $CENY = .3$, *and the case* $IFUN{=}5$, $(NX, NY, NZ) = (0, 0, 1)$, $RMAG = 2$, $CENX = .5$, $CENY = .3$.

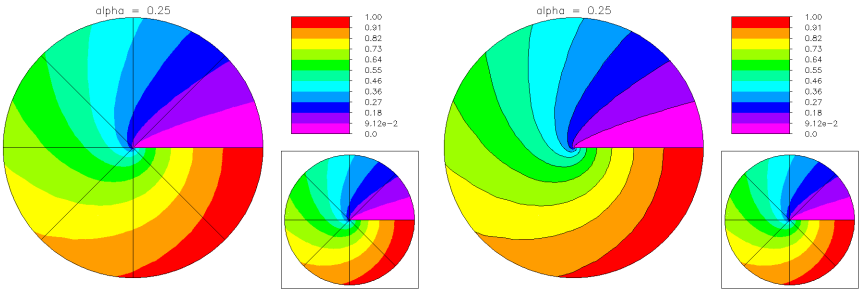

Figure 5.4. *The case* $LINES = 1$ *and the case* $LINES = 3$. *The corresponding picture for* $LINES = 0$ *is in Figure 5.1.*

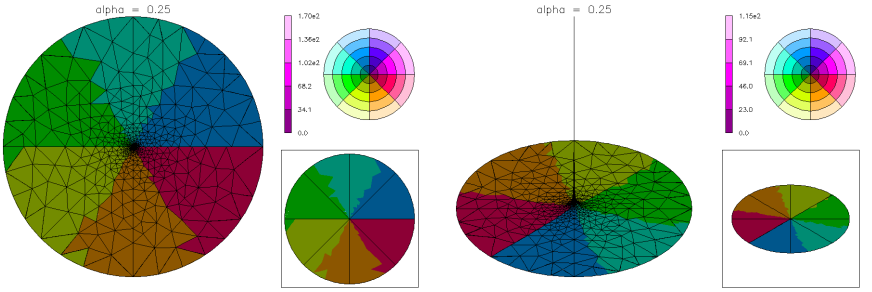

Figure 5.5. *The case IFUN* $= 2$*, ICONT* $= 1$*.* $(NX, NY, NZ) = (0, 0, 1)$ *and* $(NX, NY, NZ) = (1, 1, 1)$*.*

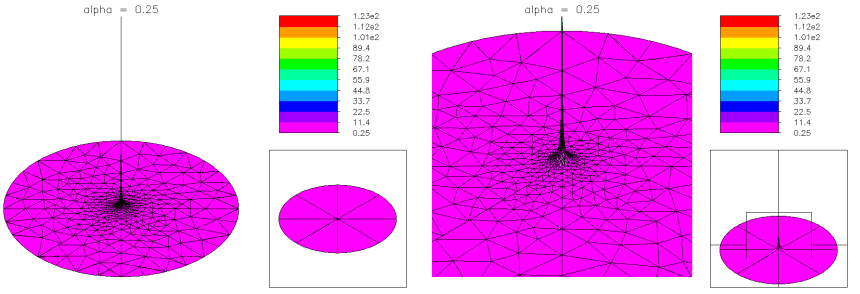

Figure 5.6. *The case IFUN* $= 1$*, ICONT* $= 1$*.* $(NX, NY, NZ) = (1, 1, 1)$*. In the picture on the right RMAG* $= 2$*, CENX* $= .5$*, and CENY* $= .3$*.*

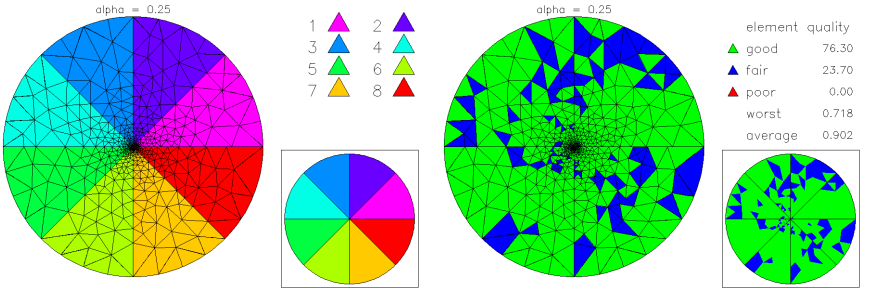

Figure 5.7. *Triangles colored by label (INPLSW* $= 0$*) and by quality (INPLSW* $= 2$*).*

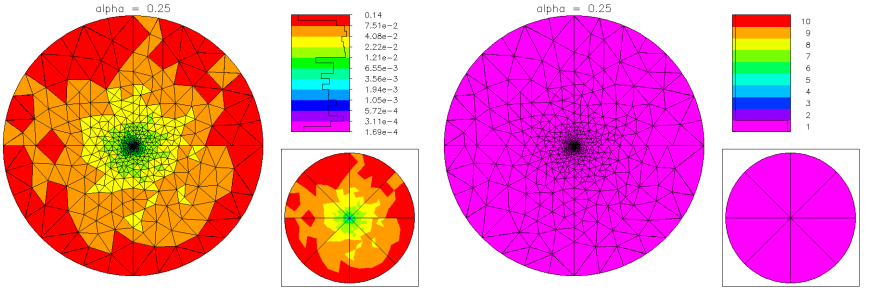

Figure 5.8. *Triangles colored by size (INPLSW* $= 6$*) and by polynomial degree (INPLSW* $= 5$*).*

IFUN	displayed function
0	the solution u_h
1	the scalar function $\mid \nabla u_h \mid$
2	the vector function ∇u_h
3	the alternate function QXY
4	the alternate vector function QXY
5	the error estimate $\|\epsilon_t\|_{\mathcal{H}^1(t)}$
6	the tangent function $\dot{u}$
7	the right singular vector ψ_r
8	the left singular vector ψ_ℓ
9	the Lagrange multiplier u_m
10	the control variable λ_h
11	the dual function ω
12	the scaling factor α_t

Table 5.1. *The values of IFUN.*

5.2.1 Surface Plots.

In the case of surface plots, *NCON* specifies the number of contours (colors) to be used. If $NCON > MXCOLR - 2$, some colors are used for more than one contour. The parameters *SMIN* and *SMAX* can be used to specify the limits of the color scale. If $SMIN < SMAX$, then these values are used as limits, with parts of the function lying outside $(SMIN, SMAX)$ colored white. Otherwise, the largest and smallest values of the displayed function are used as limits.

Each picture consists of three frames; a large plot on the left and a two-part legend on the right. The upper right contains a scale relating colors to function values; three scales are available using the switch *ISCALE* as described in Section 5.2.4. For the case $IFUN = 5$, $ICONT = 0$, a histogram showing the distribution of errors $\|\epsilon_t\|_{\mathcal{H}^1(t)}$ is also provided in this legend. Five line-drawing options using *LINES* and eleven labeling options using *NUMBRS* are also available. *RMAG*, *CENX*, and *CENY* provide a zoom-in capability as described in Section 5.2.3.

The main image can be animated using three dimensional imaging systems such as OpenGL. The viewing perspective can be statically set as well, using the triple $d = (NX, NY, NZ)$. The three-dimensional surface is projected into the plane orthogonal to d, and the function is drawn as it would appear to an observer viewing the surface from a line of sight parallel to d. The vectors (NX, NY, NZ) and $-(NX, NY, NZ)$ cause the same projection to be computed; however, different pictures are generally produced for the two cases. In the former case one observes the projection on the "front" of the plane, and in the latter case one observes the projection on the "back" of the plane. If *MXCOLR* is sufficiently large, the surface will be shaded relative to a light source directly behind the viewer, imparting some additional three-dimensional character to the picture.

The lower right-hand legend provides guidance in understanding three-dimensional

surface plots. In this case the legend contains a "flat" version of the main picture, allowing another avenue for orienting oneself with respect to the viewing perspective. Some examples of surface plots are given in Figures 5.1–5.4.

5.2.2 Vector Plots.

Color plays an important role in the vector plots. Different colors correspond to different directions in the vector field. This is illustrated in the color wheel portion of the upper right-hand legend. The number of directions is specified by the parameter *NCON*. Different intensities of the same color correspond to the magnitude of the vector; darker shades correspond to smaller magnitudes, and lighter shades correspond to higher magnitudes. The correspondence between color intensity and vector magnitude is illustrated for an example color in the upper right-hand legend. The parameters *SMIN* and *SMAX* are used to specify the limits of the color intensity scale for the magnitude of the vector. As with surface plots, if $SMIN < SMAX$, then these values are used as limits; otherwise the largest and smallest magnitudes of the vector function are used.

Three scales for the vector magnitude are available using the option switch *ISCALE*. Five line-drawing options using *LINES* and eleven labeling options using *NUMBRS* are also available, and *RMAG*, *CENX*, and *CENY* provide zoom-in capabilities. The triple *(NX,NY,NZ)* specifies a direction as in the case of surface plots. In this case the surface plotted is the *linear interpolant* of the magnitude of the vector function.[9] In this case the elements remain colored as in a two dimensional vector plot. Some examples of vector plots are given in Figures 5.5 and 5.6.

5.2.3 Parameters RMAG, CENX, and CENY.

The parameters *RMAG*, *CENX*, and *CENY* provide a zoom-in option. *RMAG* is the magnification factor relative to the picture coordinates. For example, if $RMAG = 1$ the whole picture will be drawn; if $RMAG = 2$, the picture is scaled by a factor of 2 in both directions and thus no longer fits on the output device. One must now choose a window and view only a portion of the picture. The fractions $0 \le CENX \le 1$ and $0 \le CENY \le 1$ are used for this purpose. In particular $(CENX, CENY)$ specifies the point that will appear at the center of the magnified window. If $RMAG = 1$, the values of *CENX* and *CENY* are ignored. Some examples are shown in Figure 5.3 and Figure 5.6 (right).

As an aid to understanding, the lower right legend contains a copy of the complete picture (corresponding to $RMAG = 1$). Whenever $RMAG > 1$, a small box is drawn in this legend depicting the portion of the picture appearing in the main graph. The box is supplemented by a crosshair locator, since the box becomes too small to be visible for large magnification factors.

[9] For the actual magnitude, the surface of each triangular element is not necessarily a plane, making the hidden surface problem more difficult.

5.2.4 Parameters ISCALE, LINES, NUMBRS, and MPIRGN.

The parameter *ISCALE* provides three scaling options, summarized in Table 5.2. For linear scaling, drawn contours are equally spaced with respect to the largest and smallest values of the given function $z(x, y)$. If $ISCALE = 1$, then the contours are equally spaced with respect to the largest and smallest values of $\log z$. If $ISCALE = 2$, then the contours are equally spaced with respect to largest and smallest values of the function $\sinh^{-1} z$. The logarithmic scaling clearly requires z to be positive. The $\sinh^{-1}$ scaling is always defined, having a (signed) logarithmic behavior for large $\mid z \mid$ and a linear behavior for small $\mid z \mid$. If $ISCALE = 1$ and $z \leq 0$ at some node, then *TRIPLT* defaults to the $\sinh^{-1}$ scaling. In Figure 5.1, the solution u_h was drawn using the linear scale ($ISCALE = 0$), while the error estimate was drawn using the logarithmic scale ($ISCALE = 1$).

Five line drawing options are available, specified through the parameter *LINES*, as summarized in Table 5.2. If $LINES = 0$, *TRIPLT* will draw edges of all triangles in the mesh. If $LINES = 1$, only boundary edges and edges separating triangles from different regions are drawn. The case $LINES = 2$ is similar to the case $LINES = 1$, except that here boundary edges and edges separating triangles from different processors are drawn. When $LINES = 3$ for surface plots, *TRIPLT* draws boundary triangle edges and contour lines separating contours of different colors. This option produces a traditional contour map on monochrome devices and thus is useful when $MXCOLR = 2$. Some examples for $LINES = 1$ and $LINES = 3$ are shown in Figure 5.4. The option *LINES=3* is not implemented for vector plots. The option *LINES=-1* displays the underling (typically refined) graphics triangulation that was actually used by *TRIPLT* in making the image; this is mainly of interest for debugging.

Eleven labeling options are available in *TRIPLT*; these are specified through the parameter *NUMBRS*, as summarized in Table 5.2. When $NUMBRS \neq 0$, three-dimensional plotting is disabled; the result will be a "flat" (but labeled) surface. Some examples are shown in Figures 2.1 and 2.2.

In making images using MPI, the usual situation is that each processor contributes its part of the image, corresponding to its refined subdomain. However, in certain situations (such as debugging), one may wish to see the complete image as it exists on an individual processor. The parameter *MPIRGN* allows this. When $MPIGRN = 0$, its default value, then all processors contribute to a given image in the usual way. When $MPIGRN = I$ for $1 \leq I \leq NPROC$, then the complete image from processor I is drawn.

5.2.5 Parameters ICRSN and ITRGT.

When *NDF* becomes very large, the amount of data used to make an image may become too large for animated display systems like OpenGL or for Postscript files of reasonable size.[10] In this situation, one may wish to compress the data and make a lower resolution image. The parameter *ICRSN* indicates whether or not to coarsen

[10] Raster graphics images like those produced by X-Windows displays and XPM files are largely independent of the size of the underlying data set.

ISCALE	scale
0	linear
1	logarithmic
2	$\sinh^{-1}$
LINES	line drawing option
0	all triangle edges
1	boundary/interface edges
2	load balance boundary edges
3	contours
-1	underlying graphics triangulation
NUMBRS	labeling option
0	no labels
1	triangles/subregions
2	vertices
3	edges
4	curved edges
5	edge type
6	edge labels
7	processor
8	vertex type
9	degrees of freedom
10	element degree
MPIRGN	image option
0	all processors contribute
$I > 0$	draw image from processor I
ICRSN	coarsening option
0	no coarsening
1	coarsen global subspace
ICONT	smoothing option
0	no smoothing
1	smooth piecewise constant function

Table 5.2. *The values of ISCALE, LINES, NUMBRS, MPIRGN, ICRSN, and ICONT.*

the global subspace, as indicated in Table 5.2. If $ICRSN = 1$, then the parameter *ITRGT* specifies the target number of degrees of freedom for the coarsened subspace. The coarsening option is very much like the mesh coarsening option in *TRIGEN*; many of the same subroutines are used, and the overall coarsening strategy is the same. However, the coarsening criteria is different. When MPI is on ($MPISW = 1$),

each processor independently coarsens the subspace for its subregion to a target of $ITRGT/NPROC$ degrees of freedom. Thus, when the subspaces are later combined, the global subspace appearing in the image will have at most $ITRGT$ degrees of freedom.

When the mesh is coarsened, all numbering options are disabled; $NUMBRS = 0$ is always used. The setting $LINES = 0$ is reset to $LINES = 1$, and $ICONT = 1$ is always used.

5.2.6 Some Algorithmic Details.

The main algorithms of interest in *TRIPLT* are those for hidden line and surface removal. In the general case of a surface plot, one must make comparisons between various triangles to determine whether a given triangle blocks another with respect to the viewer. Since the triangular mesh is generally unstructured, our goal is to organize the data to minimize the number of comparisons between triangles.

Generally, for surface plots in which $(NX, NY, NZ) \neq (0, 0, 1)$, a partial order is constructed in which elements farthest from the viewer are ordered first, and those closest to the viewer are ordered last. The elements are then drawn and colored in order, with the elements closer to the viewer (possibly) overwriting some elements that are farther away. The notion of distance from the viewer is defined with respect to the x and y coordinates only, so that the same ordering is computed independent of the function being graphed. A typical element is compared only to elements with which it shares a common edge; it is ordered before any edge neighbors closer to the viewer and after any neighbors farther away. Since any element has at most three neighbors, this greatly limits the number of comparisons necessary and completely solves the ordering problem for a convex domain with no holes.

Unfortunately, many domains are not convex and have holes, so that elements with boundary edges must be treated as special cases. Thus we make a list of triangles with boundary edges, sort them with respect to the direction (in the (x, y) plane) perpendicular to the (NX, NY) components of the viewing direction. Boundary edges are also sorted by whether they face "backward" or "forward" with respect to (NX, NY). With these preliminary calculations done, all pairs of relevant triangles that *might* conflict are tested and appropriate ordering constraints imposed. For a mesh with NTF triangles, the number of boundary triangles is $O(\sqrt{NTF})$, so that in the worst case (every boundary element compared with every other boundary element), this will still be only $O(NTF)$ work. Since only $O(NTF)$ work is required for the interior elements, the overall work is still $O(NTF)$.

5.3 Subroutine INPLT.

Subroutine *INPLT* is a graphics routine for displaying the input data defining a triangulation or a skeleton. *INPLT* is called using the statement

Call INPLT(VX, VY, SF, ITNODE, IBNDRY, ITDOF,
IP, RP, SP, SXY)

The arrays *VX*, *VY*, *IBNDRY*, *ITNODE*, and *SF* define either a triangulation or a skeleton (*INPLT* uses the value of *ITNODE(3,1)*, which is zero for a skeleton and positive for a triangulation, to distinguish these cases). The string variable *ITITLE* is displayed as a banner above the graph. Variables in the *IP*, *RP*, and *SP* arrays used by *INPLT* are shown in Tables 2.6–2.8. *INPLT* was used to make Figures 3.1 **??**, and **??**, among others in this manual.

INPLSW	triangulation	skeleton
0	user label	user label
1	load balance	uniform color
2	element quality	subregion
3	largest angle	
4	smallest angle	
5	mesh grading	
6	polynomial degree	
7	element diameter	
8	polynomial degree	

Table 5.3. *The values of INPLSW.*

5.3.1 Triangle Plots.

For triangle plots, the elements in the triangulation are colored to depict some feature of the mesh. The available options are controlled by the switch *INPLSW* as summarized in Table 5.3.

If $INPLSW = 0$, the elements in the mesh are colored according to the user supplied labels in *ITNODE(5,I)*; all elements with the same label will have the same color. If $INPLSW = 1$, the elements in the mesh are colored according to the load balance (*ITNODE(4,I)*).

For $2 \le INPLSW \le 5$, *INPLT* colors the elements of the triangulation according to their quality, measured by $q(t)$ in (3.1), their largest angle, their smallest angle, and the local mesh grading, respectively. For each of these measures, five numbers are printed in the upper right legend. The row labeled "average" refers to the average of that quantity over all elements in the mesh; "worst" reports the smallest value of $q(t)$, largest angle, smallest angle, or the steepest local grade over all of the elements. The rows labeled "good," "fair," and "poor" report the percentage of elements in each category and depict the corresponding colors.

For $q(t)$, good means $q(t) \ge \sqrt{3}/2$, fair means $.6 \le q(t) < \sqrt{3}/2$, and poor means $q(t) < .6$. For large angles, good means $A(t) \le \pi/2$, fair means $\pi/2 < A(t) \le 2\pi/3$, and poor means $A(t) > 2\pi/3$ ($A(t)$ is the largest angle). For small angles, good means $\arccos(4/5) \le a(t)$, fair means $\arccos(13/14) \le a(t) < \arccos(4/5)$ and poor means $a(t) < \arccos(13/14)$ ($a(t)$ is the smallest angle). Triangles that are good in terms of $q(t)$ are (necessarily) also good in terms of large and small angles.

Those that are fair in terms of $q(t)$ must be good or fair in terms of large and small angles (but not conversely). The local mesh grading g_v at any vertex v in the mesh is the ratio of the largest to smallest lengths among all the element edges having v as an endpoint. The mesh grade for an element $g(t)$ is the maximum of g_v among its three vertices. For mesh grading, good means $g(t) < 2$, fair means $2 \leq g(t) \leq 3$ and poor means $g(t) > 3$. In Bank and Yserentant [38], control of mesh grading is seen to be a crucial point in creating nonuniform meshes where the $\mathcal{L}_2(\Omega)$ projection of a function $u \in \mathcal{H}^1(\Omega)$ is stable in the $\mathcal{H}^1(\Omega)$ norm.

When *INPLSW* = 6, *INPLT* produces an image in which each element is colored according to its polynomial degree. A histogram showing the distribution of element degrees appears in the legend. When *INPLSW* = 7, *INPLT* produces an image in which each element is colored according to its size. A histogram showing the distribution of element sizes appears in the legend. Although any scaling option available through *ISCALE* can be used, generally the logarithmic scaling (*ISCALE* = 1) produces the most useful image. Some example images made using *INPLT* are shown in Figures 5.7 and 5.8.

The meanings and use of *RMAG*, *CENX*, *CENY*, and *MXCOLR* are identical to *TRIPLT*. Labeling options using *NUMBRS* are summarized in Table 5.2. *INPLT* was used with various *NUMBRS* options to produce Figure 2.1 although the legends on the right-hand sides of the pictures were deleted. For the main graph, three line-drawing options are available using *LINES*, as summarized in Table 5.2.

The meaning and use of parameter *MPIRGN* is the same in subroutine *INPLT* as in *TRIPLT*. Subroutine *INPLT* also allows mesh coarsening, but the criterion is different. In *INPLT*, each element is a single color and the images are two dimensional, and the coarsening criterion reflects these differences. As with *TRIPLT*, *NUMBRS* = 0 is always specified for a coarsened mesh and *LINES* = 0 is reset to *LINES* = 1.

5.3.2 Skeleton Plots.

As with triangle plots, the subregions of the skeleton are colored according to the option specified by *INPLSW* as summarized in Table 5.3. If *INPLSW* = 0, the subregions are colored according to the user supplied labels in *ITNODE(5,I)*, similar to the case of a triangulation. If *INPLSW* = 1, each subregion is given the same color, while if *INPLSW* = 2, each subregion is given a different color.

Subroutine *INPLT* draws a skeleton by first creating a crude triangulation based on the skeleton, and then drawing the triangulation. Here shape regularity and overall quality of the triangulation is not an issue; rather, keeping the number of elements small and computing the triangulation quickly are important. The option *LINES* = −1 displays the underlying triangulation used in the skeleton plot. It was included mainly for debugging purposes.

The parameters *RMAG*, *CENX*, *CENY*, and *MXCOLR* are the same as for triangle plots. Labeling options using *NUMBRS* are summarized in Table 5.2. There are no coarsening or parallel computation options available for skeleton plots. *INPLT* was used with various *NUMBRS* options to produce Figure 2.2.

5.4 Subroutine GPHPLT.

Subroutine *GPHPLT* displays an assortment of data related to the performance of various algorithms and subroutines in *PLTMG* and *TRIGEN* using a graphical format.

GPHPLT is called using the statement

Call GPHPLT(IP, RP, SP)

GPHPLT makes use of the arrays *TIME* and *HIST*, that reside in a common block initialized by *PLTMG* and *TRIGEN* when $IFIRST \neq 0$. The string variable *GTITLE* is displayed as a banner above the graph. Other variables in the *IP*, *RP*, and *SP* arrays used by *GPHPLT* are shown in Tables 2.6–2.8.

IGRSW	displayed graph
0	Newton iteration convergence history
1	CSCG/CSBCG iteration convergence history
-1	matrix statistics
2	individual subroutine timing statistics
-2	time pie chart
3	the continuation path
-3	load balance
4	error estimates for $\mathcal{H}^1$ norm
-4	error estimates for $\mathcal{L}_2$ norm
5	the *IP* array
-5	the *SP* array
6	the *RP* array

Table 5.4. *The values of IGRSW.*

IGRSW is an integer switch for selecting the displayed graph; the available possibilities are summarized in Table 5.4.

5.4.1 Iteration Information.

For the cases $IGRSW = -1, 0, 1$, information about various iterations and preconditioners is displayed. In all three cases, the same three graphs are drawn. The large main window contains the information indicated in Table 5.4 for the corresponding value of *IGRSW*. The other two graphs appear in the two smaller frames on the right. Examples are shown in Figures 5.9– 5.10.

In the case $IGRSW = 0$, in the main window *GPHPLT* graphs the functions

$$\mathcal{R}_k = \log_{10}\left\{\frac{\|\mathcal{G}_k\|}{\|\mathcal{G}_0\|}\right\} \qquad \text{and} \qquad \mathcal{E}_k = \log_{10}\left\{\frac{\|\delta\mathcal{U}_k\|}{\|\mathcal{U}_k\|}\right\}.$$

$\mathcal{G}_k$ is the residual for the Newton iteration, while δS_k is the incremental change in

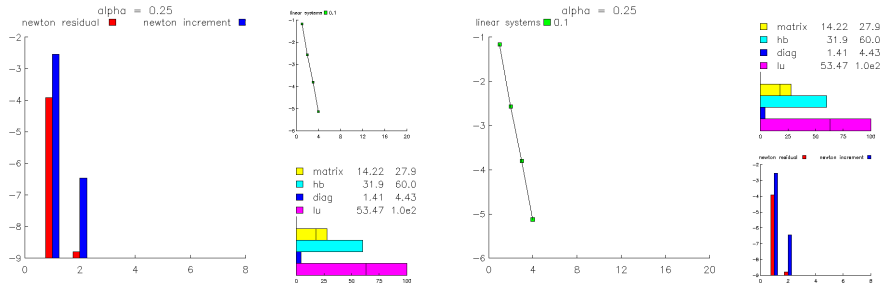

Figure 5.9. *The cases* $IGRSW = 0$ *and* $IGRSW = 1$.

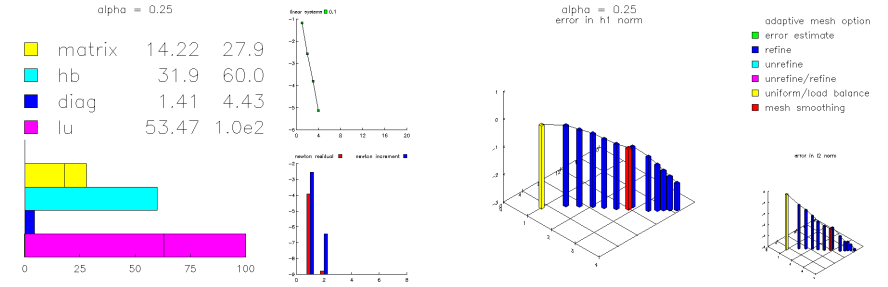

Figure 5.10. *The cases* $IGRSW = -1$ *and* $IGRSW = 4$ *with* $(MX, MY, MZ) = (1, -1, 1)$.

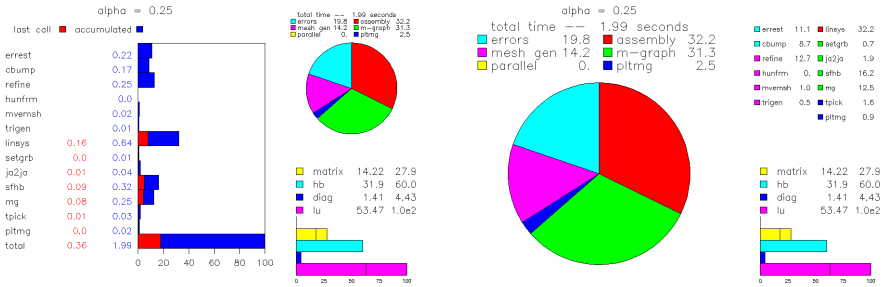

Figure 5.11. *The cases* $IGRSW = 2$ *and* $IGRSW = -2$.

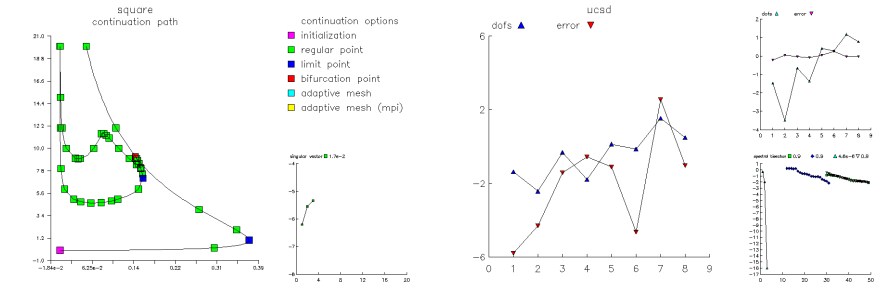

Figure 5.12. *The cases* $IGRSW = 3$ *and* $IGRSW = -3$.

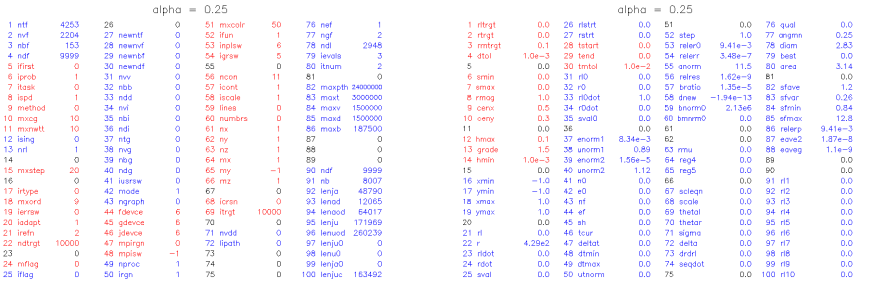

Figure 5.13. *The cases IGRSW* $= 5$ *and IGRSW* $= 6$.

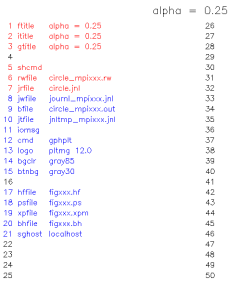

Figure 5.14. *The case IGRSW* $= -5$.

the solution S_k. The precise meaning of $\mathcal{G}_k$ and S_k varies according to the system of nonlinear equations solved for each problem class addressed by *PLTMG*. Both convergence histories are plotted in a bar graph of $\mathcal{R}_k$ and $\mathcal{E}_k$ versus iteration index k.

The convergence history for the most recently solved set of equations is displayed. When this corresponds to a regular (serial) solution ($IPROB > 0$), the relative residuals are red bars, while the solution increments are blue. At most, information about the last twenty Newton iterations is displayed. When $IPROB < 0$, the Newton iteration employs the parallel domain decomposition solver in place of the simple preconditioned linear solver. In this case, the residuals are magenta bars, and the solution increments are cyan.

Nominally, the rate of convergence for Newton's method should asymptotically be quadratic; however, the convergence becomes linear when systems of linear equations involving the Jacobian matrix are only approximately solved.

In the case $IGRSW = 1$, in the main window *GPHPLT* graphs the function

$$\mathcal{S}(k) = \log_{10}\left\{\frac{\|r_k\|}{\|r_0\|}\right\}.$$

Here r_k is the residual of a set of linear equations to be solved and k is the iteration number. The displayed histories are for linear systems solved in the most recent Newton iteration. Up to four such systems are solved in each Newton step, depending on the value of *IPROB*. In all cases, only information about the last twenty iterations is saved and displayed.

Either the composite step conjugate gradient method or composite step bi-conjugate gradient method is used [9, 8], preconditioned by the solver specified by *METHOD*. Each individual step is marked with a small icon; a color pair (green, red), (blue, yellow), (cyan, magenta), (white, black) is assigned to each history. In each case, for simple steps the icon is colored with the first color (e.g., green), while for composite steps the icon is colored with the second color (e.g., red).

In the case $IGRSW = -1$, in the main window statistics related to the the sparse matrix and its factorizations is displayed. Potential information about five matrices is given

1. The stiffness matrix, colored yellow.
2. The *ILU* factorization, colored green.
3. The *HB* factorization, colored cyan.
4. The block diagonal factorization, colored blue.
5. The complete *LU* factorization, colored magenta.

The first four correspond to matrices and factorizations that have been computed; *ILU* and *HB* and block diagonal factorization data appear only if they have been selected by the parameter *METHOD*. The complete *LU* factorization data is included for reference, and indicates data relevant to sparse Gaussian Elimination with the minimum degree ordering.

At the top, two columns of figures appear. The first is the average number of nonzeros per row in the matrix. The second is the same, but given as a percentage relative to sparse Gaussian Elimination. Below is a bar graph reflecting the actual storage used. This is different from the numerical data, in that if the matrices are symmetric, only the diagonal and upper triangle are stored. The storage bar for Gaussian Elimination (*LU*) is hypothetical only. In each colored bar, a vertical black line might appear; this indicates the size of the *JA* or *JU* arrays relative to the corresponding *A* or *U* arrays.

5.4.2 Timing Statistics.

If $IGRSW = 2$, *GPHPLT* prints a summary of timing statistics for *PLTMG* and *TRIGEN*. An example is given in Figure 5.11. Statistics are given both for the total accumulated time since initialization ($IFIRST = 1$) and for the time spent during the last call to *PLTMG* or *TRIGEN*. The timings are itemized with respect to subroutines that carry out major computational tasks in the package. These subroutines are listed in Table 5.5. Depending on the problem, some of these routines may not be called.

A bar graph is drawn illustrating the percentage of time spent in each routine. Each bar in the graph is partitioned into a part corresponding to the last call to *PLTMG* (red) and a part corresponding to all preceding calls (blue). The timing pie graph described below appears in the upper right frame.

If $IGRSW = -2$, *GPHPLT* displays a pie graph summarizing the same information. Each routine in Table 5.5 is assigned to one of six categories: linear system assembly (red), multigraph solver (green), mesh generation (magenta), a posteriori error estimation (cyan), parallel processing routines (yellow), and other *PLTMG* routines (blue). A pie graph showing the fraction of total time spent in each of the six categories is drawn in the main frame. Details of individual contributions from the subroutines listed in Table 5.5 are summarized in the upper right frame. Sample output is shown in Figure 5.11.

When $MPISW = 1$, the times displayed for $IGRSW = \pm 2$ are time averaged across all processors. In this case, in the lower right frame, a graph displaying the deviation from the average time for each processor is drawn.

5.4.3 Continuation Path.

When $IGRSW = 3$, *GPHPLT* displays the continuation path generated by the continuation procedure $IPROB = 3$. Target points are marked by small boxes, generally using different colors for different values of *ITASK*. A legend appears in the upper right frame summarizing the possibilities. Up to one hundred target points generated by calls to *PLTMG* are saved and displayed. Successive points are interpolated using parabolic arcs matching the values of (λ, ρ) and the tangent vectors $(\dot\lambda, \dot\rho)$. In the lower right frame appears a convergence history for the most recent singular vector computation. Sample output is shown in Figure 5.12.

5.4.4 Parallel Statistics

When $IGRSW = -3$, *GPHPLT* plots the functions

$$T_k = \log_2 \left\{ \frac{NPROC \cdot NTF(\Omega_k)}{\sum_k NTF(\Omega_k)} \right\} \quad \text{and} \quad E_k = \log_2 \left\{ \frac{NPROC \|\epsilon_t\|_{\mathcal{H}^1(\Omega_k)}}{\sum_k \|\epsilon_t\|_{\mathcal{H}^1(\Omega_k)}} \right\}$$

where $1 \le k \le NPROC$. Both curves appear in the large frame. When $MPISW = 1$ the information from all processors is obtained by an exchange of data using the MPI library. This is the most useful situation. When $MPISW = -1$, the same graph is made using local data on the given processor; this case is typically not interesting. In the upper right frame is a similar graph for the distribution of error and elements following the initial load balancing step ($IADAPT = 7$). In the lower right frame appear convergence histories for eigenvalue computations in the load balancing phase. Convergence histories are shown for the four most recent problems. Sample output is shown in Figure 5.12.

5.4.5 Error Estimates.

In the case $IGRSW = 4$, *GPHPLT* graphs the function

$$\mathcal{F}_1(NDF, TIME) = \log_{10} \left\{ \frac{\|\epsilon_t\|_{\mathcal{H}^1(\Omega)}}{\|u_h\|_{\mathcal{H}^1(\Omega)}} \right\},$$

and in the case $IGRSW = -4$, *GPHPLT* graphs the function

$$\mathcal{F}_0(NDF, TIME) = \log_{10}\left\{\frac{\|\epsilon_t\|_{\mathcal{L}_2(\Omega)}}{\|u_h\|_{\mathcal{L}_2(\Omega)}}\right\}.$$

Here ϵ_t is the computed approximation of the error $u - u_h$. While it is hoped that these approximations accurately reflect the true state of affairs, the estimates are based on a posteriori calculations involving only the computed solution. Some judgment of the validity of such computations may be required. An example is shown in Figure 5.10.

Error estimates are plotted as a function of both *NDF* and *TIME*. In particular, $\mathcal{F}_j$ is graphed versus $\log_{10} NDF$ and $\log_{10} TIME$ in a three-dimensional graph. All data points (up to the 20 most recent) for which error estimates are available are marked with rectangular cylinders of different colors. A legend appears in the upper right frame summarizing the possibilities. In the case $IGRSW = 4$, the plot of $\mathcal{F}_0$ appears in the lower right frame; if $IGRSW = -4$, the plot of $\mathcal{F}_1$ in the lower right frame.

The triple $d = (MX, MY, MZ)$ specifies the viewing perspective for these graphs in a fashion similar to *(NX,NY,NZ)* for surface plots. The choice $(1, -1, 1)$ is a reasonable default. The choice $(0, -1, 0)$ yields a traditional two-dimensional graph of $\log_{10} \mathcal{F}_j$ versus $\log_{10} NDF$. The choice $(1, 0, 0)$ yields a two-dimensional graph of $\log_{10} \mathcal{F}_j$ versus $\log_{10} TIME$. The main image can be animated using three dimensional imaging systems such as OpenGL.

5.4.6 Displaying Data Arrays.

The options $|\, IGRSW \,| \geq 5$, *GPHPLT* displays the *IP*, *RP*, or *SP* arrays. Unlike other graphics options, here the entire graphics window is treated as a single frame. In the case of the *IP* and *RP* arrays, all 100 entries, their names, and their current values are displayed. Entries that can be interactively reset in the *ATEST* driver are colored red, unused entries appear in black, and all other entries are colored blue. This situation is similar for the *SP* array, except only the first 50 entries are displayed (the remainder are all presently unused). Examples are shown in Figures 5.13–5.14.

subroutine	main function
TGEN	create triangulation from skeleton
REFINE	adaptively refine the triangulation
UNREFN	adaptively unrefine the triangulation
HUNFRM	uniformly h-refine the triangulation
PUNFRM	uniformly p-refine the triangulation
MVEMSH	adaptively smooth the mesh points
ERREST	compute error estimates for u_h
CBUMP	recover derivatives for error estimation
CDLFN	compute dual function
EXPTH	MPI exchange *IPATH* data
EXFLAG	MPI exchange error flag data
BCAST	broadcast mesh to all processors
LDBAL	compute a load balance
LDEV	solve eigenvalue subproblem in load balance
CUTR	reorganize data structures for reconciling mesh
PASTE	reconcile mesh along interface of *IRGN*
PASTE1	reconcile mesh along interface not part of *IRGN*
TRIGEN	all other time spent in *TRIGEN*
SETGRB	compute block *JA* array
SETGR2	compute DD interface *JA* array
JA2JA	min degree / reordering
SFBILU	block *ILU* factorization
SFHB	*HB* matrix factorization
MG	solve equations using CSCG/CSBCG iteration
BLK3	solve equations for $IPROB = \pm 3$
BLK4	solve equations for $IPROB = \pm 4$
BLK5	solve equations for $IPROB = \pm 5$
LINSYS	assemble linear system
RGNSYS	assemble linear system for DD
CEV	compute the singular value μ and vectors ψ_r and ψ_ℓ
SWBRCH	switch branches at a bifurcation point
PREDCT	compute the steplength σ for continuation
TPICK	line search for Newton iteration
TPICKD	line search for Newton/DD iteration
PLTMG	all other time spent in *PLTMG*

Table 5.5. *Subroutines timed by GPHPLT.*

Chapter 6

Test Driver

6.1 Overview.

Program *ATEST* is the test driver used in the development and testing of the *PLTMG* package. *ATEST* is a flexible program in that it accepts simple command strings directing it to call subroutines or perform other tasks. It is not limited to a fixed sequence of tasks on a particular run; any routine can be called as often as desired, with certain parameters reset for each call at the discretion of the user.

The program *ATEST* can operate in four modes, governed by the switch *MODE*. If $MODE = -1$, *ATEST* runs as an interactive program, accepting commands from the user via a terminal window. If $MODE = 0$, *ATEST* runs interactively, accepting commands from the user via an X-Windows interface. This interface is based on the Motif widget set and can be used only in environments supporting X-Windows. If $MODE = 1$, *ATEST* runs as a batch program, reading commands from a journal file and sending all output to appropriate output files. Finally, if $MODE = -2$, *ATEST* runs as a slave mode under MPI; this mode cannot be directly set by the user, but is set by *ATEST* if it determines that it is a slave node in a parallel computation. In this situation, the user specifies *MODE* only for the master node, which can be any of the three other options.

A common command syntax is used for all modes. This is described first for the case $MODE = -1$ in Section 6.2. The extensions used in the X-Windows interface are described in Section 6.3.

Several files are written by *ATEST*. The file *BFILE* contains a complete record of all commands and printed output produced during the session. The file *JWFILE* contains a record of all commands read and processed during the session, formatted as a journal file. See Section 6.8 for a discussion of journal files. *ATEST* also creates a temporary file *JTFILE* used in connection with the journal command. While most commands invoke one of the major routines in the package, there are a few utility routines (e.g. for reading and writing files) which are documented in Sections 6.7–6.10.

6.2 Terminal Mode.

In terminal mode, commands are entered from a terminal window in character strings of 80 characters, counting blanks. The syntax of a command can take several forms, but the root command is always a single letter. The commands that are currently recognized by *ATEST* are summarized in Table 6.1.

Command	Action
s	call *PLTMG*
t	call *TRIGEN*
f	call *TRIPLT*
g	call *GPHPLT*
i	call *INPLT*
r	read data set from a file
w	write data set to a file
u	call *USRCMD*
j	read journal file
k	execute shell command
p	MPI toggle
q	quit

Table 6.1. *Available commands for ATEST.*

The terminal window prompt is the string *command:*. At this prompt, one can enter a command string (e.g., s), reset parameters as described below, or enter a blank line to see a list of the available commands. In this latter case the terminal window will appear as follows.

```
command:
pltmg  s    trigen t    triplt f    gphplt g    inplt  i    read   r
write  w    usrcmd u    journl j    shell  k    mpi    p    quit   q

command:
```

A syntax error in a given command string causes the entire string to be ignored. *ATEST* will display the string *command error* and present the command prompt for a new input string.

The most simple commands are just single lower case letters as shown in Table 6.1. However, associated with most commands are various parameters which can be reset before calling the given routine. To see a listing of the parameters associated with a given command and their current values, without executing the command itself, enter the command in upper case at the command prompt. For example, the command F will display the parameters which can be interactively reset in connection with *TRIPLT*.

```
command:F
```

```
ifun   f  0         iscale s  0         lines  l  0         numbrs n  0
fdevce d  0         nx     nx 0         ny     ny 0         nz     nz 1
ncon   c  11        icont  ic 0         icrsn  cr 0         itrgt  it 10000
mxcolr mc 256       smin   sn 0.0       smax   sx 0.0       rmag   m  1.0
cenx   cx 0.5       ceny   cy 0.5       mpirgn mr 0
ftitle t  "alpha = 0.25"

command:
```

There are fourteen integer parameters, five real parameters, and one string parameter affecting subroutine *TRIPLT* that can be interactively reset by the user. To the right of each parameter is a one- or two-letter alias (to avoid typing long names), followed by the current value.

To reset some parameters associated with a command c (c = *s, f, g,* etc.), without invoking the command itself, one can type a string of the form

```
command:C name1=value1, name2=value2, ... , namek=valuek
```

Note that the root command appears in upper case. The *namek* refer to variable names or their aliases, and *valuek* refer to integer, real, or string values. Several parameters can be reset, with different entries separated by commas. Values for integer parameters should be integers, while values for real parameters can be specified using integer, fixed point, or exponential notation. There are three types of string parameters: *short*, *long* and *file*. Short strings are typically single words and can not contain any blank characters. Files are typically file names, and they also can not contain any blank characters. All other strings are long, and can contain any printable ASCII characters other than double quotes. Values of long string parameters should appear within double quotes. Short and file string parameters are not enclosed with double quotes. Blank spaces are ignored everywhere but within the value field of a long string parameter. A syntax error in the input line (e.g., a misspelled variable name) causes the entire command to be ignored and no variables to be reset. *ATEST* will respond *command error* and then ask for the next command. For example, here we reset $ISCALE = 1$, $NCON = 20$, $CENX = .3$, $RMAG = 10$, and $FTITLE =$ *A new title for Circle*. Subroutine *TRIPLT* is not called, but the parameters are updated and redisplayed as

```
command:F s=1, ncon=20, cenx=.3, rmag=1.e1, t="A new title for Circle"
ifun   f  0         iscale s  1         lines  l  0         numbrs n  0
fdevce d  0         nx     nx 0         ny     ny 0         nz     nz 1
ncon   c  20        icont  ic 0         icrsn  cr 0         itrgt  it 10000
mxcolr mc 256       smin   sn 0.0       smax   sx 0.0       rmag   m  10.0
cenx   cx 0.3       ceny   cy 0.5       mpirgn mr 0
ftitle t  "A new title for Circle"

command:
```

One can reset some parameters for a given command c, and then invoke the command itself, using a string of the form

```
command:c name1=value1, name2=value2, ... , namek=valuek
```

Note that the only difference is that the root command now appears in lower case rather than upper case. Thus

```
command:f s=1, ncon=20, cenx=.3, rmag=1.e1, t="A new title for Circle"
```

resets the indicated parameters as in the previous example. However, instead of displaying the updated values, subroutine *TRIPLT* is called.

Finally, the graphics and MPI commands (f, i, g, and p) have a short form allowing one crucial parameter (*IFUN*, *INPLSW*, *IGRSW*, and *MPISW*, respectively) to be reset without typing even the alias. For example,

```
command:f5
```

is the short form for

```
command:f ifun=5
```

The short and long forms of these commands cannot be mixed. Thus

```
command:f5, ncon=10
```

is not valid.

6.3 X-Windows Mode.

When $MODE = 0$, the driver *ATEST* creates an X-Windows interface for the *PLTMG* package. The functional capabilities are the same as for the terminal window mode, but the possibilities for data entry are more varied. An example of the X-Windows interface appears in Figure 6.1.

The main display contains two elements. The upper portion of the display contains *command buttons*. The bottom portion of the display is the *history window*. The interface supports up to ten graphics displays. The command buttons stand in one to one correspondence with the basic *ATEST* command set shown in Table 6.1. In particular, clicking the left mouse button (button one) with the pointer over a command button is equivalent to the typed lower-case version of that command. For example, clicking mouse button one on the *TRIPLT* command button causes subroutine *TRIPLT* to be called as in the command f. On the other hand, clicking on the right mouse button (button three) with the pointer over a command button is equivalent to the upper case version of the command. Clicking mouse button three on the *TRIPLT* command button causes the parameters for the *TRIPLT* command to be displayed in a popup reset window, as in the typed command F. This is shown is figure 6.2.

The parameters associated with a given command are displayed in the reset window in a format similar to terminal mode. However, each parameter value is displayed in one line text-editing window, and can be reset by typing in the new value. For some parameter names (e.g., *IFUN* in Figure 6.2), the name appears

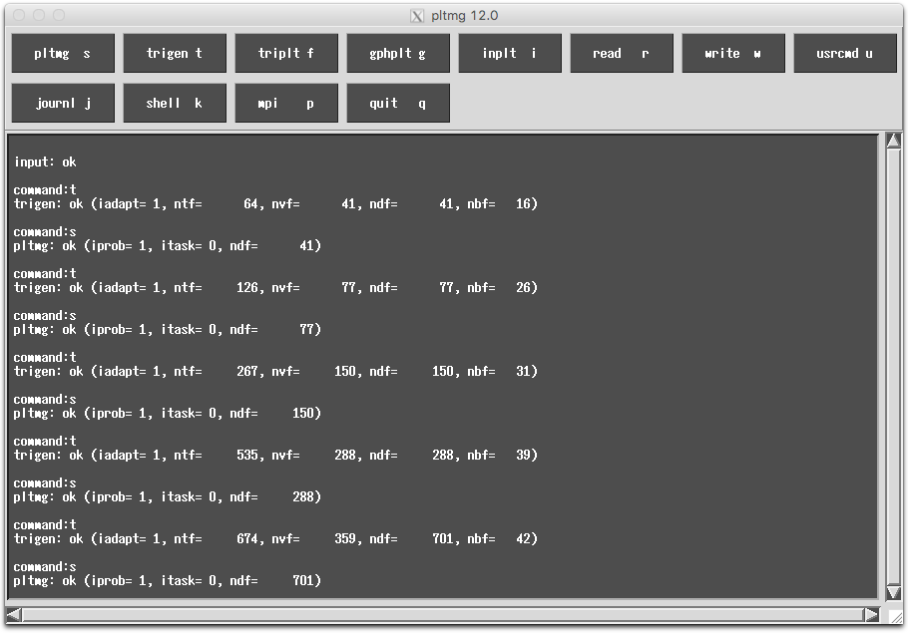

Figure 6.1. *The X-Windows interface.*

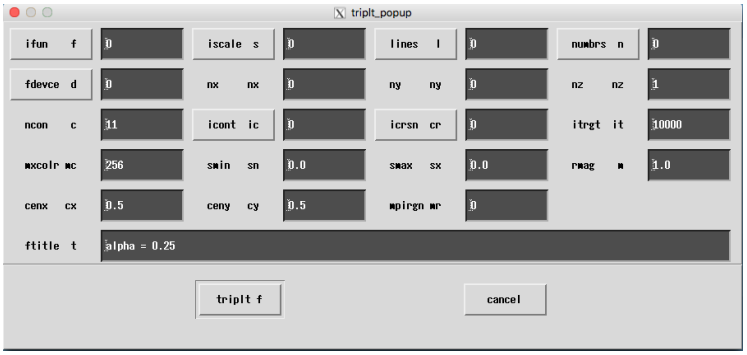

Figure 6.2. *An example reset window.*

in a raised button. Clicking on the name causes a display of radio buttons, listing available options for the given parameter, to pop up. Clicking on the appropriate option causes the parameter to be reset to the corresponding value. The radio button popup associated with the parameter *IFUN* appears in Figure 6.3.

For file selection commands (*READ*, *WRITE*, and *JOURNL*), the generic reset window is replaced by the Motif file-selection widget. The file-selection popup for the *JOURNAL* command is shown in Figure 6.4.

The history window displays the contents of the output file, *BFILE*, as it is

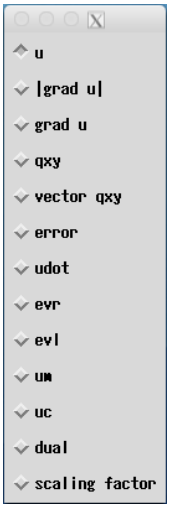

Figure 6.3. *An example radio buttons popup.*

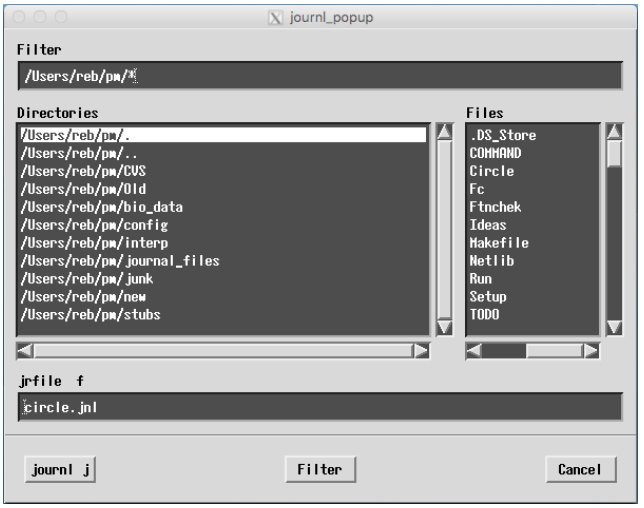

Figure 6.4. *An example file selection popup.*

created. If the file becomes sufficiently large, only the tail of the file is displayed.

The X-Windows driver supports ten graphics displays (numbered 0-9). The parameter $NGRAPH$, $1 \leq NGRAPH \leq 10$, states the number of windows to create initially. Graphics displays can be dismissed and recreated as necessary. These windows use only X-Windows primitives, and display static images which cannot be manipulated (e.g. rotated) with the mouse. Graphics popups can be resized in the usual way, but maintain a 3/2 aspect ratio. Also, any existing image is erased upon resize, and must be redrawn.

When executing a journal file in X-Windows mode, if a graphics command is executed, depending on the graphics device selected, *ATEST* can pause after the picture is drawn, and create a small popup *continue* button. In this case, *ATEST* waits until the user dismisses the *continue* popup before continuing to execute the journal file. This allows time for the user to view the picture before processing the next command in the journal file.

The X-Windows display can be interactively resized in the usual way. However, *ATEST* will adjust the user-specified resizing such that an overall aspect ratio of 3/2 is maintained. *ATEST* also imposes a minimum size requirement on the main window.

The string parameters *BGCLR* and *BTNBG* allow the user to specify the background and button background colors for the main display. Motif automatically defines the remaining colors used in the display. These parameters can be given any of the named colors supported by X-Windows. The string parameter *LOGO* is provided to X-Windows for use as titlebars and other identifiers.

Finally, we remark that the X-Windows interface does not follow the pattern of many X-Windows programs, in that the *PLTMG* package was not integrated into the X-Windows system with the X-Windows interface serving as the main routine. Indeed, the X-Windows interface is realized as a collection of C language subroutines called by a Fortran driver. These routines use the same database of Fortran character strings as the terminal window interface to define their displays, and return command strings of the same type described in the terminal windows interface. Both the X-Windows interface and the terminal window interface are quite generic, in that neither contains direct links to any of the main routines in the package. Thus changes in the behavior of routines comprising the package have no impact on the interface routines and at most modest impact on the database of character strings that define the displays.

6.4 Batch Mode.

When $MODE = 1$, the *ATEST* driver runs as a batch program. All commands are read from the journal file specified in *JRFILE*. Graphics output should be directed to files (BH, Postscript, and XPM) rather than to interactive displays.

6.5 Parallel Processing

When run as a parallel program using *NPROC* processors, *ATEST* uses a master-slave model. One process, the master process, runs in terminal, X-Windows, or batch mode, and the remaining $NPROC - 1$ slave processes all run with $MODE = -2$. Slave nodes receive command strings from the master node via MPI communication. At any given time, the parallel computation is in one of two possible states that specify how slave nodes should process commands. Somewhat arbitrarily, the two states are denoted “off” and “on”. When MPI is on, all processors execute all commands from the user, whether entered interactively or through a journal file. When MPI is off, only the master process executes most commands. Slave nodes

remain active and still receive and evaluate the command strings they receive. Some commands (namely p and q) continue to be executed and some parameter updates continue on all processors in the off state. However, in the off state, slave nodes are mainly waiting for MPI to be turned on again.

The p command is used to switch between the on and off states of MPI. When $MPISW = 1$, MPI is on, and when $MPISW = -1$, MPI is off. The p command is unusual in that it can behave as a toggle; executing p with no argument switches the MPI state. The p command can also be employed in the usual way to explicitly set the MPI state using the parameter *MPISW* (e.g., $p1$ turns on MPI, while $p-1$ turns off MPI). The *MPI* command button in X-Windows mode is a bit unusual; when *MPI* is on, the *MPI* command button changes color (to the background color of the main display). When *MPI* is off the *MPI* command button returns to its usual color.

A common and effective way to use MPI is to create a journal file that contains a script for the entire computation (including p commands) The j command issued in the MPI on state directs all processors to run the journal file. The master process will then execute the entire script, while the slave nodes execute the parts of the journal file that correspond to the on state.

An issue with respect to file names arises in the context of parallel processing. Some files, for example a journal file, are intended to be read by all processors. In other situations, for example writing data files, each processor is intended to process its own version of the file. Then name conflicts can potentially become catastrophic if all nodes read and write files on the same file system. To resolve this conflict in a simple way that allows the user to easily specify on a case-by-case basis if the file is a single file or a file with distinct copies on each node, *ATEST* scans all file names, looking for the characteristic string *MPIXXX*. If found, this string is replaced by *MPI001*, *MPI002*, etc, where the integer part denotes the processor. Thus, for example if one sets

JRFILE = MYFILE.JNL

all nodes process the same file with the name *MYFILE.JNL*. If one sets

RWFILE = MYFILE_MPIXXX.RW

node one would process the file *MYFILE_MPI001.RW*, node two would process the file *MYFILE_MPI002.RW*, and so on.

6.6 Array Dimensions and Initialization.

ATEST has six labeled *common* blocks:

```
common /atest1/ip(100),rp(100),sp(100)
common /atest2/iu(100),ru(100),su(100)
common /atest3/mode,jnlsw,jnlr,jnlw,ibatch
common /atest4/jcmd,cmdtyp,list
```

```
common /atest5/idevce
common /atest6/nproc,myid,mpisw,mpiint,mpiflt
```

The *IP*, *RP*, and *SP* arrays are described in Section 2.7. The arrays *IU*, *RU*, and *SU* are not directly used by *ATEST* or any of the other routines. They are provided to the user for storing integer, real, and string parameters associated with a particular problem. The advantages in using these arrays are that they are saved and read in the *w* and *r* commands; the common block *ATEST2* can be included in subroutines *A1XY*, *A2XY*, etc., where the parameters may be needed; and they can form part of the interface for resetting problem parameters using *USRCMD*. *ATEST3* contains internal control parameters used by *ATEST*; each has a corresponding location in the *IP* array. *ATEST4* contains string and integer variables that are used for internal communication among the user interface routines. The block *ATEST5* contains an integer specifying the current graphics output device, while *ATEST6* contains parameters relevant to MPI.

The input data arrays *ITNODE(5,MAXT)*, *ITDOF(8,MAXT)*, *E(MAXT,2)*, *IBNDRY(7,MAXB)*, *SF(2,MAXB)*, *VX(MAXV)*, *VY(MAXV)*, *GF(MAXD,7)*, and *IPATH(6,MAXPTH)* are declared at the beginning of *ATEST*. The sizes of the arrays, *MAXT*, *MAXV*, *MAXD*, *MAXB*, and *MAXPTH*, are specified at the beginning of *ATEST* using *parameter* statements; changing sizes to suit a particular computing environment or problem is thus a simple matter.

To use *ATEST*, the user must provide Fortran subroutines *A1XY*, *A2XY*, *FXY*, *GNXY*, *GDXY*, *P1XY*, *P2XY*, *SXY*, and *QXY*. Subroutine *USRCMD* should be provided, if only as a dummy routine. The user must also supply subroutine *GDATA*, in which the input arrays *VX*, *VY*, *SF*, *ITNODE*, and *IBNDRY* are specified, along with some parameters in *IP*, *RP*, *SP*, and possibly *IU*, *RU*, and *SU*. Other entries of the *IP*, *RP*, and *SP* arrays not required to be provided by the user through *GDATA* are given default values at the beginning of *ATEST*, but can be reset by the user as desired.

6.7 Reading and Writing Files.

The *w* and *r* commands are used to save and restore data sets. The arrays *IP*, *RP*, *SP*, *IU*, *RU*, *SU*, *VX*, *VY*, *SF*, *IBNDRY*, *ITNODE*, *ITDOF*, *IPATH*, *E*, and common blocks *PLTMG6* and *PLTMG7* are written to (*w* command) or read from (*r* command) the file *RWFILE*. Data files are formatted as machine independent binary files using the XDR protocol. The *w* and *r* commands can be used with both the triangulation and skeleton data structures.

One can use the *w* and *r* commands to save and restore the solution at various points along a continuation path. One can also save solutions in the current run for post processing (graphics, etc.), which can then occur in a later run.

The parameter *MPIRGN* is also useful in this setting. When $MPISW = 1$ and *MPIRGN=0*, then a *r* or *w* command will cause all processors to read or write the specified file. However, if one would like to read or write a file on just one processor (e.g., for debugging), one can set $MPISW = 1$ and *MPIRGN=I*, for $1 \le I \le NPROC$, and the file will be read or written only by processor I.

6.8 Journal Files.

The *j* command causes *ATEST* to read its command strings from the file *JRFILE*, rather than accepting them interactively from the user. It is the only option available in batch mode. A journal file is an ASCII file containing a sequence of command strings as described in Section 6.2. The symbol # appearing as the first character in a line causes that line to be interpreted as a comment. When the end of the file is reached *ATEST* returns to terminal or X-Windows mode and again accepts commands interactively. If a *q* command is encountered in a journal file, *ATEST* will exit.

6.9 Shell Command.

The *k* command causes the string stored in the variable *SHCMD* to be executed by the user's shell. It is included mainly as a convenience, in particular as a means to include system file manipulation commands within journal files.

6.10 Subroutine USRCMD.

The *u* command is used to call the user supplied routine *USRCMD*.

Call USRCMD(VX, VY, SF, ITNODE, IBNDRY, IP, RP, SP,
IU, RU, SU)

This routine is written by the user to perform any tasks not covered by other commands. In our experience, the most frequent use of *USRCMD* has been to reset parameters unique to a particular problem.

USRCMD is affected by the variable *IUSRSW*. If $IUSRSW = 0$, the return from *USRCMD* causes *ATEST* to present the command prompt. If $IUSRSW \neq 0$, the return from *USRCMD* results in a branch to the user supplied routine *GDATA* before presenting the command prompt. This switch is useful if modified parameters affect the geometry of the region, boundary conditions, etc., requiring modifications of the input arrays.

Since the most frequent use of *USRCMD* is to modify problem dependent parameters, we now describe how to build an interface within *USRCMD* allowing one to reset parameters in a fashion similar to the other commands. This is done via subroutine *USRSET*, which is called as follows:

Call USRSET(FILE, LEN, IU, RU, SU)

IU, *RU*, and *SU* are integer, real, and *CHARACTER*80* arrays, respectively, of size 100 containing the parameters to be reset. It is often convenient to use the *IU*, *RU*, and *SU* arrays provided by *ATEST* in common block *ATEST2* for this purpose. *FILE* is a *CHARACTER*80* array of length *LEN*, described below. In terminal mode, the command *u* creates a display listing the user parameters and their current values, similar to the upper case form of other commands. Commands

of the form

```
command:u name1=value1, name2=value2, ... , namek=valuek
```

reset the indicated parameters and then display the updated values. In X-Windows mode, pressing the *USRCMD* command button with mouse button one pops up a reset window, similar to pressing mouse button three for the other commands.

The array *FILE* contains a list of commands that define the variables to be reset, and characterize the reset display. The commands in *FILE* have a syntax similar to the basic scripting language we have defined for *ATEST* itself. However, in this case there are just two basic commands: n (name variable) and s (string for radio button). These are summarized in Table 6.2.

Parameters associated with n command			
Name	Alias	Type	Value
vname	n	short	maximum of 6 characters
alias	a	short	maximum of 2 characters
vtype	t	short	i (int), r (real), s (short), l (long), f (file)
index	i	int	pointer to *IU*, *RU*, *SU*

Parameters associated with s command			
Name	Alias	Type	Value
vname	n	short	variable name
value	v	-	depends on vname
label	l	long	label associated with value in radio buttons

Table 6.2. *Command syntax for USRSET.*

Note that integer variables are stored in the *IU* array, real variables in the *RU* array, and short, long and file strings are all stored as entries in the *SU* array. In order to correctly define the reset window, all four variables associated with the n command should be defined in each n command. Similarly, the three variables associated with the s command should all be defined in each s command. Otherwise, the syntax for each command follows the usual rules of the scripting language. Below is an example code fragment that could define a simple *FILE* array.

FILE(1) = 'N I=1, N=NTRI, A=NT, T=I'
FILE(2) = 'N I=2, N=IBC , A=BC, T=I'
FILE(3) = 'S N=IBC, V=1, L="NEUMANN BC"'
FILE(4) = 'S N=IBC, V=2, L="DIRICHLET BC"'
LEN = 4

The first two lines are n commands that define two integer variables. The first line defines a variable with name *NTRI*, alias *NT*, that is stored as *IU(1)*. The

second defines a variable *IBC*, alias *BC*, that is stored as *IU(2)*. The variable *IBC* can take on two values, 1 and 2, that are associated with Neumann and Dirichlet boundary conditions, respectively. The third and fourth lines above are *s* commands that define the structure of a radio box associated with the *IBC* name in the X-Windows popup. Note that since the *LABEL* is a long string, its value must be enclosed in double quotes.

6.11 Subroutine GDATA.

The user provides subroutine *GDATA*, which defines the region through an initial triangulation or a skeleton. A call to *GDATA* is among the first executable statements in *ATEST*.

Call GDATA(VX, VY, SF, ITNODE, IBNDRY, IP, RP, SP,
IU, RU, SU, SXY)

Through this call the user is minimally expected to supply values for *NTF*, *NVF*, and *NBF* in the *IP* array, as well as the relevant values for the input arrays *VX*, *VY*, *SF*, *ITNODE*, and *IBNDRY*. Entries in *RP*, *SP*, *IU* and *RU*, as well as parameters in *IP* other than those mentioned above, may be optionally specified in *GDATA*.

6.12 Machine Dependent Routines.

During the initial installation of the package, the user must provide several machine dependent routines associated with timing and graphics. Default versions of these routines are provided with the package, which should work without modification in many environments, and in any event can serve as a model for a new implementation.

Fortran module *MTHDEF*, is used throughout the package to specify the precision of the floating point arithmetic to be used. The timing routine *TIMER* is used by *PLTMG* and *TRIGEN*. The graphics routines *TRIPLT*, *GPHPLT*, and *INPLT* address the graphics output device through the routines *PLTUTL*, *PFRAME*, *PLINE*, and *PFILL*. These routines are documented in detail below.

6.12.1 Arithmetic Specification.

This version of *PLTMG* uses module *MTHDEF* to specify the precision of arithmetic to be used. In particular, *PLTMG* is no longer supplied in single and double precision versions, since either version can easily be created just by resetting some parameters in *MTHDEF*

Below appears the default version of *MTHDEF*.

```
      module mthdef
c
      integer(kind=4), parameter :: isngl=4
      integer(kind=4), parameter :: rsngl=4
      integer(kind=4), parameter :: rdble=8
```

```
        integer(kind=4), parameter :: iknd=isngl
        integer(kind=4), parameter :: rknd=rdble
c
        end module
```

The parameters *RSNGL*, and *RDBLE* define single and double precision arithmetic, respectively. *ISNGL* defines integers. These three definitions should work with no change on most systems. The parameter *RKND* can be set to *RSNGL* for a single precision version of the code, or to *RDBLE* for a double precision version. *IKND* should be set it *ISNGL*.

6.12.2 Timing Routine.

Subroutine *TIMER* has the calling sequence

Subroutine TIMER(ISW)

Here *ISW* is an integer. The array *TIME* stored in common block *PLTMG7* records the time spent in major subroutines called by *PLTMG* and *TRIGEN*. *TIMER* should call an appropriate system routine to determine the current time each time it is entered, and then take various actions depending on the value of *ISW*. The cases $ISW = -2$ and $ISW = -1$ request initialization of the *TIME* array, while $1 \leq ISW \leq 50$ request an individual entry in the *TIME* array be updated. The current time is saved as it is needed for the next call to *TIMER*. Subroutine *TIMER* is machine independent except for the call to the system clock. An example of *TIMER*, calling the function *CPU_TIME*, is given below. It is quite likely that this routine will function properly on most modern systems with no change.

```
        subroutine timer(isw)
c
            use mthdef
            implicit real(kind=rknd) (a-h,o-z)
            implicit integer(kind=iknd) (i-n)
            integer(kind=iknd), save :: len=50
            real(kind=rknd), save :: tx=0.0e0_rknd
            common /pltmg7/time(3,50),hist(22,30)
c
c       call the clock and return the time in seconds
c       (time differences are used to compute the elapsed time)
c
        ty=tx
        call cpu_time(tx)
c
c       update time array (1.0e-10_rknd is below resolution of timer)
c
        if(isw>0) then
            dt=max(tx-ty,1.0e-10_rknd)
            time(1,isw)=time(1,isw)+dt
            time(2,isw)=time(2,isw)+dt
        else if(isw==-1) then
            do i=1,len
                time(1,i)=0.0e0_rknd
```

```
    enddo
else if(isw==-2) then
    do i=1,len
        time(1,i)=0.0e0_rknd
        time(2,i)=0.0e0_rknd
        time(3,i)=0.0e0_rknd
    enddo
endif
return
end
```

6.12.3 Graphics Interface.

The four device dependent routines in the graphics package are

Subroutine PLTUTL(NCOLOR, RED, GREEN, BLUE)
Subroutine PFRAME(IFRAME)
Subroutine PLINE(X, Y, Z, N, ICOLOR)
Subroutine PFILL(X, Y, Z, N, ICOLOR)

Subroutine *PLTUTL* takes various actions depending on the value of the integer *NCOLOR*. $NCOLOR > 0$ specifies initialization; *NCOLOR* denotes the number of colors to be used and satisfies $2 \le NCOLOR \le MXCOLR$. *RED*, *GREEN*, and *BLUE* are vectors of length *NCOLOR*. The entries *RED(i)*, *GREEN(i)*, and *BLUE(i)*, $1 \le i \le NCOLOR$, are floating point numbers on the interval $[0, 1]$, corresponding to *rgb* values for the ith color. Color number 1 is always white ($RED(1) = GREEN(1) = BLUE(1) = 1.0$), and color number 2 is always black ($RED(2) = GREEN(2) = BLUE(2) = 0.0$). The *rgb* values of the remaining entries depend on the picture to be drawn and the value of *MXCOLR*. *PLTUTL* should create a color map with the required colors, as these will be referenced in future calls to *PLINE* and *PFILL*. If *PLTUTL* is called with $NCOLOR < 0$, the drawing is complete and any necessary post processing should be carried out (e.g., close the plot file).

The drawing space used by the graphics routines is always assumed to be either the unit square $(0, 1) \times (0, 1)$ or the rectangle $(0, 1.5) \times (0, 1)$. For devices that have a so-called *Z*-buffer, the drawing space is either the unit cube $(0, 1) \times (0, 1) \times (0, 1)$ or the brick $(0, 1.5) \times (0, 1) \times (0, 1)$. The graphics display itself is always viewed as rectangular with aspect ratio 3/2, which is either a single rectangular frame or three square frames. These frames are numbered 1 to 4 as illustrated in Figure 6.5. The graphics routines write their output to various *lists*. A list consists of a frame, and certain attributes (rotating/non-rotating, lighted/non-lighted). Some attributes may not have realizations for certain graphics devices. The nine available lists are summarized in Table 6.3.

When graphics is initiated for a certain list, say list k, subroutine *PFRAME(k)* is called to indicate that subsequent calls of *PLINE* and *PFILL* contain data to be written to list k. $PFRAME(-k)$ indicates that the output to the given list should be terminated. By convention, graphics routines are allowed only one open list at a

time. Therefore, when *PFRAME* is invoked with a positive argument, the given list should be opened and the mapping from the unit cube or brick to the actual device coordinates for the given list should be computed. If rotation or lighting attributes are available, these should be set as specified in Table 6.3. When *PFRAME* is invoked with a negative argument, the given list should be closed.

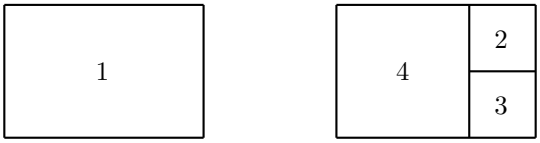

Figure 6.5. *Frame definitions.*

list	frame	rotating	lighted
1	1	no	no
2	2	no	no
3	3	no	no
4	4	no	no
5	4	yes	no
6	4	yes	no
7	4	yes	yes
8	4	yes	yes
9	4	no	yes

Table 6.3. *list specifications for pframe.*

Subroutine *PLINE* has arguments *X*, *Y*, *Z*, *N*, and *ICOLOR*. *X*, *Y*, and *Z* are vectors of length $N \geq 2$. The points *(X(i),Y(i),Z(i))* lie in the unit cube or the brick $(0, 1.5) \times (0, 1) \times (0, 1)$. The *Z* coordinate is useful only for devices that have a *Z*-buffer, and can be ignored in other cases. *ICOLOR* is an integer between 1 and *NCOLOR*, where *NCOLOR* was the argument that initialized *PLTUTL*, indicating the color to be used. *PLINE* should draw the given polyline *(X(i),Y(i),Z(i))* to *(X(i+1),Y(i+1),Z(i+1))*, $1 \leq i \leq N - 1$, with the specified color in the proper frame.

Subroutine *PFILL* has arguments *X*, *Y*, *Z*, *N*, and *ICOLOR*. *X*, *Y*, and *Z* are vectors of length $N \geq 3$. The points *(X(i),Y(i),Z(i))* lie in the unit cube or the brick $(0, 1.5) \times (0, 1) \times (0, 1)$, and define an *N*-sided (planar) polygonal region with sides *(X(i),Y(i),Z(i))* to *(X(i+1),Y(i+1),Z(i+1))* for $1 \leq i \leq N - 1$, and *(X(N),Y(N),Z(N))* to *(X(1),Y(1),Z(1))*. *ICOLOR* is an integer between 1 and *NCOLOR*, where *NCOLOR* was the argument that initialized *PLTUTL*, indicating

the color to be used. *PFILL* should color the specified polygon with the specified color in the proper frame.

IDEVCE	output driver
0–3	*SG* sockets 0–3
4	BH file
5	Postscript file
6	XPM file
7–10	X-Windows displays 0-3

Table 6.4. *Default graphics devices.*

The default installation of the package includes several standard output graphics devices. These are described in Table 6.4. *SG* is an OpenGL program written by Mike Holst that is available separately. It can receive input from a specified INET socket. *ATEST* allows up to four *SG* displays to be accessed. Because it is socket based, *SG* and *ATEST* can be running on different computers; the parameter *SGHOST* is the name of the host computer running *SG*. Since it is based on OpenGL the graphics displays are animated, and images can be manipulated with the mouse.

BH is the protocol developed for communication between *ATEST* and *SG*. BH files are essentially file versions of *SG* images. The parameter *BHFILE* gives the file name. The parameter *BHFILE* is scanned for the string *FIGXXX*. If found, this string is replaced by *FIG001*, *FIG002*, etc, with the counter incremented for each image. This allows the single parameter *BHFILE* to specify a family of separate BH files. The parameter *BHFILE* is also scanned for the string *MPIXXX*. If found, this string is replaced by *MPI001*, *MPI002*, etc, where the integer part denotes the processor. This avoids potential name conflicts when running *ATEST* as a parallel program. The BH file itself is a device independent binary file written using XDR. These files can be saved and later displayed using the *SG* program.

If the *SG* interface is not available or not desired, an alternate interface composed of stub routines is provided with the default installation of the program. The alternate interface has the same routines as the regular *SG* interface, but with all calls to routines and functions in the *MALOC* library deleted. Using the stub routines, an executable can be created without loading the *MALOC* library to resolve external references. However, if the stub routines are used, the *SG* and BH graphics options are disabled.

Postscript and XPM are both ASCII files. The parameters *PSFILE* and *XPFILE* specify the file names. These names are scanned for the strings *FIGXXX* and *MPIXXX*, that are replaced if found as described above in the case of *BHFILE*. Devices 7–10 refer to X-Windows graphics displays. Up to four such displays may be used (although the *ATEST* driver itself allows up to ten). These graphics windows display static pixmaps (raster images similar to XPM files) that cannot be animated or manipulated, other than resizing the window. X-Windows graphics

displays are only available when $MODE = 0$.

6.12.4 X-Windows Interface.

The X-Windows interface uses several X-Windows libraries, as well as the Motif widget set, and thus can be used only in environments that support the X-Windows system. It is based on the release X11R6. Our intent was to make the interface as generic and simple as possible. Since the *PLTMG* package is constantly evolving, the interface is structured to run arbitrary Fortran programs, so that in the future, large changes in the package need not cause correspondingly large changes in the interface. The X-Windows interface is written in C.

If the X-Windows libraries that support the X-Windows interface are not available, one can use substitute stub routines in place of the regular interface. These alternative stub routines are supplied with the default installation of the package, and are similar to those in the regular X-Windows interface, except that all calls to routines and functions in the X-Windows libraries have been deleted. Using the stub routines, an executable can be created without the need to load X-Windows libraries to resolve external references. However, in this case the X-Windows interface ($MODE = 0$) is completely disabled. This includes X-Windows graphics options ($7 \leq IDEVCE \leq 10$).

6.12.5 MPI Interface

The communication used in parallel processing is provided by calls to the MPI library. This library is not provided as part of the *PLTMG* package. The calls to the MPI library are all made from Fortran, and we have concentrated all calls into just a few subroutines. Thus the vast majority of the code comprising the main *PLTMG* routines is self-contained. If the MPI library is not available, one can use substitute stub routines supplied with the default installation in place of the regular interface. The stub routines are similar to the those in the regular interface, except that all calls to routines and functions in the MPI library have been deleted. Using the stub routines, an executable can be created without the need to load the MPI library to resolve external references. In this case, all the parallel computing options provided by *PLTMG*, *TRIGEN*, and the graphics routines are disabled.

Chapter 7
Test Problems

7.1 Overview.

In this chapter, we briefly document the test problem data sets included with the *PLTMG* source code. These problems encompass a variety of applications and exercise most features of the package. Each data set minimally consists of functions *A1XY*, *A2XY*, *FXY*, *GNXY*, *GDXY*, *P1XY*, *P2XY*, and *QXY* and subroutines *USRCMD* and *GDATA*. Problem specific routines are also included.

7.2 Test Problem CIRCLE.

In this problem, we solve the equation

$$-\nabla \cdot (a \nabla u) = 0,$$

where Ω is the unit circle with a crack along the positive x axis. Homogeneous Dirichlet boundary conditions are imposed on the top of the crack, and homogeneous Neumann boundary conditions are imposed below the crack. The coefficient $a \equiv a_k$ is piecewise constant in the eight sectors

$$\Omega_k = \{(r,\theta) |\, 0 \le r \le 1,\, (k-1)\pi/4 \le \theta \le k\pi/4\}.$$

The domain Ω is defined by a triangulation consisting of eight similar triangles, shown in Figure 7.1, that correspond to the eight sectors of constant a. On the boundary of the circle, nonhomogeneous boundary conditions are imposed such that the true solution in sector Ω_k is given by

$$u = r^\alpha (\beta_k \sin \alpha\theta + \gamma_k \cos \alpha\theta). \tag{7.1}$$

The exponent α is chosen to correspond to the leading singularity arising from the geometry, change of boundary conditions, and coefficient jumps at the origin. The coefficients β_k and γ_k are chosen to insure continuity of the solution u and the normal component of the flux $a\nabla u \cdot n$ across the interfaces, and to satisfy the

boundary conditions along the crack. For example, in the case $a_k = 1$ for all k, $\alpha = 1/4$ and

$$u = r^\alpha \sin \alpha\theta.$$

The *USRCMD* for this test problem has ten parameters that can be set. *IBC* determines the boundary conditions. If $IBC = 2$, the boundary conditions on the outer boundary of the circle are nonhomogeneous Dirichlet chosen such that (7.1) is the exact solution; if $IBC = 1$, nonhomogeneous Neumann boundary conditions are imposed on the circular part of the boundary in a similar fashion. One can also alter the geometry of the domain using the parameter *NTRI*, where $1 \le NTRI \le 8$. If $NTRI = 8$ the entire circle is used as the domain; if $NTRI < 8$, only the first *NTRI* sectors are used. Some examples are shown in Figure 7.1. Eight parameters,

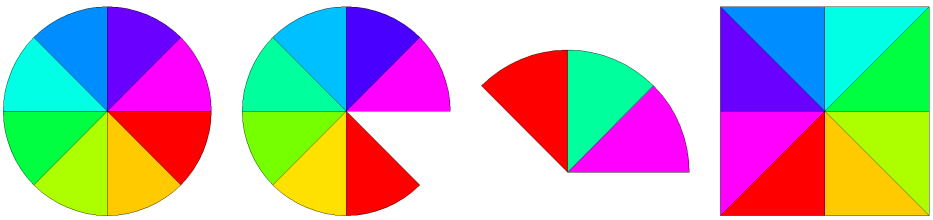

Figure 7.1. *On the far right is the square domain for problems SQUARE, OB and CONTROL. The remaining domains are for test problem CIRCLE with* $NTRI = 8$, $NTRI = 7$ *and* $NTRI = 3$.

A1, *A2*,...,*A8* define the coefficients a_k. Given the a_k and *NTRI*, the values of α, β_k and γ_k are computed in *GDATA* by solving appropriate nonlinear equations. Since the exact solution is known, we can compute the exact error. For this test problem, the function *QXY* is defined to be the exact error for graphics options and the true solution (7.1) otherwise.

7.3 Test Problem SQUARE.

In this test problem, a complicated equation is solved on a simple domain. The domain is always the unit square shown in Figure 7.1; boundary conditions on each side of the square can be independently specified as Dirichlet or natural, or pairs of opposite sides can be specified as periodic. The region is specified as a triangulation.

The coefficient functions are defined by

$$a_1 = A1X\,\frac{\partial u}{\partial x} + A1Y\,\frac{\partial u}{\partial y} + A1U\,u,$$

$$a_2 = A2X\,\frac{\partial u}{\partial x} + A2Y\,\frac{\partial u}{\partial y} + A2U\,u,$$

$$f = -BUX\,\frac{\partial u}{\partial x} - BUY\,\frac{\partial u}{\partial y} - CU0 - CU1\,u - CU2\,u^2 - CAHN\,(u - u^3)$$

$$- CIR\left(\frac{\partial u}{\partial x}(y - .5) - \frac{\partial u}{\partial y}(x - .5)\right) - CEXP\,e^u - CSIN\,\sin u, -F0(y - x)$$

$$g_1 = -DU0 - DU1\,u,$$

$$g_2 = -EU0,$$

and the functional ρ is defined by

$$p_1 = u^2,$$
$$p_2 = 0.$$

All of these nineteen parameters can be set using *USRCMD*, and any can be used as the continuation parameter λ by specifying the parameter *ICONT* in *USRCMD* as in Table 7.1. With this variety of nonlinearities, one can exercise most continuation features of *PLTMG*. If $ICONT = 0$, then none of the parameters is

ICONT	λ	*ICONT*	λ
0	none	10	*CU1*
1	*A1X*	11	*CU2*
2	*A1Y*	12	*CAHN*
3	*A1U*	13	*CEXP*
4	*A2X*	14	*CIR*
5	*A2Y*	15	*CSIN*
6	*A2U*	16	*DU0*
7	*BUX*	17	*DU1*
8	*BUY*	18	*EU0*
9	*CU0*	19	*F0*

Table 7.1. *Possible settings for ICONT.*

regarded as λ, and one should set $IPROB = 1$ to signify that the problem does not involve continuation.

One can also set the integer parameters *LEFT*, *RIGHT*, *TOP*, and *BOTTOM* in *USRCMD*. These refer to the four sides of the square in an obvious fashion and can be individually set to 2 for Dirichlet boundary conditions or to 1 for natural boundary conditions for the given side of the square. A pair of opposite edges can be set to 0 (e.g., $TOP = BOTTOM = 0$), and *IBNDRY* will then be set for periodic boundary conditions.

7.4 Test Problem DOMAINS.

In this test problem, a simple equation is solved on a variety of complicated domains. This test problem was designed mainly to exercise *TRIGEN*.

The problem to be solved is the linear partial differential equation

$$a_1 = A1X\,\frac{\partial u}{\partial x} + A1Y\,\frac{\partial u}{\partial y} + A1U\,u,$$
$$a_2 = A2X\,\frac{\partial u}{\partial x} + A2Y\,\frac{\partial u}{\partial y} + A2U\,u,$$
$$f = -BUX\,\frac{\partial u}{\partial x} - BUY\,\frac{\partial u}{\partial y} - CU1\,u - CU0$$

with a combination of homogeneous Dirichlet, homogeneous Neumann, and periodic boundary conditions. The parameters *A1X*, *A1Y*, *A1U*, *A2X*, *A2Y*, *A2U*, *BUX*, *BUY*, *CU0*, and *CU1* can all be set in *USRCMD*. The parameter *DOMAIN*, satisfying $1 \le DOMAIN \le 21$, specifies the domain to be used. The various possibilities are shown in Figure 7.2. All domains are defined by skeletons, so *TRIGEN* must be called to generate a triangulation.

7.5 Test Problem NACA.

Test problem *NACA* solves the equation of potential flow in one of several domains. The equation is of the form

$$-\nabla \cdot \rho(\nabla u)\nabla u = 0,$$

where

$$\rho(\nabla u) = (1 - u_x^2 - u_y^2)^{\frac{1}{\gamma - 1}}$$

and $\gamma = 1.4$. The local Mach number is computed in QXY and is given by

$$q = \sqrt{\frac{2c}{\gamma - 1}},$$
$$c = \frac{1}{1 - u_x^2 - u_y^2} - 1.$$

There are four domain options, chosen using the parameter *DOMAIN* in *USRCMD*. These domains are shown in Figure 7.3. All regions are defined as skeletons, so *TRIGEN* must be used to generate a triangulation.

Neumann boundary conditions are imposed everywhere so each domain has $ISING = 1$. There are several parameters in *USRCMD* that affect these problems. The parameter *MINF*, specifying the Mach number at infinity M_∞, sets the boundary conditions on the outer boundary and is also the continuation parameter λ for these problems. The parameter *ANGLE* specifies the angle of attack (in degrees). The parameter *SIZE* sets the radius of the outer boundary. When the local Mach number is less than one the flow is subsonic; *PLTMG* will work well in regions where the flow is entirely subsonic. As the M_∞ is increased, the solution will begin to

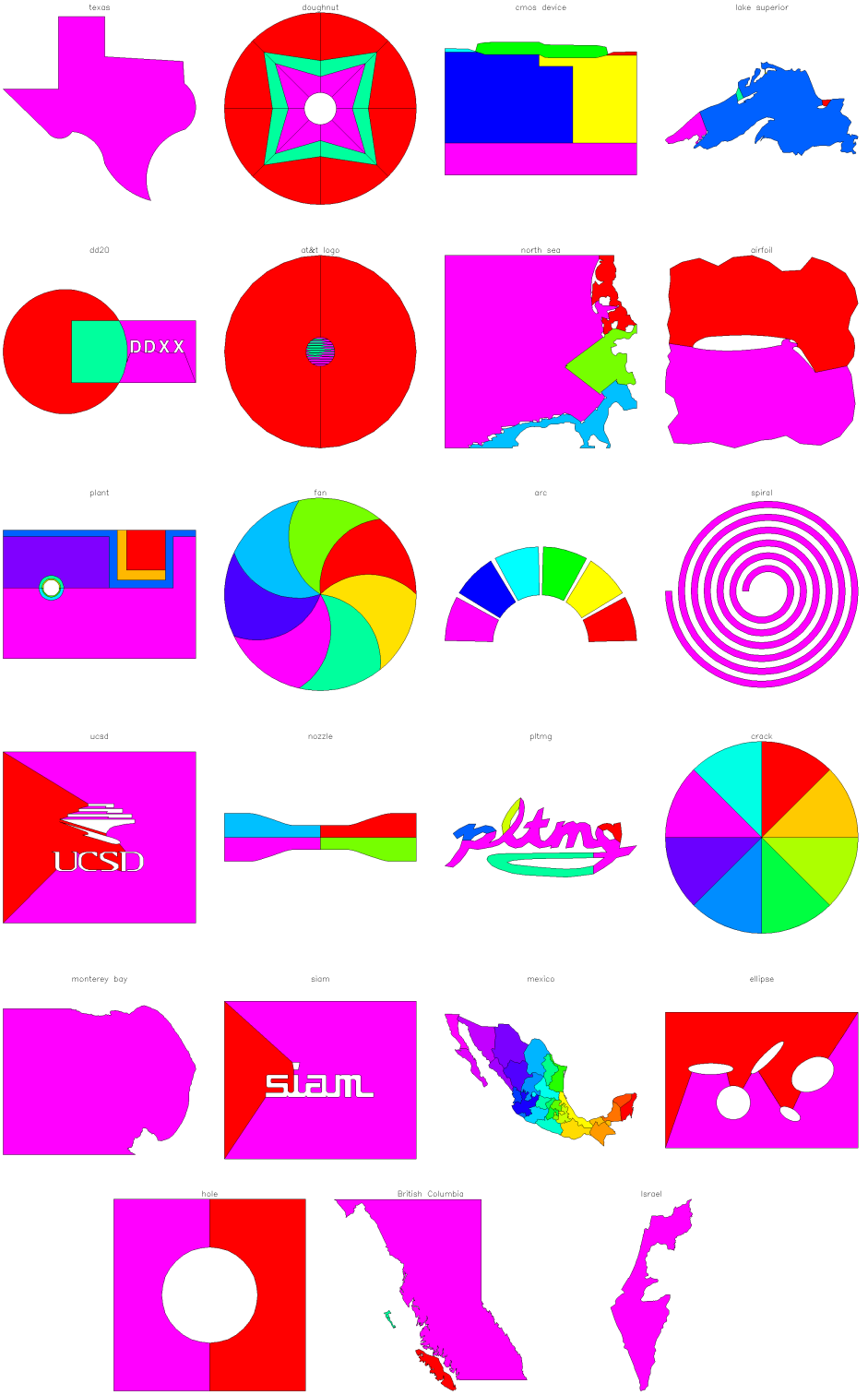

Figure 7.2. *The domains for* $DOMAIN = i$, $1 \leq i \leq 23$.

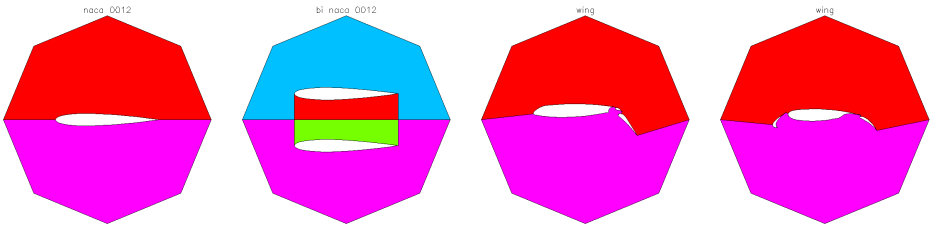

Figure 7.3. *The domains for DOMAIN* $= i$*,* $1 \le i \le 4$*, with SIZE* $= 1$*.*

develop regions of supersonic flow near the airfoils; *PLTMG* will continue to work as these regions are forming, but eventually will fail, as the underlying discretization used by *PLTMG* is not really appropriate for hyperbolic problems.

7.6 Test Problem JCN.

Test problem *JCN* solves the convection diffusion equation

$$-\nabla \cdot (\nabla u + \beta u) = 0,$$

where β is piecewise constant. The region is shown in Figure 7.4. The domain is specified by skeleton, so *TRIGEN* must be used to generate a triangulation.

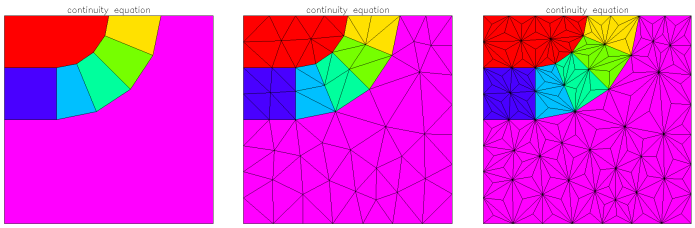

Figure 7.4. *The domain for test problem JCN (left), a triangulation produced by TRIGEN (middle), and the corresponding triangulation after a call to USRCMD with OBTUSE* $= 1$ *(right).*

This problem is an idealized model of the current continuity equation from the semiconductor device model that we have used to study the stability of discretizations used in device simulation. The problem has seven regions; $\beta = 0$ in regions one and seven. In the other five regions it has a magnitude of approximately 10^4 and is directed radially in each of the five subregions. The solution develops steep gradients at the junction between region seven and the five adjoining subregions.

Constant nonhomogeneous Dirichlet boundary conditions are specified along the bottom of the domain and on the left-hand portion of the top of the domain. Homogeneous Neumann boundary conditions are imposed elsewhere. The parameters *TOP* and *BOTTOM* in *USRCMD* can be used to reset the Dirichlet boundary

conditions on the top and bottom of the domain. The parameter DU can be used to adjust the size of β in regions 2–5; in particular, the magnitude of β in these five regions is proportional to DU.

Our original purpose in constructing this example was to test the sensitivity of various upwinding techniques [6] to poor element geometries. Since the goal of *TRIGEN* is to produce elements with good geometries, the *USRCMD* for this problem includes a procedure for systematically degrading the quality of the triangulation by introducing new elements with obtuse angles. If $OBTUSE = 1$ in *USRCMD*, then each triangle in the current mesh is divided into three new triangles by connecting its barycenter to its vertices. An example is shown in Figure 7.4. Repeated application of this procedure will produce triangulations with interior angles arbitrarily close to π.

7.7 Test Problem OB.

Test problem *OB* solves the a simple obstacle problem, with coefficient functions defined by

$$
\begin{aligned}
p_1 &= AX\left(\frac{\partial u}{\partial x}\right)^2 + AY\left(\frac{\partial u}{\partial y}\right)^2 + CU\,u^2 - 2su,\\
s &= \big(AX(IX\pi)^2 + AY(IY\pi)^2 - CU\big)\sin(IX\pi x)\sin(IY\pi y),\\
\underline{u} &= BDLW + CFLW\sin(IXL\pi x)\sin(IYL\pi y),\\
\overline{u} &= BDUP + CFUP\sin(IXU\pi x)\sin(IYU\pi y),\\
g_1 &= 0.
\end{aligned}
$$

The domain Ω is the unit square with homogeneous Dirichlet boundary conditions. The input data structure is a triangulation consisting of eight right triangles, shown in Figure 7.1. The parameters AX, AY, CU, $BDLW$, $BDUP$, $CFLW$, $CFUP$ and the integers IX, IY, IXL, IYL, IXU, IYU can all be set by the user in *USRCMD*. The exact solution to this problem in the absence of the obstacle is $u = \sin(IX\pi x)\sin(IY\pi y)$. This problem is mainly designed to test the cases $IPROB = \pm 2$ in *PLTMG*.

7.8 Test Problem MNSURF.

Test problem *MNSURF* solves the a simple minimal surface problem with an obstacle. The coefficient functions are given by

$$p_1 = \sqrt{1 + \left(\frac{\partial u}{\partial x}\right)^2 + \left(\frac{\partial u}{\partial y}\right)^2}$$

$$\underline{u} = \begin{cases} 1 & \text{in } \Omega_1 \\ -1 & \text{in } \Omega_2 \\ \ell & \text{in } \Omega_I \end{cases}$$

$$\overline{u} = 1.5$$

$$g_1 = 0,$$

$$g_2 = 0.$$

The domain Ω is the unit square with a mixture of homogeneous Dirichlet and Neumann boundary conditions. The domain is given as a skeleton, and is shown in Figure 7.5. The region Ω_1 is the inner square with side $1/2$, and Ω_2 is the outer region. The region Ω_I is the small band separating Ω_1 and Ω_2, consisting of four narrow trapezoids. In each of the four trapezoids, $\underline{u}$ is a linear polynomial in x or y that interpolates between -1 and 1, insuring continuity of $\underline{u}$. The parameter *THETA*, which can be set in *USRCMD*, controls the width of the band. The upper bound $\overline{u}$ is chosen such that it does not affect the solution. As with test problem *OB*, this problem is mainly designed to test the cases $IPROB = \pm 2$ in *PLTMG*.

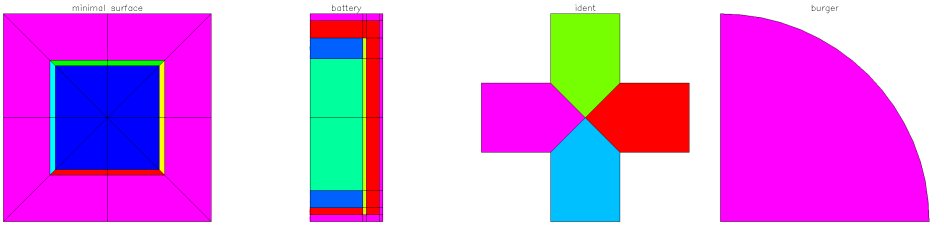

Figure 7.5. *The domains for test problems MNSURF, BATTERY, IDENT, and BURGER (left to right).*

7.9 Test Problem BURGER.

Test problem *BURGER* solves the nonlinear convection dominated flow

$$-\epsilon \Delta u + u_y + u u_x = 0.$$

This is really a time dependent Burger's equation in one space dimension. In this setting, the y space variable plays the role of time, and we have added a small diffusion term. This problem is solved as a two dimensional steady state problem. Some

analysis of this approach to solving time dependent partial differential equations is given in [33].

The small parameter $\epsilon > 0$ and can be set in *USRCMD*. The domain Ω is the quarter circle shown in Figure 7.5, and is specified as a skeleton. Natural (homogeneous Neumann) boundary conditions are applied along the circular arc, while Dirichlet boundary conditions are specified on the left side ($x = 0$) and the bottom ($y = 0$) as

$$g_2 = \begin{cases} 1 & 0 \le x \le 1/4 \\ 3/2 - 2x & 1/4 \le x \le 3/4 \\ 0 & 3/4 \le x \le 2 \end{cases}.$$

This combination of boundary conditions gives rise to a solution similar to the so-called "λ shock" of Burger's equation.

7.10 Test Problem BATTERY.

In this test problem we solve the linear elliptic problem

$$-a_1 u_{xx} - a_2 u_{yy} - f = 0$$

where the piecewise constant values of the coefficients are given in Table 7.2. The

Region	a_1	a_2	f	side	c	α
1	25	25	0	left	0	0
2	7	0.8	1	top	1	3
3	5.0	10^{-4}	1	right	2	2
4	0.2	0.2	0	bottom	3	1
5	0.05	0.05	0			

Table 7.2. *Coefficient definitions.*

domain Ω is shown in Figure 7.5 and is specified as a skeleton. The five subregions are given labels in *ITNODE(5,*)*, allowing us to conveniently define the coefficient functions. The boundary conditions are natural boundary conditions of the form

$$g_1 = c - \alpha u.$$

Here c and α are piecewise constant functions defined using *IBNDRY(6,*)*, as indicated in Table 7.2. The data for this problem was supplied by Leszek Demkowicz.

7.11 Test Problem CONTROL.

This problem tests the cases *IPROB* $= \pm 5$. The differential equation (constraint) is

$$-\Delta u = \lambda(C0 + C1\,u + C2\,u^2 + C3\,u^3) + F0 + F1\,u + F2\,u^2 + F3\,u^3$$

in Ω, with Dirichlet boundary conditions

$$u = DBC$$

on $\partial\Omega$. The objective function ρ is given by

$$\rho(u, \lambda) = \int_\Omega (u - u_0)^2 + \beta|\nabla(u - u_0)|^2 + \gamma\lambda^2 \, dx.$$

Ω is the unit square, defined as a triangulation similar to test problem *SQUARE*; see Figure 7.1. The function u_0 and the bounds on λ are given by

$$u_0 = \sin(IX\pi x)\sin(IY\pi y),$$
$$BDLW \le \lambda \le BDUP.$$

The constants $BETA = \beta$. $GAMMA = \gamma$, *BDLW*, *BDUP*, *DBC*, *C0*, *C1*, *C2*, *C3*, *F0*, *F1*, *F2*, and *F3*, and the integers *IX* and fIY can all be reset in *USRCMD*.

7.12 Test Problem IDENT.

This problem tests the cases $IPROB = \pm 4$. The differential equation is

$$-(1 + A^2)\Delta u + C2\, u^2 + C1\, u - C0 \; = 0.$$

The domain Ω is specified as a skeleton, and is shown in Figure 7.5. The boundary conditions are a combination of homogeneous Neumann and Dirichlet, except for the vertical edge on the right where the (possibly) nonhomogeneous Dirichlet boundary condition

$$u = D$$

is imposed. The five parameters *A*, *C0*, *C1*, *C2*, and *D* can be set in *USRCMD*, and any combination of them can be used as scalar parameters λ_i in the optimization problem. This is done setting the switches *IRL* (also set in *USRCMD*) indicated in Table 7.3. For example, setting $IRL1 = 1$ makes *A* an optimization parameter, while setting $IRL1 = 0$ keeps *A* at its current fixed value.

switch	λ_j
IRL1	*A*
IRL2	*C0*
IRL3	*C1*
IRL4	*C2*
IRL5	*D*

Table 7.3. *IRL switches.*

The objective function ρ is given by

$$\rho(u, \lambda) = \int_\Omega e^{-20(x^2+y^2)}(u - 1)^2 \, dx,$$

which tries to make the solution $u = 1$ near the origin, located at the center of Ω.

7.13 Test Problem BOX.

Test problem *BOX* tests the moving boundary optimization option in *PLTMG* (*IPROB* = 4 and *ITASK* = 8). The domain is a 1×1 square with a square hole, illustrated in Figure 7.6. The hole is free to move around within the square, with its position governed by three parameters: (x_c, y_c) denoting the coordinates of the center of the square, and θ denoting its angle of rotation. Any combination of these three parameters may be chosen as optimization parameters, as summarized in Table 7.4.

switch	λ_j
IRL1	x_c
IRL2	y_c
IRL3	θ

Table 7.4. *IRL switches.*

The objective function is given by

$$\rho(u, \lambda) = \min \int_\Omega \nabla u^2 + \delta \sum_{i=1}^{NRL} \lambda_i^2 \, dx.$$

The boundary value problem and inequality constraints are given by

$$\begin{aligned} -\Delta u &= 1 && \text{in } \Omega \\ u &= 0 && \text{on } \partial\Omega \\ \underline{\lambda}_i \le \lambda_i \le \overline{\lambda}_i, & && \text{for } 1 \le i \le NRL. \end{aligned}$$

7.14 Test Problem MESSAGE.

In this test problem, a simple equation is solved on a domain consisting of a message with up to ten lines. This test problem was designed mainly for fun, and to make software demonstrations more interesting.

The problem to be solved is the linear partial differential equation

$$\begin{aligned} a_1 &= A1X \frac{\partial u}{\partial x} + A1Y \frac{\partial u}{\partial y} + A1U \, u, \\ a_2 &= A2X \frac{\partial u}{\partial x} + A2Y \frac{\partial u}{\partial y} + A2U \, u, \\ f &= -BUX \frac{\partial u}{\partial x} - BUY \frac{\partial u}{\partial y} - CU1 \, u - CU0 \end{aligned}$$

with homogeneous Dirichlet boundary conditions. The parameters *A1X*, *A1Y*, *A1U*, *A2X*, *A2Y*, *A2U*, *BUX*, *BUY*, *CU0*, and *CU1* can all be set in *USRCMD*. String

parameters *LINE0*, *LINE1*, ... , *LINE9* can be set in *USRCMD* to a user specified message. Upper case and lower case letters, numbers, and several symbols found on a standard keyboard are available. Two possible domains are shown in Figure 7.6. All domains are defined by skeletons, so *TRIGEN* must be called to generate a triangulation.

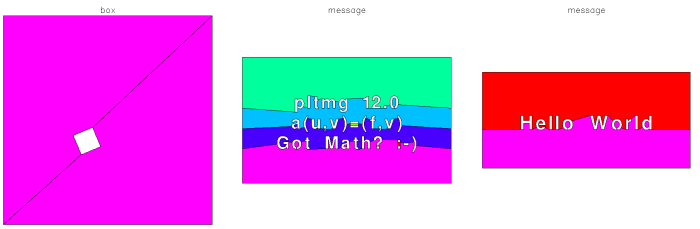

Figure 7.6. *The domain for test problem BOX, and two sample domains for test problem MESSAGE.*

7.15 Test Problem USMAP.

In this test problem, a simple equation is solved on one of 51 domains; 50 are outlines of individual states in the United States, and the last is an outline of the continental U. S. As with test problem *MESSAGE*, this test problem was designed mainly for fun.

The problem to be solved is the linear partial differential equation

$$a_1 = A1X\,\frac{\partial u}{\partial x} + A1Y\,\frac{\partial u}{\partial y} + A1U\,u,$$

$$a_2 = A2X\,\frac{\partial u}{\partial x} + A2Y\,\frac{\partial u}{\partial y} + A2U\,u,$$

$$f = -BUX\,\frac{\partial u}{\partial x} - BUY\,\frac{\partial u}{\partial y} - CU1\,u - CU0$$

with homogeneous Dirichlet boundary conditions. The parameters *A1X*, *A1Y*, *A1U*, *A2X*, *A2Y*, *A2U*, *BUX*, *BUY*, *CU0*, and *CU1* can all be set in *USRCMD*.

All domains are specified as skeletons, derived from PostScript and PDF files from the National Digital Map Library at the University of Virginia. The parameter *ISTATE*, $1 \le ISTATE \le 51$, specifies the domain. The parameter *ICTY* takes on values 0 and 1; if $ICTY = 1$, county lines (state lines in the case of the U. S. map) are included as part of the skeleton. If $ICTY = 0$, the skeleton consists of just the outline of the state or country. Several domains (e. g. Michigan, Hawaii) are not connected. Many have small islands[11] that can be excluded from the skeleton by setting the parameter $ISLE = 0$. If $ISLE = 1$, all small islands are included as part of the skeleton. Several domains are shown in Figure 7.7. Since all domains are defined by skeletons, *TRIGEN* must be called to generate a triangulation.

[11] The definition of small is problem dependent and depends on the judgment of the author.

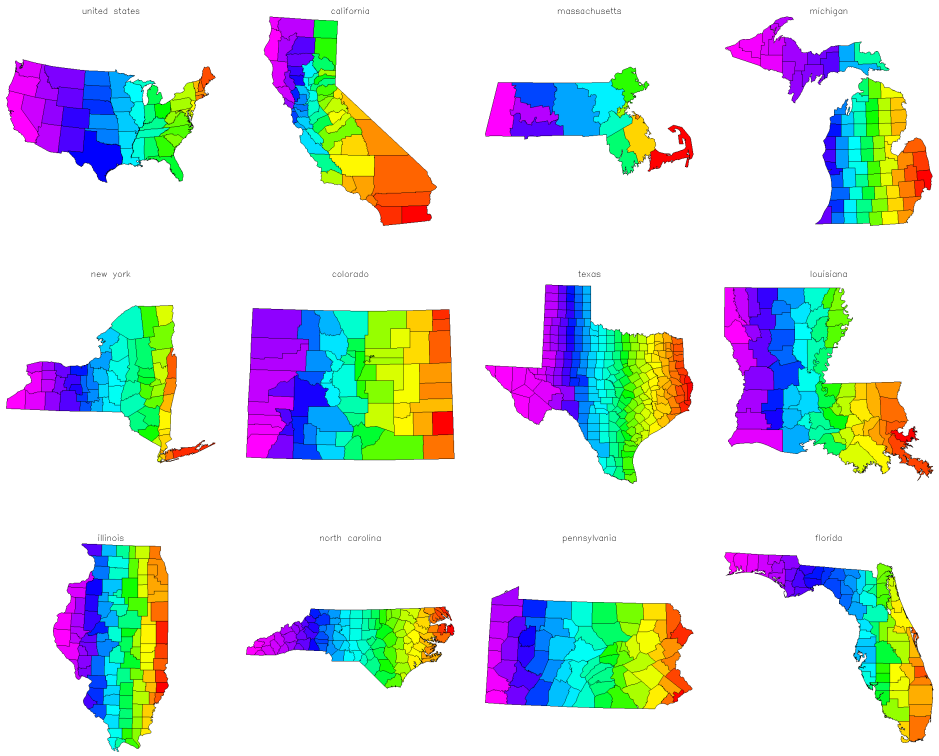

Figure 7.7. *Sample domains for test problem USMAP. ICNTY* $= 1$ *and ISLE* $= 0$ *for all domains.*

Bibliography

[1] I. Babuška and W. C. Rheinboldt, *Error estimates for adaptive finite element computations*, SIAM J. Numer. Anal., 15 (1978), pp. 736–754.

[2] Ivo Babuška and Theofanis Strouboulis, *The finite element method and its reliability*, Numerical Mathematics and Scientific Computation, The Clarendon Press Oxford University Press, New York, 2001.

[3] Randolph E. Bank, *Multigraph users' guide - version 1.0*, tech. report, Department of Mathematics, University of California at San Diego, 2001.

[4] ——, *A domain decomposition solver for a parallel adaptive meshing paradigm*, in Domain Decomposition Methods in Science and Engineering XVI, Olof B. Widlund and David E. Keyes, eds., vol. 55 of Lecture Notes in Computational Science and Engineering, Springer-Verlag, 2006, pp. 3–14.

[5] ——, *Some variants of the Bank-Holst parallel adaptive meshing paradigm*, Computing and Visualization in Science, 9 (2006), pp. 133–144.

[6] R. E. Bank, J. F. Bürgler, W. Fichtner, and R. K. Smith, *Some upwinding techniques for finite element approximations of convection-diffusion equations*, Numer. Math., 58 (1990), pp. 185–202.

[7] Randolph E. Bank and Tony F. Chan, *PLTMGC: A multi-grid continuation program for parameterized nonlinear elliptic systems*, SIAM J. Sci. and Stat. Computing, 7 (1986), pp. 540–559.

[8] ——, *An analysis of the composite step biconjugate gradient method*, Numer. Math., 66 (1993), pp. 295–319.

[9] ——, *The composite step biconjugate gradient algorithm for nonsymmetric linear systems*, Numerical Algorithms, 7 (1994), pp. 1–16.

[10] Randolph E. Bank, William M. Coughran, and Lawrence C. Cowsar, *Analysis of the finite volume Scharfetter-Gummel method for steady convection diffusion equations*, Computing and Visualization in Science, 1 (1998), pp. 123–136.

[11] Randolph E. Bank and Chris Deotte, *The influence of partitioning on domain decomposition convergence rates*, Computing and Visualization in Science, (accepted).

[12] ——, *Adventures in adaptivity*, Computing and Visualization in Science, (submitted).

[13] Randolph E. Bank, Philip E. Gill, and Roummel F. Marcia, *Interior methods for a class of elliptic variational inequalities*, in Large-scale PDE-constrained Optimization, Lorenz T. Biegler, Omar Ghattas, Matthias Heinkenschloss, and Bart van Bloemen Waanders, eds., vol. 30 of Lecture Notes in Computational Science and Engineering, Berlin, Heidelberg and New York, 2003, Springer-Verlag, pp. 218–235.

[14] Randolph E. Bank and Michael J. Holst, *A new paradigm for parallel adaptive meshing algorithms*, SIAM J. on Scientific Computing, 22 (2000), pp. 1411–1443.

[15] ——, *A new paradigm for parallel adaptive meshing algorithms*, SIAM Review, 45 (2003), pp. 292–323.

[16] Randolph E. Bank and Peter K. Jimack, *A new parallel domain decomposition method for the adaptive finite element solution of elliptic partial differential equations*, Concurrency and Computation: Practice and Experience, 13 (2001), pp. 327–350.

[17] Randolph E. Bank, Peter K. Jimack, Sarfraz A. Nadeem, and Sergei V. Nepomnyaschikh, *A weakly overlapping domain decomposition preconditioner for the finite element solution of elliptic partial differential equations*, SIAM J. on Scientific Computing, 23 (2002), pp. 1817–1841.

[18] Randolph E. Bank and Shaoying Lu, *A domain decomposition solver for a parallel adaptive meshing paradigm*, SIAM J. on Scientific Computing, 45 (2003), pp. 292–323.

[19] Randolph E. Bank and Hans D. Mittelmann, *Continuation and multigrid for nonlinear elliptic systems*, in Multigrid Methods II: Proceedings, Cologne 1985, vol. 1228 of Lecture Notes in Mathematics, Springer-Verlag, Heidelberg, 1986, pp. 24–38.

[20] ——, *Stepsize selection in continuation procedures and damped Newton's method*, J. Comput. Appl. Math., 26 (1989), pp. 67–78.

[21] Randolph E. Bank and Hieu Nguyen, *Domain decomposition and hp-adaptive finite elements*, in Domain Decomposition Methods in Science and Engineering XIX, Yunqing Huang, Ralf Kornhuber, Olof Widlund, and Jinchao Xu, eds., vol. 78 of Lecture Notes in Computational Science and Engineering, Springer-Verlag, 2011, pp. 3–13.

[22] ——, *hp adaptive finite elements based on derivative recovery and superconvergence*, Computing and Visualization in Science, 14 (2012), pp. 287–299. Original Article.

[23] ——, *Mesh regularization in the Bank-Holst parallel hp adaptive meshing*, in Domain Decomposition Methods in Science and Engineering XX, Randolph Bank, Michael Holst, Olof Widlund, and Jinchao Xu, eds., vol. 91 of Lecture Notes in Computational Science and Engineering, Springer-Verlag, 2013, pp. 103–110.

[24] ——, *A parallel hp-adaptive finite element method*, in Scientific Computing and Applications VIII, Jichun Li, ed., vol. 586 of Contemporary Mathematics, American Mathematical Society, 2013, pp. 23–33.

[25] Randolph E. Bank and Jeffery S. Ovall, *Dual functions for a parallel adaptive method*, SIAM J. on Scientific Computing, 29 (2007), pp. 1511–1524.

[26] ——, *Some remarks on interpolation and best approximation*, Numerische Mathematik, (submitted).

[27] Randolph E. Bank, Aseih Parsania, and Stefan Sauter, *Saturation estimates for hp-finite element mathods*, Computing and Visualization in Science, 16 (2013), pp. 195–218.

[28] Randolph E. Bank and Donald J. Rose, *Global approximate Newton methods*, Numer. Math., 37 (1981), pp. 279–295.

[29] ——, *A multi-level Newton method for nonlinear finite element equations*, Math. Comp., 39 (1982), pp. 453–465.

[30] Randolph E. Bank and R. Kent Smith, *Mesh smoothing using a posteriori error estimates*, SIAM J. Numer. Anal., 34 (1997), pp. 979–997.

[31] Randolph E. Bank and R. Kent Smith, *Multigraph algorithms based on sparse Gaussian elimination*, in Thirteenth International Symposium on Domain Decomposition Methods for Partial Differential Equations, Domain Decomposition Press, Bergen, 2001, pp. 15–26.

[32] ——, *An algebraic multilevel multigraph algorithm*, SIAM J. on Scientific Computing, 25 (2002), pp. 1572–1592.

[33] Randolph E. Bank, Panayot Vassilevski, and Ludmil Zikatanov, *Arbitrary dimension convection-diffusion scheme for sapce-time discretizations*, Journal of Computational and Applied Mathematics, (accepted).

[34] Randolph E. Bank and Panayot S. Vassilevski, *Convergence analysis of a domain decomposition paradigm*, Computing and Visualization in Science, 11 (2008), pp. 333–350.

[35] Randolph E. Bank and Jinchao Xu, *Asymptotically exact a posteriori error estimators, part I: Grids with superconvergence*, SIAM J. Numerical Analysis, 41 (2003), pp. 2294–2312.

[36] ——, *Asymptotically exact a posteriori error estimators, part II: General unstructured grids*, SIAM J. Numerical Analysis, 41 (2003), pp. 2313–2332.

[37] Randolph E. Bank, Jinchao Xu, and Bin Zheng, *Superconvergent derivative recovery for Lagrange triangular elements of degree p on unstructured grids*, SIAM J. Numerical Analysis, 45 (2007), pp. 2032–2046.

[38] Randolph E. Bank and Harry Yserentant, *On the H^1-stability of the L_2-projection onto finite element spaces*, Numerische Mathematik, 126 (2014), pp. 361–381.

[39] ——, *A note on interpolation, best approximation, and the saturation property*, Numerische Mathematik, (to appear).

[40] Mark W. Beall and Mark S. Shephard, *A general topology-based mesh data structure*, Internat. J. Numer. Methods Engrg., 40 (1997), pp. 1573–1596.

[41] X. Cai and K. Samuelsson, *Parallel multilevel methods with adaptivity on unstructured grids*, 1999. Preprint.

[42] T. F. Chan, P. Ciarlet, and W. K. Szeto, *On the optimality of the median cut spectral bisection method*, SIAM J. Sci. Comput., 18 (1997), pp. 943–948.

[43] H. L. deCougny, K. D. Devine, J. E. Flaherty, R. M. Loy, C. Ozturan, and M. S. Shephard, *Load balancing for the parallel adaptive solution of partial differential equations*, Appl. Num. Math., 16 (1994), pp. 157–182.

[44] C. Deotte, *Domain Partitioning Methods for Elpiptic Partial Differential Equations*, PhD thesis, University of California at San Diego, 2014.

[45] J. E. Flaherty, R. M. Loy, C. Ozturan, M. S. Shephard, B. K. Szymanski, J. D. Teresco, and L. H. Ziantz, *Parallel structures and dynamic load balancing for adaptive finite element computation*, Appl. Num. Math., 26 (1998), pp. 241–263.

[46] Andrew V. Knyazev, *Toward the optimal preconditioned eigensolver: locally optimal block preconditioned conjugate gradient method*, SIAM J. Sci. Comput., 23 (2001), pp. 517–541 (electronic). Copper Mountain Conference (2000).

[47] Scott Kohn, John Weare, M. Elizabeth Ong, and Scott B. Baden, *Software abstractions and computational issues in parallel structured adaptive mesh methods for electronic structure calculations*, in Workshop on Structured Adaptive Mesh Refinement Grid Methods, Institute for Mathematics and Its Applications, University of Minnesota, Minneapolis, MN., 1997.

[48] Shaoying Lu, *Parallel Adaptive Multigrid Algorithms*, PhD thesis, Department of Mathematics, University of California at San Diego, 2004.

[49] William F. Mitchell, *A comparison of adaptive refinement techniques for elliptic problems*, ACM Trans. Math. Software, 15 (1989), pp. 326–347.

[50] ——, *The full domain partition approach to distributing adaptive grids*, Applied Numerical Mathematics, 26 (1998), pp. 265–275.

[51] ——, *A parallel multigrid method using the full domain partition*, Electronic Transactions on Numerical Analysis, 6 (1998), pp. 224–233.

[52] Hans D. Mittelmann, *Multi-grid continuation and spurious solutions for nonlinear boundary value problems*, Rocky Mountain J. Math., 18 (1988), pp. 387–401.

[53] H. D. Mittelmann and H. Weber, *Multigrid solution of bifurcation problems*, SIAM J. Sci. Stat. Comp., 6 (1985), pp. 49–60.

[54] Hieu Nguyen, *p- and fully automatic hp- adaptive finite element methods for elliptic Partial Differential Equations*, PhD thesis, University of California, San Diego, 2010.

[55] Jeffrey S. Ovall, *Duality-Based Adaptive Refinement for Elliptic PDEs*, PhD thesis, Department of Mathematics, University of California at San Diego, 2004.

[56] B. N. Parlett, *The Symmetric Eigenvalue Problem*, Prentice Hall, Englewood Cliffs, New Jersey, 1980.

[57] Alex Pothen, Horst D. Simon, and Kang-Pu Liou, *Partitioning sparse matrices with eigenvectors of graphs*, SIAM J. Matrix Anal. Appl., 11 (1990), pp. 430–452.

[58] M. C. Rivara, *Mesh refinement processes based on the generalized bisection of simplices*, SIAM J. Numer. Anal., 21 (1984), pp. 604–613.

[59] P. M. Selwood, M. Berzins, and P. M. Dew, *3D parallel mesh adaptivity: Data structures and algorithms*, in Parallel Processing for Scientific Computing, Philadelphia, 1997, SIAM.

[60] Horst D. Simon and Shang-Hua Teng, *How good is recursive bisection?*, SIAM J. Sci. Comput., 18 (1997), pp. 1436–1445.

[61] Rudiger Verfürth, *A Posteriori Error Estimation and Adaptive Mesh Refinement Techniques*, Teubner Skripten zur Numerik, B. G. Teubner, Stuttgart, 1995.

[62] C. Walshaw and M. Berzins, *Dynamic load balancing for pde solvers on adaptive unstructured meshes*, Concurrency: Practice and Experience, 7 (1995), pp. 17–28.

[63] A. Weiser, *Local-Mesh, Local-Order Adaptive Finite Element Methods with A-Posteriori Error Estimators for Elliptic Partial Differential Equations*, PhD thesis, Yale University, 1981.

[64] Linbo Zhang, Tao Cui, and Hui Liu, *A set of symmetric quadrature rules on triangles and tetrahedra*, J. Comput. Math., 27 (2009), pp. 89–96.

Index